POLITECNICO DI TORINO

Master's Degree in MECHATRONIC ENGINEERING

Master's Degree Thesis

Impact of Time Gap Policies on Adaptive Cruise Control Performance

Supervisors

Prof. ANDREA TONOLI

PhD Candidate STEFANO FAVELLI

Candidate

YANRONG LI

JULY 2025

Abstract

In recent years, the rapid advancement of autonomous driving and intelligent connected vehicle technologies has significantly accelerated the development and deployment of Advanced Driver Assistance Systems (ADAS). Among them, Adaptive Cruise Control (ACC) plays a central role by automatically regulating inter-vehicle distance and longitudinal speed, thereby improving both driving safety and ride comfort. However, most existing commercial ACC systems still rely on a small set of predefined, discrete time gap values (e.g., 1.0 s, 1.5 s, 2.0 s), which lack adaptability to varying traffic conditions, driver intent, and road types. This rigidity limits the system's ability to achieve an optimal trade-off among multiple performance objectives.

This study investigates the impact of different time gap policies on the overall performance of ACC systems. A unified simulation platform was developed, comprising a vehicle dynamics model, a longitudinal controller, and three representative time gap strategies: Constant Time Gap (CTG), Constant Safety Factor (CSF), and Human Driving Behavior (HDB). These strategies were systematically tested under both urban and highway driving cycles—including WLTP Class 3, Artemis Urban, China City Cycle, HWFET, US06, and Artemis Motorway—using a multi-criteria evaluation framework that encompasses energy consumption, ride comfort, and following safety.

Simulation results indicate that in urban environments, the HDB strategy—based on statistical modeling of naturalistic human driving behavior—demonstrates superior responsiveness and adaptability in handling frequent acceleration, deceleration, and short halts. In contrast, the CSF strategy, with its longer headway and speed-dependent safe distance formulation, exhibits significant advantages in highway scenarios by reducing acceleration fluctuations and stabilizing energy consumption. The CTG strategy, while structurally simple, achieves a balanced performance across all indicators, making it suitable as a conservative baseline. Notably, certain HDB configurations yielded higher energy consumption than the ACC-free baseline in high-speed conditions, highlighting the need for scenario-specific parameter tuning.

Keywords: Adaptive Cruise Control (ACC), Time Gap Policy, Urban Driving Cycle, Highway Driving Cycle, Energy Efficiency, Ride Comfort, Multi-objective Performance Optimization

Table of Contents

Chapter 1

Introduction

1.1 Background

With the continuous evolution of artificial intelligence technologies and the increasing deployment of in-vehicle communication systems, autonomous driving has gradually become one of the core directions in the development of Intelligent Connected Vehicles (ICVs). In order to standardize terminology and define capability levels for various automated driving systems, the Society of Automotive Engineers (SAE) first published the taxonomy and definitions for on-road motor vehicle automation systems in 2014 under the standard SAE J3016, which was subsequently revised in 2021 as SAE J3016-202104 [1]. This standard systematically categorizes driving automation into six levels, from Level 0 (no automation) to Level 5 (full automation), thereby providing a unified reference framework for technical development, regulatory policymaking, and commercial deployment of automated driving systems. The core concepts of the standard revolve around two key definitions: the Dynamic Driving Task (DDT) and the Operational Design Domain (ODD).

- **DDT** encompasses all real-time operational and tactical functions required to operate a vehicle in active traffic, including longitudinal control (acceleration and deceleration), lateral control (steering), object and event detection and response, and fallback performance.
- **ODD** refers to the specific conditions under which a given driving automation system is designed to function safely, including parameters such as roadway type, speed range, and environmental conditions (e.g., weather, lighting, and traffic scenarios).

The SAE J3016-defined six-level classification is illustrated in the figure below,

clearly showing the progressive reduction in human driver involvement as the level of automation increases [2].

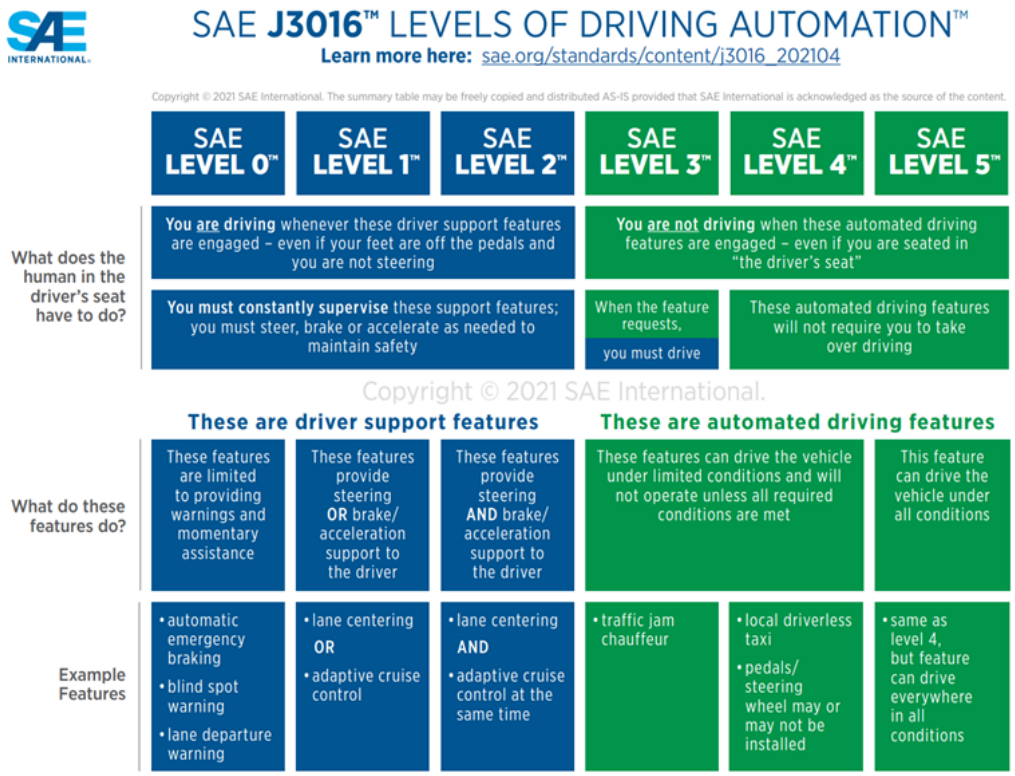

Figure 1.1: Levels of Driving Automation

Within this classification framework, Level 1 (Driver Assistance) and Level 2 (Partial Automation) represent the most technologically mature and commercially widespread stages of driving automation to date. A Level 1 system is capable of performing either longitudinal or lateral control under specific conditions—for instance, maintaining a preset speed through cruise control, or keeping the vehicle centered within the lane via lane-keeping assist. Such systems typically rely on onboard sensors such as radar and cameras to perceive the driving environment; however, the human driver remains fully responsible for all aspects of the driving task. The system merely offers limited assistance in well-defined scenarios.

In contrast, Level 2 systems exhibit a significant leap in both perception and

control capabilities. These systems can simultaneously execute longitudinal (acceleration/deceleration) and lateral (steering) control within a defined Operational Design Domain (ODD). Common functional combinations include Adaptive Cruise Control (ACC) paired with Lane Centering Assistance (LCA), and may extend to fully automated stop-and-go control in low-speed congested traffic. Level 2 systems rely heavily on multi-sensor fusion techniques and are often supported by high-definition maps, enabling automation in more complex driving scenarios. Nonetheless, the human driver is still required to maintain full attention and be ready to take over control at any time to ensure operational safety.

Although Level 1 and Level 2 systems have made significant progress in terms of functional design, they still face numerous technical challenges in areas such as perception reliability, control decoupling, human–machine interface design, functional safety, and regulatory compliance. The performance of single-sensor systems is often degraded under adverse conditions such as glare, rain, or snow, necessitating the integration of LiDAR or Vehicle-to-Everything (V2X) communication to enhance redundancy. Furthermore, fault-tolerant behavior and system fallback mechanisms must comply with the ISO 26262 functional safety standard to ensure protection in the event of system failure. At the legal level, the allocation of liability and driver monitoring requirements vary significantly across jurisdictions, adding further complexity to cross-regional deployment.

Looking forward, the evolution of L1/L2 systems is expected to follow a trajectory of gradual expansion of applicable scenarios, continuous refinement of control strategies, and data-driven performance optimization, paving the way toward higher levels of autonomous driving capability.

As for Level 3 and above, while these systems are theoretically capable of fully executing the Dynamic Driving Task (DDT) without human intervention, real-world deployment remains constrained by multiple factors—most notably the "long tail" perception problem, the lack of a mature Safety of the Intended Functionality (SOTIF) evaluation framework, and the regulatory lag across global markets. Consequently, current research and industrial efforts are largely focused on enhancing the robustness and multi-objective performance of L1/L2 systems in real-world environments, thereby establishing a reliable foundation for the future transition toward higher levels of driving automation.

As a core subsystem of ADAS, Adaptive Cruise Control (ACC) integrates sensor technologies, control algorithms, and vehicle dynamics models to enable automated longitudinal distance control. This significantly enhances driving safety and comfort while serving as a critical foundation for the deployment of higher-level autonomous

driving systems (Level 3 and above). The primary function of ACC is to monitor the relative distance and velocity to the preceding vehicle in real time. By leveraging accurate vehicle dynamics modeling and real-time responsiveness of the control system, it dynamically adjusts the ego vehicle's speed through closed-loop control logic to maintain a preset time gap—the temporal spacing between the ego vehicle and the preceding vehicle (measured in seconds). This time gap not only underpins longitudinal vehicle control but also constitutes a key variable influencing the system's multi-objective performance, including energy efficiency, comfort, safety, and traffic throughput [3].

Different time gap settings affect not only driving safety but also directly determine energy consumption levels, ride comfort, and traffic flow. While a shorter time gap improves road capacity and responsiveness, it risks causing string instability and increases the likelihood of collisions. Conversely, longer time gaps may reduce energy efficiency and traffic throughput. Therefore, designing rational and adaptive time gap policies is of vital importance for optimizing the overall performance of ACC systems.

However, existing ACC systems still exhibit significant limitations in the design of time gap policies. While some commercial vehicles support manual adjustment of gap levels (e.g., "short," "medium," "long" modes), these presets are largely based on empirical rules or fixed parameters and lack adaptability to dynamic driving environments such as stop-and-go city traffic, highway cruising, or mountainous roads. For instance, urban driving cycles demand shorter time gaps for prompt reactions, whereas highway conditions prioritize energy efficiency and braking safety over longer distances.

Moreover, conventional research has focused predominantly on control algorithm optimization (e.g., PID, MPC), while systematic evaluation and multi-objective trade-off analyses of time gap strategies remain at a preliminary stage. Discussions of how time gap parameters influence traffic flow stability and capacity are also relatively scarce [4]. As a result, existing ACC systems often encounter performance bottlenecks such as delayed response, excessive energy consumption, or compromised comfort in complex road environments, falling short of the performance requirements expected from intelligent driving systems.

Against this backdrop, the present research focuses on the deep impact of time gap policies on ACC system performance. By constructing a standardized simulation platform, we systematically evaluate three representative policies—Constant Time Gap (CTG), Constant Safety Factor (CSF), and Human Driving Behavior (HDB)—in diverse driving scenarios. This study aims to uncover the internal

patterns by which these policies influence energy consumption and comfort, providing both theoretical insights and engineering guidance for the next generation of intelligent driving systems.

1.2 Problem Statement and Research Motivation

1.2.1 Static Nature of Existing Strategies and Limited Adaptability to Dynamic Scenarios

Most current ACC systems adopt the Constant Time Gap (CTG) strategy, where a fixed time gap (e.g., 1.5 or 2.0 s) is maintained regardless of driving context. While this approach simplifies control logic, its static nature fails to account for the dynamic characteristics of real-world traffic scenarios. For example, in urban conditions, frequent stop-and-go movements and lane changes require shorter time gaps for responsiveness, whereas highway cruising necessitates longer gaps to optimize energy efficiency and ensure driving stability.

The "one-size-fits-all" approach of fixed-gap strategies often leads to suboptimal performance in complex environments, manifested as frequent braking due to small gaps in city traffic or low traffic efficiency due to overly large gaps on highways. More critically, these static gaps can lead to increased fuel consumption and poor energy utilization [5].

1.2.2 Conflicting Multi-Objective Requirements and Need for Integrated Optimization

The design of time gap strategies must simultaneously address four core performance objectives: safety, energy efficiency, ride comfort, and traffic throughput. However, these goals often conflict. For instance, a shorter gap increases road capacity but leads to frequent acceleration and deceleration, resulting in higher energy consumption and discomfort. On the other hand, a longer gap reduces fuel consumption and improves stability, but compromises road utilization efficiency.

Moreover, safety requires the minimum following distance to cover emergency braking conditions, whereas energy-efficient driving prefers fewer throttle and braking actions. Balancing these trade-offs and achieving an integrated optimization framework poses a significant challenge in ACC strategy design.

1.2.3 Lack of Systematic Evaluation and Quantitative Analysis Frameworks

Although alternative strategies—such as Human Driving Behavior (HDB) models and Constant Safety Factor (CSF) methods—have been proposed, most studies focus on optimizing individual strategies under limited conditions. A unified evaluation platform that allows for cross-strategy comparisons under standardized conditions remains absent.

Additionally, inconsistent use of driving cycles, controller designs, and performance metrics across existing studies limits the universality and comparability of their findings. This fragmented research landscape hinders the standardization and real-world implementation of advanced time gap policies.

1.3 Challenges and Research Significance

1.3.1 Complex Parameter Design and Lack of Unified Standards

Optimizing time gap strategies requires multi-dimensional parameter tuning. Taking CSF as an example, its core parameters include maximum deceleration factors, safety buffers, and braking thresholds. These must be adapted to the vehicle's dynamic characteristics, road adhesion conditions, and traffic density. However, due to the absence of a standardized design framework, parameter calibration often relies on expert heuristics, making large-scale deployment difficult.

1.3.2 High Requirements for Simulation Platform Integration

To fairly compare different time gap policies, a unified simulation platform must be established with consistent control structures, vehicle models, and driving scenarios. The vehicle dynamics model must accurately represent powertrain efficiency and braking behavior, while the driving scenarios must reflect realistic features of urban and highway conditions. Additionally, the quantification of energy and comfort indicators must rely on physical models and human perception thresholds, placing high demands on both computational efficiency and simulation fidelity.

1.3.3 Complex Interactions Between Multidimensional Performance Metrics

Trade-offs between energy consumption and comfort are especially prominent under complex traffic conditions. For instance, to save energy, vehicles prefer steady cruising, but if the lead vehicle frequently changes speed, large time gaps can cause delayed responses and ride discomfort. Therefore, a multidimensional performance analysis—including per-kilometer energy consumption, RMS of acceleration, and peak jerk—is necessary to reveal the performance characteristics and applicable domains of each policy.

Despite these challenges, this study aims to provide a comprehensive performance evaluation of time gap strategies. The results will offer data support for current ACC system optimization and lay a theoretical foundation for next-generation intelligent driving technologies—such as cooperative ACC and V2X-integrated control—highlighting the study's academic and engineering value.

1.4 Research Objectives and Scope

This study adopts a "baseline without ACC or time gap policy" as the reference condition. On top of this, a unified simulation platform is built to evaluate and compare the performance of three policies (CTG, CSF, HDB) across both urban and highway driving scenarios. The specific objectives are as follows:

- **Establish a Unified Simulation Platform:** Based on the MATLAB/Simulink environment, develop a consistent framework integrating a longitudinal vehicle dynamics model (including powertrain, drivetrain, and braking subsystems), a PID controller, and a configurable time gap module to ensure fair and repeatable comparisons.
- **Model Time Gap Strategies and Define Parameters:** Implement detailed models of the CTG, CSF, and HDB strategies. Clearly define their control logic, parameter definitions, and physical underpinnings, providing standardized interfaces for simulation testing.
- **Design Representative Driving Cycles:** Select representative urban cycles (e.g., WLTP Class 3, Artemis Urban, China City Cycle) and highway cycles (e.g., HWFET, US06, Artemis Motorway) to cover a range of acceleration, deceleration, and cruising scenarios.
- **Construct a Multi-Metric Performance Evaluation System:** Evaluate system performance across four dimensions: energy consumption, comfort, safety, and traffic efficiency. Metrics include energy per kilometer, peak jerk, RMS acceleration, minimum distance, and maximum distance.

- **Comprehensive Comparison and Scenario-Based Recommendations:** Evaluate system performance across four dimensions: energy consumption, comfort, safety, and traffic efficiency. Metrics include energy per kilometer, peak jerk, RMS acceleration, minimum distance, and maximum distance.

1.5 Thesis Structure

The structure of the thesis is as follows:

- **Chapter 1:** Presents the research background, defines the problem, states the motivation, outlines challenges and significance, introduces research objectives, and describes the thesis framework.
- **Chapter 2:** Reviews ACC fundamentals, mainstream control methods, and the current state of research on time gap policies.
- **Chapter 3:** Details the vehicle dynamics model, controller design, and mathematical modeling and parameterization of CTG, CSF, and HDB strategies.
- **Chapter 4:** Evaluates strategy performance under urban driving cycles, comparing energy and comfort metrics.
- **Chapter 5:** Assesses strategy adaptability and stability under highway conditions.
- **Chapter 6:** Summarizes key findings, identifies limitations, and outlines directions for future research.

Chapter 2

Theoretical Background and Related Work

2.1 Overview of Adaptive Cruise Control (ACC) Systems

2.1.1 Development Background and Functional Framework of ACC

With the rising demands for traffic safety and the rapid development of intelligent vehicle technologies, Adaptive Cruise Control (ACC) has become one of the core modules for longitudinal control and has been widely deployed in modern passenger vehicles. By integrating multi-modal sensor fusion and advanced control algorithms, ACC systems autonomously regulate the longitudinal motion of the vehicle. The core function lies in perceiving the dynamic state of the preceding vehicle (e.g., relative velocity, distance, and trajectory) and outputting desired acceleration or braking commands in real-time, thereby maintaining a safe, stable, and efficient car-following state under various traffic scenarios [6].

From a control-theoretic perspective, the essence of ACC is a closed-loop feedback system with a target time gap or desired distance as the control objective. Its design aims to dynamically balance the multi-objective conflicts among safety (e.g., minimum safe distance), comfort (e.g., acceleration smoothness), and energy efficiency (e.g., powertrain optimization) [7].

Key Definitions and Principles:

1. Target Time Gap (Time Gap): Time gap is defined as the time interval

(in seconds) maintained between the ego vehicle and the preceding vehicle. A shorter T_g (e.g., 1.0s) may increase road capacity but leads to frequent acceleration and deceleration, reducing ride comfort. Conversely, a larger T_g (e.g., 2.5s) enhances following stability but compromises traffic flow efficiency [8].

2. Perception Components and Sensor Fusion: Unlike conventional Cruise Control (CC) systems that only rely on speed sensors, ACC systems utilize a fusion of radar, LiDAR, and camera data to capture environmental information:

- **Millimeter-wave radar:** Operates in the 77GHz band to detect range and relative velocity; works in all weather conditions but with low spatial resolution.
- **LiDAR:** Emits laser pulses to generate precise 3D point clouds; offers accurate object detection but is sensitive to weather (e.g., rain, fog).
- **Cameras:** Employ computer vision algorithms to detect lane markings, preceding vehicles, and traffic signs; sensitive to illumination.

Sensor fusion methods such as Kalman filtering or deep learning enhance redundancy and reduce the likelihood of misperceptions.

3. Control Algorithms and Closed-Loop Structure: Based on perceived data, the control algorithm generates the desired acceleration command to actuate the vehicle's throttle or brake systems. Mainstream algorithms include:

- **Proportional–Integral–Derivative Control (PID):** A classic technique adjusting output via proportional, integral, and derivative terms; simple but limited in handling nonlinearities or constraints.
- **Model Predictive Control (MPC):** Uses receding-horizon optimization to derive optimal control sequences satisfying multi-objective constraints; computationally intensive.
- **Linear Quadratic Regulator (LQR):** Based on state-space modeling and minimizing a quadratic cost function; effective but heavily reliant on model accuracy.

All the above operate in a feedback loop to ensure system stability and adaptability in dynamic traffic [7][9].

Comparison with Conventional Cruise Control (CC):

Traditional CC systems only maintain a constant driver-set speed and cannot adapt to the behavior of a lead vehicle. In scenarios such as sudden deceleration or cut-ins, manual braking is required, creating safety risks. In contrast, ACC offers the following enhancements:

- **Dynamic following:** Adjusts speed in real time to maintain a preset time gap or safe distance.
- **Multi-objective optimization:** Balances safety, comfort (e.g., jerk minimization), and energy efficiency.
- **Emergency braking support:** Activates Automatic Emergency Braking (AEB) upon imminent collision risks to reduce accident probability.

2.1.2 ACC System Control Flow and Decision Hierarchy

As an advanced longitudinal driver assistance system, Adaptive Cruise Control (ACC) adopts a hierarchical architecture comprising three key functional layers: the Perception Layer, the Decision Layer, and the Execution Layer. These layers operate collaboratively to ensure the system's adaptability in dynamic traffic environments.

Perception Layer:

The perception layer functions as the data input interface of the ACC system, primarily responsible for acquiring dynamic information from both the ego vehicle and the surrounding environment. It relies on multi-sensor fusion technologies to achieve environmental perception and object recognition. Core tasks include:

1. Data Acquisition:

- **Ego vehicle state:** Obtained via the vehicle CAN bus, including speed (v_{ego}), acceleration (a_{ego}), etc.
- **Preceding vehicle state:** Detected by radar or LiDAR, including relative distance (D_{rel}), relative speed (Δv), and azimuth angle.
- **Environmental features:** Detected using cameras and deep learning algorithms to recognize lane lines, traffic signs, and obstacles; combined with radar point clouds for multi-target tracking (MTT).

2. Data Preprocessing:

- **Signal filtering:** Kalman Filter or Particle Filter is applied to denoise sensor data and estimate states.

- **Sensor fusion:** Algorithms integrate radar, camera, and vehicle dynamics data to enhance perception accuracy and redundancy.

Decision Layer:

As the control center of the ACC system, the decision layer generates optimal longitudinal motion commands based on perception inputs and predefined control targets (e.g., time gap or desired distance). Its processes include:

1. Target Specification:

- **Time gap strategy:** Based on driver-selected gap level (e.g., 1.0s, 1.5s, 2.0s), calculate the target distance $D_{des} = v_{ego} \cdot T_g$, where T_g is the selected time gap.

2. Control Algorithms:

- **Classical control:** PID controllers adjust acceleration based on the error in inter-vehicle distance.
- **Model Predictive Control (MPC):** Solves a receding-horizon optimization problem with constraints for safety, comfort, and energy efficiency.
- **Learning-based methods:** Employ reinforcement learning or deep neural networks to tune control parameters in complex traffic environments adaptively.

Execution Layer:

The execution layer translates control commands into vehicle motion through actuation components. Key elements include:

1. Powertrain Actuation:

- **Electronic throttle:** Modulates engine torque by adjusting throttle valve opening.
- **Motor controller (for EVs):** Regulates motor speed and output torque based on control input.

2. Braking Systems:

- **E-Booster:** Adjusts hydraulic brake force in response to deceleration commands.
- **Brake-by-wire systems:** Enable precise force distribution and redundancy control.

3. Feedback Monitoring:

- Real-time dynamic feedback is obtained via wheel speed sensors and Inertial Measurement Units (IMUs) to correct actuation errors.

2.1.3 Common ACC Control Algorithms and Evolution

Since its inception, ACC control strategies have progressed from classical linear control to advanced intelligent optimization control. Based on complexity and modeling principles, mainstream ACC control algorithms fall into three categories: PID control, Model Predictive Control (MPC), and intelligent control approaches.

Proportional–Integral–Derivative (PID) Control

As one of the most widely used traditional controllers, PID regulates system output based on the error between the desired and actual values through proportional (P), integral (I), and derivative (D) terms. The control law is given by:

$$u(t) = K_p \cdot e(t) + K_i \cdot \int_0^t e(\tau)d\tau + K_d \cdot \frac{d}{dt}e(t) \tag{2.1}$$

In ACC systems, PID typically adjusts the error between the desired and actual following distance. Advantages include simplicity, intuitive parameter tuning, and low computational cost, making it suitable for constant-speed or gradually changing scenarios. However, due to its low dependence on system models, PID struggles with abrupt changes or predictive control requirements and may suffer from overshooting or lagging behaviors [10].

Model Predictive Control (MPC)

MPC is an advanced control technique that uses dynamic models to predict future system behavior and solve an optimal control sequence over a finite horizon, executing only the first control input at each time step.

- **Advantages of MPC:**
  - Handles system constraints (e.g., maximum acceleration, minimum gap)
  - Supports multi-objective optimization (e.g., energy, comfort, responsiveness)
  - Exhibits strong foresight and adaptability in complex scenarios

Due to its high computational load and dependency on accurate models, MPC is currently more common in research or premium applications, with real-time

implementation challenges in mass-production vehicles [11].

Intelligent Control Methods

With the advancement of artificial intelligence, intelligent control techniques such as fuzzy logic, neural networks, and reinforcement learning are increasingly being applied to ACC systems. These approaches emphasize data-driven modeling and behavioral learning, providing adaptability and generalization in uncertain or nonlinear environments.

- **Reinforcement learning:** Continuously optimizes control policies through environmental interaction, enabling adaptive behavior in diverse traffic scenarios.
- **Fuzzy control:** Encodes human driving experience into rule-based systems, suitable for high-uncertainty or nonlinear cases [12].

Despite their promising theoretical potential, intelligent methods currently face challenges such as a lack of interpretability, high reliance on training data, and weak transferability. Hence, PID and MPC remain dominant in practical implementations, with intelligent control serving as a complementary or exploratory direction [13].

2.2 Principles and Classification of Time Gap policies

2.2.1 Definition and Control Significance of Time Gap

In Adaptive Cruise Control (ACC) systems, the time gap is a key control variable that governs longitudinal car-following behavior. Its definition and optimization directly influence the system's safety, comfort, and energy efficiency. This section elaborates on the concept from two perspectives: mathematical definition and multi-objective impact.

Definition and Physical Interpretation of Time Gap

1. Mathematical Definition:

The time gap T_g is mathematically defined as:

$$T_g = \frac{D_{actual}}{v_{ego}} \tag{2.2}$$

where D_{actual} represents the exact distance (m) between the ego vehicle and the preceding vehicle, and v_{ego} is the current speed of the ego vehicle (m/s). The unit of T_g is seconds, and it intuitively reflects the time required for the ego vehicle to reach the preceding vehicle's current position at its present speed.

2. Physical Significance:

Physically, the time gap can be interpreted as the time it would take for the ego vehicle to collide with the lead vehicle if the latter suddenly stopped and no additional braking were applied. For instance, when $T_g = 2.0\,\mathrm{s}$, the ego vehicle must come to a complete stop within two seconds to avoid collision.

This parameter not only quantifies the longitudinal safety margin but also implicitly reflects the conservativeness of the control strategy:

- **Low T_g (e.g., 1.0 s):** Indicates an aggressive policy that prioritizes shorter gaps to improve traffic flow capacity.
- **High T_g (e.g., 3.0 s):** Reflects a conservative policy that favors increased buffer time to reduce the risk of collisions.

Multi-Objective Impact Mechanism of Time Gap

The selection of time gap values in ACC systems entails a dynamic trade-off among safety, comfort, and energy efficiency. The impacts are detailed as follows:

1. Safety Dimension:

- **Short Time Gap ($T_g < 1.5\,\mathrm{s}$)**
  - **Advantage:** Shorter inter-vehicle spacing can increase traffic throughput, particularly in congested urban scenarios.
  - **Risk:** Inadequate braking buffer increases collision risk in case of sudden deceleration by the lead vehicle. The safety condition must satisfy:

$$D_{actual} \geq v_{ego} \cdot T_g + \frac{v_{ego}^2}{2a_{max}} \tag{2.3}$$

    where a_{max} is the maximum deceleration capability of the ego vehicle.
- **Long Time Gap ($T_g > 2.5\,\mathrm{s}$)**
  - **Advantage:** Provides ample safety margin and significantly reduces the likelihood of rear-end collisions.

  - **Disadvantage:** Excessive gap increases the chance of being cut in by other vehicles, thereby elevating control complexity and triggering additional braking events.

2. Comfort Dimension:

- **Short Time Gap ($T_g < 1.5\,\mathrm{s}$)**

  Frequent acceleration and deceleration increase the rate of change of acceleration (jerk), causing discomfort for passengers.

  - **Typical scenario:** In urban stop-and-go traffic, excessively short gaps often lead to the "nodding effect" where passengers experience abrupt forward/backward movements.

- **Long Time Gap ($T_g > 2.5\,\mathrm{s}$)**

  Smooth acceleration profiles result in better ride comfort. However, excessively large gaps may undermine the driver's perceived confidence in the system due to the impression of sluggish system response.

3. Energy Efficiency Dimension:

- **Short Time Gap ($T_g < 1.5\,\mathrm{s}$)**

  Frequent throttle-brake switching elevates energy consumption, including higher fuel usage for ICE vehicles and greater electricity consumption in EVs.

  - Research indicates that for every 0.5-second reduction in T_g, urban energy consumption may increase by approximately 8%–12% under typical driving conditions.

- **Long Time Gap ($T_g > 2.5\,\mathrm{s}$)**

  Increases the proportion of steady cruising, reduces drivetrain load, and improves powertrain efficiency. However, excessive gaps may result in inefficient coasting when trailing a slower vehicle unnecessarily.

2.2.2 Constant Time Gap (CTG) Policy

The Constant Time Gap (CTG) policy is one of the most widely adopted time gap control methods in Adaptive Cruise Control (ACC) systems, particularly dominant in mass-produced passenger vehicles. This strategy maintains a constant time interval T_{gap}, dynamically adjusting the expected inter-vehicular distance between the ego and preceding vehicles. The primary goal is to ensure baseline safety while simplifying control logic:

$$D_{des} = T_{gap} \cdot V_{ego} + D_{min} \tag{2.4}$$

Where:

- D_{des}: Desired following distance
- T_{gap}: Constant time gap
- V_{ego}: Ego vehicle speed
- D_{min}: Minimum static safety distance, typically set to 2–5 meters

Due to its simplicity, clarity, and ease of engineering implementation, the CTG strategy is favored in industry. The control logic of CTG can be easily embedded into traditional PID or LQR control frameworks, and it has proven effective in preventing rear-end collisions under low- to mid-speed conditions [14].

Control Logic Modeling

In simulation modeling, the CTG strategy operates by setting a constant T_{gap} and updating the desired spacing D_{des} in real-time based on the ego vehicle's speed V_{ego}. The controller calculates the control error as the difference between the actual spacing D_{act} and the desired spacing:

$$e(t) = D_{act}(t) - D_{des}(t) \tag{2.5}$$

This error is input into the controller (e.g., PID or MPC) to compute the required acceleration command, which is then executed via actuators (throttle/brake system) to regulate the ego vehicle's speed, achieving desired longitudinal motion.

Parameter Tuning and Vehicle Behavior Analysis

The key parameter in the CTG strategy is the value of T_{gap}, which influences both steady-state and transient responses of the system, as well as ride comfort and energy efficiency.

- **Smaller T_{gap} (e.g., 1.0 s):**

  Provides quicker response and higher road utilization, but leads to more frequent braking and acceleration, thereby degrading comfort and increasing energy consumption-especially in low-speed stop-and-go traffic.

- **Larger T_{gap} (e.g., 2.5 s):**

  Improves system stability and mitigates hard braking events, beneficial for energy saving and comfort. However, it may reduce lane capacity and result in excessive spacing in high-speed scenarios.

To enhance user-friendliness, many commercial ACC systems offer selectable discrete time gap modes, such as:

Mode	Time gap
Near	1.0 s
Medium	1.5 s
Far	2.0–2.5 s

However, these settings are often empirical and lack adaptability to changing traffic conditions, road topology, or driver intentions [15].

Advantages and Limitations

- **Advantages:**
  - **Simplicity:**
    Linear model and control logic integrate easily with classical controllers such as PID, reducing development cost.
  - **Real-time efficiency:**
    Low computational overhead; suitable for embedded automotive ECUs.
  - **Baseline safety guarantee:**
    The inclusion of D_{min} provides static redundancy, reducing risk in extreme scenarios.
- **Limitations:**
  - **Low environmental adaptability:**
    A fixed T_{gap} cannot handle dynamic situations such as cut-ins or road gradient changes.
  - **Multi-objective trade-off:**
    Cannot simultaneously optimize safety, comfort, and efficiency (e.g., short gap improves efficiency but worsens comfort).
  - **Manual dependence:**
    Time gap selection often requires user input, increasing cognitive load and risk of inappropriate selection (e.g., short gap in high-speed conditions).

Engineering Applications

Numerous automakers have implemented the CTG policy in production ACC systems. For instance, drivers are often allowed to choose from three fixed time gap levels. Alternatively, time gap values can be automatically linked to driving modes (e.g., Eco, Normal, Sport), with each mode corresponding to a different T_{gap} setting to match powertrain responsiveness and fuel economy strategies.

2.2.3 Constant Safety Factor (CSF) Policy

The Constant Safety Factor (CSF) policy is a time gap strategy that emphasizes physical constraints derived from braking dynamics and safety redundancy. Its primary objective is to ensure collision avoidance capability in emergency braking scenarios by explicitly modeling vehicle dynamics parameters such as maximum deceleration and system latency.

Compared to empirically-based CTG strategies, CSF introduces a rigorous formulation using safety coefficients, enhancing the physical interpretability and theoretical soundness of control logic, making it particularly suitable for high-demand safety applications such as commercial vehicles and autonomous driving systems.

Control Logic Modeling

According to kinematic theory, the stopping distance of the ego vehicle under emergency braking is expressed as:

$$D_{stop} = \frac{v_{ego}^2}{2a_{dmax}} \tag{2.6}$$

Where:

- v_{ego}: Ego vehicle speed
- a_{dmax}: Maximum deceleration

To ensure safety, the desired spacing D_{des} must satisfy:

$$D_{des} \geq D_{stop} + D_{min} \tag{2.7}$$

To further enhance redundancy, a safety factor K ($K \in [1.0, 2.0]$) is introduced:

$$D_{des} \geq D_{min} + K \cdot D_{stop} \tag{2.8}$$

In addition, the total system response delay σ is considered, representing the end-to-end latency across perception, decision, and actuation stages (e.g., radar signal processing time, control computation delay, brake actuation lag). The final expression for the desired distance becomes:

$$D_{des} = D_{min} + \sigma \cdot v_{ego} + K \cdot D_{stop} \tag{2.9}$$

Where:

- D_{des}: desired distance

- D_{min}: Minimum static safety distance
- σ: Total system response time
- v_{ego}: Ego vehicle speed
- K: Safety factor

This model has been validated in multiple studies for its effectiveness in emergency braking, especially when latency and deceleration limits are explicitly accounted for [16].

Parameter Sensitivity Analysis

- **System Response Time σ:**
  - **Low values (e.g., 0.5 s):**
    The system reacts rapidly but may underestimate lead vehicle behavior, leading to frequent acceleration modulation and peak jerk values exceeding $\pm 2\ m/s^3$, which compromises comfort.
  - **High values (e.g., 1.5 s):**
    Enables anticipatory buffering and smoother acceleration profiles, enhancing comfort and stability. However, increased spacing may lower traffic throughput.
- **Safety Factor K:**
  - **Lower values (e.g., 1.0):**
    Reduces braking redundancy, suitable for high-adhesion road surfaces.
  - **Higher values (e.g., 1.5):**
    Improves braking safety under low-adhesion conditions (e.g., rain or snow) but may result in excessively long following distances.

Advantages and Limitations

- **Advantages**
  - **Safety-prioritized design:**
    Explicitly models braking dynamics and system delay to ensure collision avoidance in emergencies.
  - **Physical consistency:**
    Parameters such as a_{max} and σ are directly linked to vehicle dynamics, avoiding subjective empirical settings.

- **Limitations**
  - **Model dependency:**
    Strong reliance on accurate estimation of a_{max}; environmental variability can lead to modeling errors and insufficient safety margins.
  - **Computational cost:**
    Includes nonlinear terms (e.g., speed squared), imposing higher processing demands on automotive ECUs, especially at high speeds.

Engineering Applications

The CSF strategy shows strong potential in commercial vehicles, trucks, and heavy-duty high-speed applications, where braking safety is paramount. The CSF-based control logic can significantly reduce collision risks. Some studies integrate CSF with driver intent recognition systems: in conservative modes, higher K values are applied; in aggressive modes, they are lowered to match personalized preferences.

Additionally, CSF can be embedded as a dynamic weighting term within advanced control architectures such as MPC, enabling adaptive time gap adjustment and improving overall system intelligence and robustness [17].

2.2.4 Human Driving Behavior (HDB) Policy

The Human Driving Behavior (HDB) policy is an empirically driven time gap control method derived from naturalistic driving data. Its core objective is to enhance the human-likeness and scenario adaptability of Adaptive Cruise Control (ACC) systems by modeling actual driver car-following behavior. Compared to the physics-based Constant Time Gap (CTG) and Constant Safety Factor (CSF) strategies, HDB captures the driver's regulation of following distance under varying speeds through statistical modeling, striking a balance between behavioral interpretability and engineering feasibility. This makes it a current hotspot in human–machine cooperative driving research.

Control Logic Modeling

The classical HDB model was proposed by Fancher et al. based on naturalistic driving data collected from 107 drivers[17]. The desired distance D_{des} is modeled as:

$$D_{des} = D_{min} + T_{gap} \cdot v_{ego} + G \cdot v_{ego}^2 \tag{2.10}$$

Where:

- D_{des}: Desired following distance
- D_{min}: Minimum standstill distance, typically 2–5 meters
- T_{gap}: Time gap
- v_{ego}: Ego vehicle speed
- G: Quadratic speed coefficient, accounting for increased safety margin at high speeds due to nonlinear risks (e.g., sudden deceleration of lead vehicle)

Through regression analysis, Fancher et al. further identified a negative correlation between T_{gap} and G [18]:

$$G = -0.0246 \cdot T_{gap} + 0.010819 \tag{2.11}$$

This implies that drivers tend to decrease the weight of the quadratic term as T_{gap} increases to balance safety and following efficiency. This finding reveals the underlying logic of the "risk–efficiency" trade-off in human driving behavior.

Advantages and Limitations

- **Advantages**
  - **Human-like consistency:** Derived from real-world driving behavior data, the model reflects natural driver logic and response patterns.
  - **Dynamic adaptability:** The model includes both first- and second-order speed terms to dynamically adjust following distance based on vehicle speed.
  - **Structural simplicity:** The model has a compact parameter structure and is easy to integrate into existing control frameworks, suitable for real-time embedded applications.
- **Limitations**
  - **Behavior dependency:** Model parameters are based on statistical averages of a driver population; universality may be limited under varying individual behaviors or environmental scenarios.
  - **Limited responsiveness:** The speed-squared term may be slow to respond in extreme relative velocity changes, necessitating auxiliary detection modules (e.g., abrupt braking detection).

Applications and Future Directions

As a behavior-driven time gap strategy, HDB provides high human-likeness and explainability, making it suitable for systems prioritizing naturalistic following and smooth longitudinal control. Without requiring complex environment modeling, it dynamically adjusts target distance using vehicle speed and acceleration profiles, offering generality and modeling efficiency.

In practice, HDB is structurally compatible with classical controllers such as PID or MPC, and can also be embedded as a behavioral module within higher-level predictive or reinforcement learning-based control architectures to improve human-like decision-making capability.

2.3 Evaluation Metrics for Time Gap Policies

As a critical component linking decision-making algorithms to vehicle dynamics in ACC systems, the design of time gap policies directly influences vehicle stability, passenger comfort, energy efficiency, and traffic safety. To enable systematic and comparable evaluation of different strategies, this section proposes a multi-dimensional, quantifiable, and extensible metric framework grounded in the ISO 26262 functional safety standard [19] and classical traffic flow theory.

Four main categories of metrics are defined in this study:

- Energy Efficiency
- Comfort
- Safety
- Traffic Flow Efficiency

2.3.1 Energy Efficiency

Energy consumption is a critical dimension in evaluating a time gap strategy's impact on energy optimization. The Energy Consumption Reduction Ratio (ECRR) is introduced to quantify energy savings relative to a reference condition (e.g., manual driving):

$$ECRR = \frac{E_{ref} - E_{ACC}}{E_{ref}} \times 100\% \tag{2.12}$$

Where:

- E_{ACC} : Energy consumption per kilometer under ACC strategy

- E_{ref} : Baseline energy consumption per kilometer (e.g., manual driving)

A positive ECRR indicates energy-saving benefits; a negative value implies excessive acceleration or braking, increasing consumption. ECRR is normalized and thus facilitates cross-scenario and cross-vehicle comparisons.

2.3.2 Comfort

Comfort reflects the smoothness of longitudinal motion and human acceptability. This study adopts the Acceleration Reduction Ratio (ARR) to evaluate how well a time gap strategy reduces acceleration fluctuations:

$$ARR = \frac{a_{rms,rel} - a_{rms,ACC}}{a_{rms,rel}} \times 100\% \tag{2.13}$$

Where:

- $a_{rms,ACC}$: Root mean square (RMS) value of longitudinal acceleration under adaptive cruise control (ACC) strategy
- $a_{rms,rel}$: Root mean square (RMS) value of longitudinal acceleration under reference driving

A higher ARR means better suppression of acceleration variance and greater ride comfort. ARR and ECRR are complementary and form the basis for multi-objective trade-off analysis.

2.3.3 Safety

Safety remains the top priority in ACC control. This study evaluates safety from three aspects:

1. Minimum Distance (D_{min})

- **Definition**: Smallest actual distance between ego and lead vehicle during simulation
- **Risk thresholds:**
  - $D_{min} < 2.0\,\text{m}$: Critical warning
  - $D_{min} < 1.0\,\text{m}$: Potential collision (per SAE J3016[1])

2. Time-to-Collision (TTC)

$$TTC = \frac{D_{rel}}{|\Delta V|} \tag{2.14}$$

- D_{rel}: Relative distance
- ΔV: Relative speed
- **Risk levels:**
  - $TTC < 3.0\,\text{s}$: High risk
  - $TTC < 1.5\,\text{s}$: Very high risk, triggers AEB

3. Braking Intervention Frequency (BIF)

- **Definition**: Frequency of maximum deceleration events per unit time
- **Interpretation**: High BIF indicates low adaptability to emergencies

This study does not include extreme lead vehicle braking scenarios. TTC is used here for dynamic interaction analysis rather than collision avoidance verification.

2.3.4 Traffic Flow Efficiency

Although ACC primarily addresses individual vehicle control, time gap strategies influence overall traffic performance.

Metrics include:

- **Average Speed**: Higher average speed indicates more efficient strategies
- **Vehicle Density**: Larger time gaps reduce lane capacity
- **Following Delay**: Time needed to reestablish desired spacing after lead vehicle acceleration

In this study, traffic flow indicators are supplemental but critical for collaborative scenarios (e.g., CACC, V2X systems).

2.4 Review of Existing Research

2.4.1 Research Progress

Since the 1990s, when Adaptive Cruise Control (ACC) systems were first applied in production vehicles, countries such as the United States, Germany, and Japan have continuously led technological and theoretical advancements in this field. Research related to time gap policy optimization has primarily focused on three directions:

Constant Time Gap (CTG) Strategy

CTG is one of the earliest and most widely adopted time gap control methods. Its theoretical modeling and engineering validation are relatively mature. Treiber et al., in their work *Traffic Flow Dynamics*, explored the impact of time gap settings on platoon stability and traffic throughput, highlighting that shorter time gaps may enhance capacity but also promote disturbance propagation and the formation of "stop-and-go" waves, thus reducing overall stability.

Rajamani et al., in *Vehicle Dynamics and Control* [3], analyzed CTG-based car-following performance from a control theory perspective, demonstrating its practical value in ensuring stable car-following under low- and medium-speed conditions. More recently, some studies have attempted to incorporate nonlinear correction factors or adaptive gains into CTG to improve flexibility. However, as CTG is fundamentally a static parameter model, its adaptability to dynamic and complex scenarios remains limited.

Constant Safety Factor (CSF) Strategy

CSF was initially applied in commercial and heavy-duty vehicle systems, such as truck platooning and railcar tracking. Research in this area focuses on modeling the coupling between braking capacity and safe spacing. In a study published in *IEEE Transactions on Intelligent Vehicles*, Nilsson et al. [20] proposed a CSF-based yielding control strategy that incorporates maximum deceleration and safety margins into gap estimation. Their approach significantly improved safety during congested conditions.

In addition, some studies under Model Predictive Control (MPC) frameworks have embedded CSF constraints into optimization problems to ensure safe braking while minimizing energy consumption. This demonstrates CSF's strength in balancing safety and energy efficiency.

Human Driving Behavior (HDB) Strategy

HDB has gained traction as a cutting-edge research topic, especially with the growing emphasis on human-like behavior in autonomous systems. Several research institutions have used naturalistic driving datasets to build behavior models that capture human gap adjustment logic.

For example, the SHRP 2 Naturalistic Driving Study, jointly supported by SAE and NHTSA, has provided extensive U.S. driving behavior data, enabling the development of data-driven HDB models [21]. Based on this dataset, researchers have proposed personalized time gap models using regression trees and clustering analysis to enable adaptation to diverse driving styles and road conditions [22].

2.4.2 Summary and Research Gaps

Despite the extensive progress made in ACC time gap policy research, several systematic and practical issues remain unresolved:

- **Lack of a unified testing platform:**

  Most studies employ different modeling tools, controllers, and evaluation metrics, making cross-study comparisons difficult and hindering the establishment of a standardized assessment framework.

- **Insufficient cross-policy comparisons:**

  The majority of research focuses on optimizing individual strategies without systematic horizontal comparisons based on common vehicle and control models, limiting holistic understanding.

- **Limited scenario adaptability analysis:**

  Current studies lack conclusive results on which strategy performs best under different driving conditions (e.g., urban vs. highway), which restricts deployment effectiveness.

- **Missing multi-objective trade-off frameworks:**

  There is no unified optimization methodology that balances safety, comfort, energy consumption, and throughput in an integrated manner.

Therefore, it is necessary to construct multiple time gap strategy models under a unified simulation platform and conduct multi-indicator, multi-scenario, and multi-model comparisons to assess the applicability and limitations of each policy. This forms one of the core objectives of this study.

2.5 Chapter Summary

This chapter provided a systematic review of time gap strategies within Adaptive Cruise Control systems, including theoretical foundations, mainstream control models, performance evaluation frameworks, and current research progress. It establishes a solid foundation for the modeling and simulations to be discussed in Chapter 3.

First, the control architecture of ACC systems was introduced, outlining their three-layered structure (perception–decision–execution) and the central role of speed–gap coupling. Common controllers such as PID, MPC, and learning-based algorithms were reviewed. It was emphasized that the performance of these

controllers is constrained by the rationality and flexibility of the underlying time gap policy.

Second, three representative time gap strategies were analyzed:

- **CTG**: Prioritizes engineering simplicity and low computational cost, effective in low-speed steady-state conditions, but lacks adaptability in dynamic traffic.
- **CSF**: Tightly links gap setting to vehicle braking capacity, enhancing physical safety, especially at high speeds, but requires accurate system modeling and environment perception.
- **HDB**: Focuses on imitating actual driver behavior, providing high human–machine consistency and adaptability, suitable for future user-friendly ACC systems, though it suffers from data dependency and uncertainty.

Third, a comprehensive multi-metric performance evaluation framework was proposed, covering four dimensions: energy efficiency, comfort, safety, and traffic flow. This framework provides a standardized basis for comparing strategy performance.

Lastly, the research review highlighted four main gaps: lack of a unified simulation platform, insufficient cross-policy comparison, inadequate scenario adaptability analysis, and the absence of multi-objective optimization tools. This underscores the need for systematic and quantitative comparisons of the three strategies under standardized simulation environments and typical driving conditions (urban and highway), with the aim of offering practical recommendations.

This chapter thus provides the theoretical basis and research motivation for Chapter 3, which will describe the vehicle modeling approach, controller design, and implementation of the three-time gap strategies on the simulation platform, which lays the groundwork for the performance evaluations and comparative experiments that follow.

Chapter 3

Control System Modeling and Strategy Design

3.1 Longitudinal Vehicle Modeling

3.1.1 Modeling Objectives and Framework

This study develops a forward vehicle model tailored for electric vehicles (Battery Electric Vehicles, BEV) on the MATLAB / Simulink Simscape platform, aiming to evaluate the performance of Adaptive Cruise Control (ACC) systems. The model treats the vehicle as a mass-point system and couples multiple key physical effects, including aerodynamic drag, rolling resistance, gradient resistance, tractive force, and vehicle mass. It is designed to accurately predict vehicle speed response and energy consumption behavior under predefined control inputs.

This modeling approach is widely adopted in the development of Energy Management Strategies (EMS) and Advanced Driver Assistance Systems (ADAS). It can be used directly to assess how different time-gap policies influence longitudinal dynamic performance under real-world driving conditions.

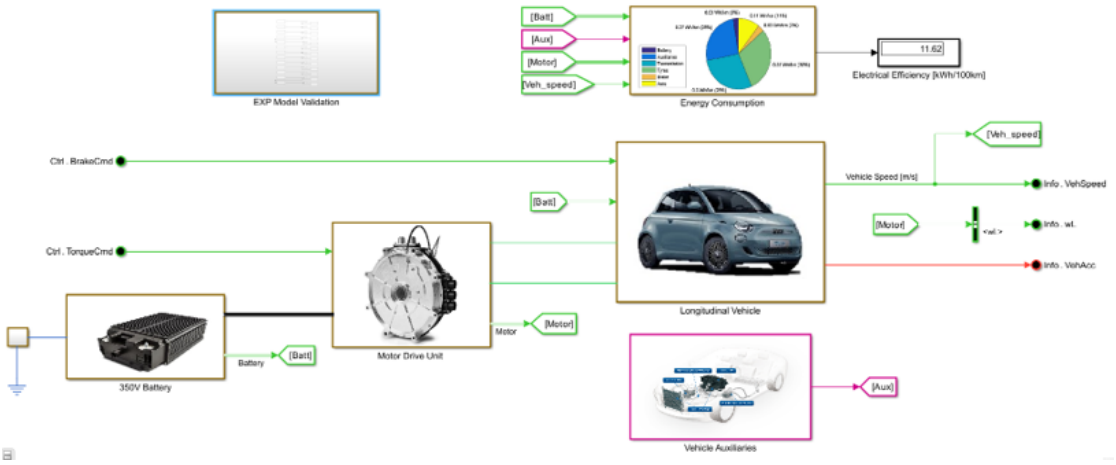

Figure 3.1: High-fidelity vehicle model developed in MATLAB/Simulink Simscape environment

3.1.2 Longitudinal Vehicle Dynamics

In the dynamic approach, the vehicle motion results from the net effect of all the forces and torques acting on a point mass, represented by the vehicle's center of gravity (CoG). The equilibrium of forces is implemented in the Simscape environment by the block called Vehicle Body of the Driveline Blockset. The graphical representation of the block and the body diagram of the equilibrium of forces are presented in Figure 3.2.

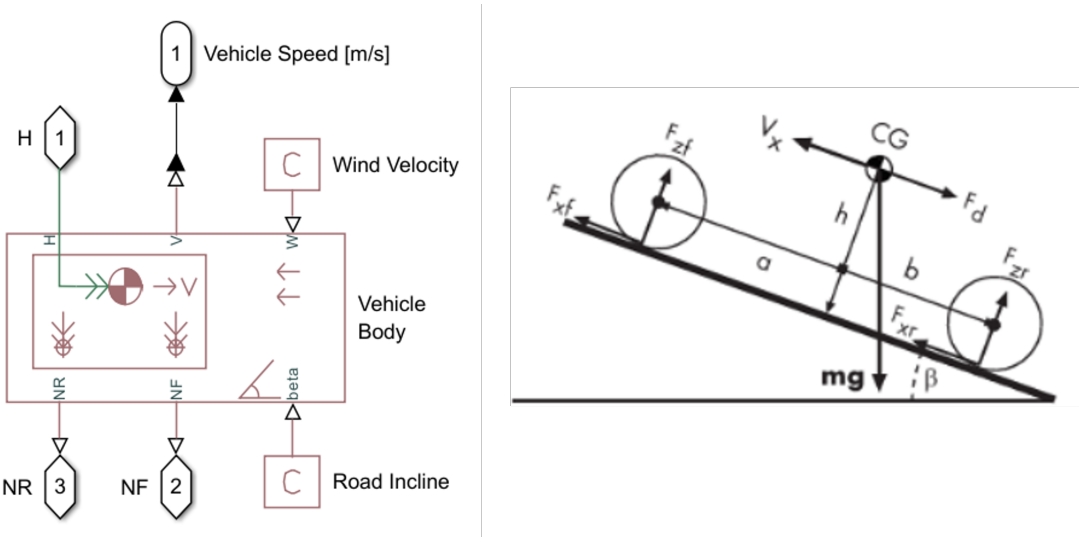

Figure 3.2: Diagram of the vehicle's longitudinal dynamics with forces acting on a point mass on an inclined plane

The fundamental equation of motion along the longitudinal axis of the vehicle is:

$$m_{app}\dot{V}_x = F_x - F_d - mg\sin\beta \tag{3.1}$$

where m_{app} is the apparent mass of the vehicle, which accounts for the inertia of rotating components such as wheels, brake discs, driveshafts, and other drivetrain elements. These components require additional torque to accelerate and therefore contribute to an effective increase in the vehicle's resistance to acceleration.

The apparent mass is computed as:

$$m_{app} = m\lambda = m(1 + k_r) \tag{3.2}$$

where m is the actual mass of the vehicle, and k_r (sometimes defined also as λ) is a dimensionless coefficient that quantifies the contribution of rotating inertias.

The remaining terms in equation (3.1) are defined as follows: V_x is the longitudinal velocity, F_x is the total traction force, F_d is the aerodynamic drag force, and β is the road slope angle, which is typically set to zero.

The traction force is distributed across the two axles:

$$F_x = n(F_{xf} + F_{xr}) \tag{3.3}$$

The aerodynamic drag is modeled as:

$$F_d = \frac{1}{2}C_d\rho A_f(V_x + V_w)^2 \cdot \text{sgn}(V_x + V_w) \tag{3.4}$$

where C_d is the drag coefficient, $\rho = 1.25\ kg/m^3$ the air density in nominal conditions, A_f the frontal area, and V_w the wind speed (always in our analysis $V_w = 0$).

The zero normal acceleration and the zero pitch torque are used to determine the normal force on each front and rear wheel. The dynamic vertical load distribution is computed respectively as:

$$F_{zf} = \frac{-h(F_d + mg\sin\beta + m\dot{V}_x) + b\ mg\cos\beta}{n(a+b)} \tag{3.5}$$

$$F_{zr} = \frac{h(F_d + mg\sin\beta + m\dot{V}_x) + a\ mg\cos\beta}{n(a+b)} \tag{3.6}$$

Finally, the wheel normal forces satisfy $F_{zf} + F_{zr} = mg\frac{\cos\beta}{n}$.

The vehicle parameters used to populate the longitudinal dynamics model of the BEV are reported in Table 3.1.

Table 3.1: Main parameters of the modeled BEV

Parameter	Value	Unit
Vehicle mass m	1443	kg
Apparent mass coefficient λ	1.006	–
Wheelbase l	2.332	m
Distance CoG to front axle a	$0.45\,l$	m
Distance CoG to rear axle b	$0.55\,l$	m
CoG height h	0.3	m
Frontal area A_f	2.15	m^2
Air density ρ	1.25	kg/m^3
Wheel radius r_w	0.3	m
Drag coefficient C_d	0.304	–

3.1.3 Tire Dynamics

The tires' longitudinal behavior is modeled using a simplified formulation derived from the Magic Formula originally developed by Pacejka (2002) [23], focusing only on the peak longitudinal force and the corresponding slip value. This approach allows for an efficient representation of the tire-road interaction in longitudinal dynamics without involving the full complexity of nonlinear tire behavior. The simplified model is implementable among the possibilities offered by the Tire (Magic Formula) block of the Driveline Blockset [24]. The model block is shown in Figure 3.3.

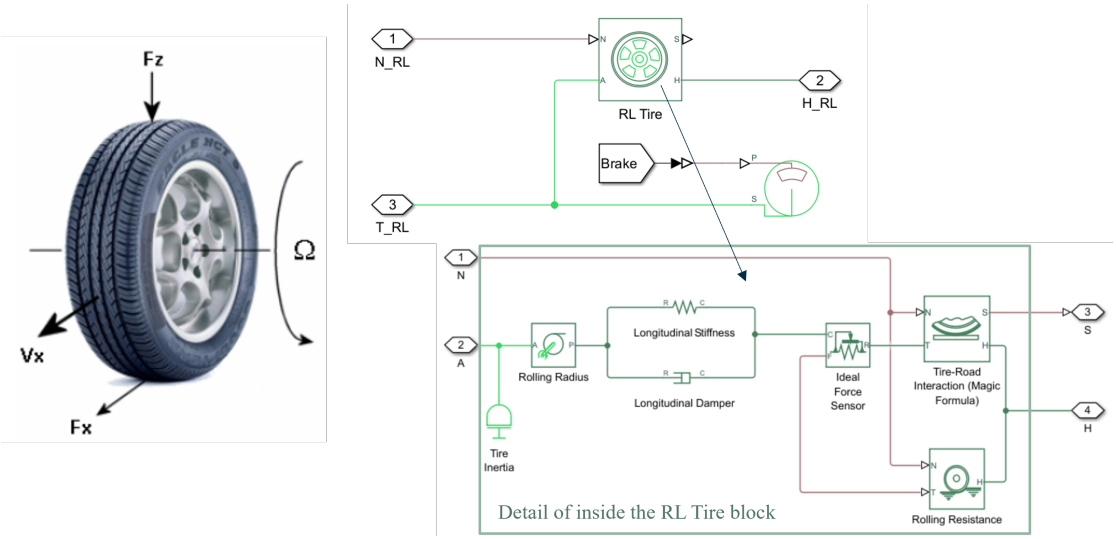

Figure 3.3: Tire dynamics model implemented in Simscape. Tire-road interaction is handled through the peak longitudinal force using a Magic Formula-based approach.

The following assumptions are adopted in this tire model:

- **No inertia**: Tire rotational inertia is neglected.
- **No compliance**: No structural compliance is considered in the tire.
- **Constant radius**: The effective rolling radius is assumed constant.
- **Constant coefficients**: Rolling resistance and Magic Formula parameters are constant and calibrated for nominal load conditions.

The longitudinal slip k and the tire's tangential velocity V_T are defined respectively as follows:

This simplified tire model is suitable for forward simulations involving straight-line acceleration or deceleration, where lateral effects and load sensitivity can be neglected, as in the case of the driving cycles considered in our analysis. The tire model is used as a power converter to pass from the translational mechanics domain to the rotational mechanics domain in Simscape.

The longitudinal force F_x generated at the tire-road interface is converted into a torque T_{wheel} applied at the wheel axle. This transformation is achieved through a translational-to-rotational converter, modeled in Simscape as a mechanical transformer. The torque at the wheel T_{wheel} is calculated as:

$$T_{wheel} = r_w F_x \tag{3.7}$$

where r_w is the effective rolling radius of the wheel. This torque is the wheel's rotational dynamics input, influencing angular acceleration and velocity.

3.1.4 Powertrain and Driveline

The electric driveline subsystem models a simplified powertrain from the DC bus to the wheel axles using Simscape Driveline Blockset components. The architecture consists of the following elements: a Motor & Drive (System Level) block connected in rotational mechanics series to a reduction gear and a differential, both taken from the standard blocks of the Gears library inside the Driveline Blockset. The resulting electric machine and driveline model is shown in Figure 3.4.

The Motor & Drive (System Level) block allows for the implementation of a closed-loop torque-controlled permanent magnet synchronous machine (PMSM). It accepts torque requests in Nm via the input port, which arrive directly from the driver or ADAS controller modules. On the electrical side, the motor is interfaced with the battery system modelled with Simscape Electrical, thus implementing a domain transformation between DC electrical power and mechanical rotational power. On the mechanical side, the torque and speed sensors are placed to monitor the respective values and obtain closed-loop control.

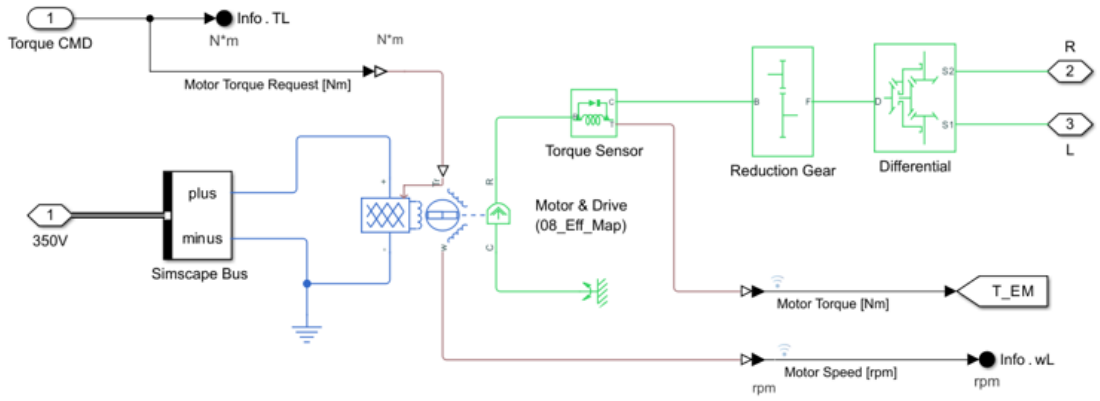

Figure 3.4: Electric machine and driveline components implemented in simulation environment.

The EM is modeled using an efficiency map and its main mechanical parameters; the rotor inertia is the primary dynamic component included in the model, as electrical dynamics (e.g., current transients) are orders of magnitude faster than inertial or mechanical responses. The relationship between mechanical shaft torque and electrical power is governed by an efficiency map. The map is derived experimentally as a function of rotational speed ω_{em} and torque T_{em}. The electrical power P_{elec} required at the battery is derived from mechanical power P_{mech} using the efficiency map as follows:

$$P_{\text{elec}} = \begin{cases} \frac{1}{\eta_{\text{em}}(\omega_{\text{em}}, T_{\text{em}})}\ \omega_{\text{em}} T_{\text{em}}, & P_{\text{elec}} \geq 0 \ \ \text{(traction)}, \\ \eta_{\text{em}}(\omega_{\text{em}}, T_{\text{em}})\ \omega_{\text{em}} T_{\text{em}}, & P_{\text{elec}} < 0 \ \ \text{(regeneration)}. \end{cases} \tag{3.8}$$

3.1.5 High-Voltage Battery

The battery is modeled with its equivalent circuit model with no dynamics. The equivalent circuit is built as a controlled voltage source with a series resistor, representing the open-circuit voltage (OCV) and internal resistance of the entire pack, respectively. This simplified model leverages standard components of the Simscape Electrical library combined to recreate the same setup proposed in the example of the HV Battery Charge/Discharge. Although being a simplified approach for battery systems modelling, the approach is one of the most effective available in the literature to implement the battery model when limited knowledge of the battery is available.

This formulation enables efficient computation of current for given power demands in system-level simulations. The computation of the battery current is the last part of the causality chain, which causes the consumption of energy to

generate the vehicle motion (i.e., the power at the wheels and the vehicle speed). To complete the energetic evaluation of the vehicle in the simulation environment, the battery power P_{batt} is integrated in time to derive the corresponding energy consumption at the battery E_{batt} and the power consumption of the auxiliaries P_{aux} is added to evaluate the total power consumption at the battery.

The following equations describe the energy consumption and the efficiency metrics used to describe the results of the simulation data:

- **Auxiliary Energy** $[kWh]$: $E_{\text{aux}} = \frac{1}{3600} \int_0^T P_{\text{aux}}(t)\, dt$
- **Total Battery Energy** $[kWh]$: $E_{\text{batt}} = \frac{1}{3600} \int_0^T [P_{\text{batt}}(t) + P_{\text{aux}}(t)]\, dt$
- **Distance Traveled** $[km]$: $d_{km} = \frac{1}{3600} \int_o^T v_{veh}(t)\, dt$
- **Tank-to-Wheel Efficiency** $[kWh/100km]$: $TtW = (E_{\text{batt}}/d_{km}) \cdot 100$

where the total time T is a function of the driving mission performed during the test.

3.2 Controller Design

3.2.1 Controller architecture and operation logic

The primary objective of an Adaptive Cruise Control (ACC) system is to maintain dynamic and safe following behavior under varying traffic conditions. To achieve this, the controller is designed using a hierarchical decoupled architecture, which consists of three main components: the upper-layer time gap policy module, the mid-layer closed-loop controller, and the lower-layer vehicle dynamics model. Among these, the closed-loop controller serves as the core of the intermediate layer. It is responsible for converting the deviation between the desired and actual inter-vehicular distance into executable longitudinal acceleration commands in real time.

From a modeling perspective, this study adopts a modular and interface-standardized design philosophy. The upper-layer strategy computes only the target distance and does not participate directly in error compensation or physical constraint handling. The controller independently processes the error signals, applies gain weighting and saturation logic, and outputs acceleration commands based on the current dynamic state of the vehicle. The bottom-layer vehicle model reflects the full physical dynamics, including the powertrain response, tire–road interaction, braking, and energy consumption, ensuring that the final acceleration/torque commands are physically executable.

The overall signal flow and control logic can be broken down into the following steps:

- **Real-Time Signal Acquisition:** The system continuously acquires key dynamic variables, including the ego vehicle speed (v_{ego}), lead vehicle speed (v_{lead}), actual inter-vehicle distance (D_{act}), and relative velocity (v_{rel}), either through onboard sensors or simulation data sources. The data refresh interval is determined by the sampling period (T_s, e.g., 0.2 s), which is selected to balance response speed and overall system stability.

- **Desired Distance Generation:** The upper-layer strategy module (CTG, CSF, or HDB) calculates and outputs the target following distance $D_{\text{des}}(t)$ for each control cycle, according to real-time operating conditions and strategy-specific parameters. Each policy enables dynamic adjustment based on the ego vehicle's instantaneous speed, acceleration, and other state variables, thereby ensuring both safety and adaptability.

- **Error Calculation and Gain Weighting:** The primary control error $e(t)$ is computed as the difference between the desired and actual inter-vehicle distances. To further enhance system stability, the controller incorporates additional error terms such as speed error (the difference between the set speed and the ego vehicle speed) and relative velocity, each weighted by specific gain coefficients.

- **Closed-Loop PID Regulation:** The controller employs a PID algorithm to calculate the target acceleration $a_{\text{des}}(t)$ based on the error signals. The gain values and functional roles of each PID component are optimized through scenario simulations and sensitivity analyses to ensure rapid error correction and overall system stability.

- **Physical Constraints and Saturation Protection:** All acceleration outputs are subjected to physical saturation limits, typically constrained within $[-4, +4]$ m/s^2, to prevent unrealistic or unachievable commands. This ensures that the system operates within the physical capabilities of real vehicles.

- **Acceleration Mapping and Torque Execution:** The desired acceleration is converted into the corresponding driving or braking torque and applied to the lower-layer Simulink vehicle dynamics model, which governs the physical vehicle response. Additional modules account for actuator delay, inertia, and other real-world implementation factors to improve simulation fidelity.

This structure forms a tightly coupled feedback loop, supporting high-fidelity simulation and real-time adjustment under various policies and driving conditions.

3.2.2 Control Performance Objectives

The controller is required to meet multiple performance objectives to ensure safe, smooth, and efficient operation under varying traffic scenarios. The specific goals include:

- **Stability**
  The system must maintain good stability in the presence of typical traffic disturbances (e.g., sudden deceleration of the lead vehicle). It should exhibit no sustained oscillation or divergence to ensure safe car-following behavior.
- **Responsiveness**
  The controller should rapidly track the target distance, correcting errors within a short time frame with minimal delay or lag.
- **Comfort**
  The output acceleration and jerk (rate of change of acceleration) must remain smooth. For passenger comfort, it is recommended that the root mean square (RMS) acceleration does not exceed 1.5 m/s^2, and jerk remains below 2.0 m/s^3.
- **Generality**
  A unified set of control parameters should apply to all time gap strategies and typical driving scenarios without the need for frequent retuning, thereby improving simulation efficiency and model portability.

3.3 Time Gap Policy Modeling

Time gap control policies are at the core of longitudinal decision-making in Adaptive Cruise Control (ACC) systems. Their primary function is to dynamically determine the target following distance between the ego and lead vehicles based on driving scenarios and vehicle operating states. A well-designed time gap strategy can significantly reduce the risk of rear-end collisions, enhance platoon stability, and improve traffic throughput. It serves as a foundation for achieving multi-objective optimization involving safety, comfort, and energy efficiency. Currently, mainstream time gap strategies include the Constant Time Gap (CTG) strategy, the Constant Safety Factor (CSF) strategy, and the Human Driving Behavior (HDB) strategy. These approaches differ in their underlying modeling principles and parameter definitions.

3.3.1 Constant Time Gap Policy (CTG)

The mathematical form of the CTG Policy is expressed as:

$$D_{des} = T_{gap} \cdot V_{ego} + D_{min} \tag{3.9}$$

Where:

- D_{des}: Desired following distance.
- T_{gap}: Constant time gap. In this study, values of 1.5 s, 2 s, 2.5 s, 3 s, 4 s, and 5 s are selected as test groups to evaluate the performance under different strategies.
- V_{ego}: Ego vehicle speed.
- D_{min}: Minimum static safety distance. In this study, it is fixed at 2 meters.

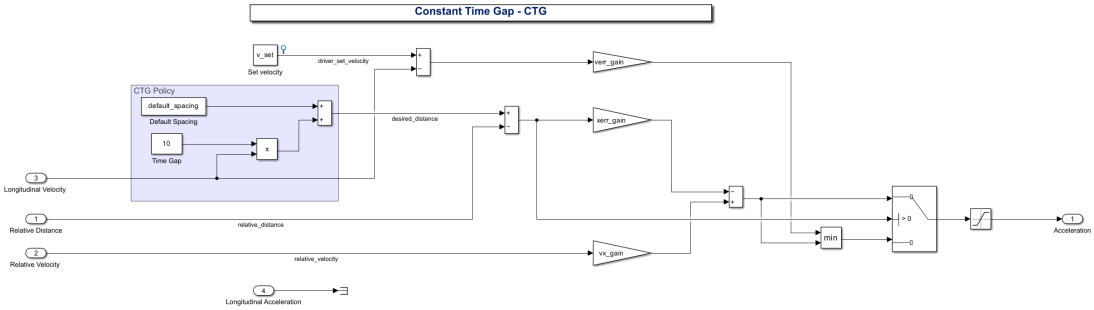

Figure 3.5: Modeling Structure of the Constant Time Gap Policy

The CTG Policy features a simple model structure, intuitive parameters, and ease of engineering implementation. Owing to its linear characteristics, it offers good adaptability to changes in traffic conditions and can operate stably in typical urban or highway scenarios where traffic density is high and speed variations are limited.

3.3.2 Constant Safety Factor Policy (CSF)

The CSF Policy extends CTG by incorporating physical braking constraints and system response delays. The desired distance is computed as:

$$D_{des} = D_{min} + \sigma \cdot v_{ego} + K \cdot \frac{v_{ego}^2}{2a_{dmax}} \tag{3.10}$$

Where:

- D_{des}: desired distance.

- D_{min}: Minimum static safety distance. In this study, it is fixed at 2 meters.
- σ: Total system response time. In this study, it is fixed at 1.5 seconds.
- v_{ego}: Ego vehicle speed.
- a_{dmax}: Maximum deceleration. In this study, it is fixed at 4 meters per second squared.
- K: Safety factor. In this study, values of 1.25, 1.5, 1.75, and 2 are selected as test groups to evaluate the performance under different strategies.

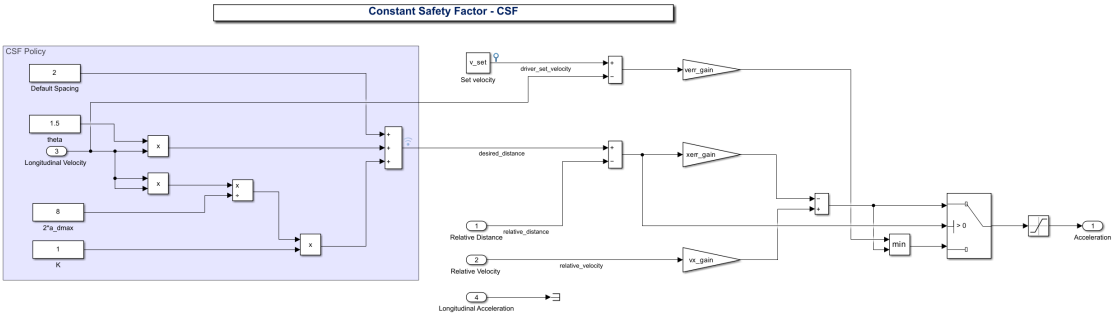

Figure 3.6: Modeling Structure of the Constant Safety Factor Policy

The CSF Policy ensures physical feasibility and accounts for response delay and emergency braking ability. It is particularly suitable for high-speed and emergency braking conditions, providing greater safety margins. However, conservative values for σ and a_{max} may lead to overly large following distances, reducing road capacity and energy efficiency.

3.3.3 Human Driving Behavior Policy (HDB)

The HDB Policy is built from large-scale naturalistic driving datasets using regression modeling. It reflects how real drivers choose longitudinal spacing across different speed ranges. A common formulation is a second-order polynomial:

$$D_{des} = D_{min} + T_{gap} \cdot v_{ego} + G \cdot v_{ego}^2 \tag{3.11}$$

Where:

- D_{des}: Desired following distance.
- D_{min}: Minimum static safety distance. In this study, it is fixed at 2 meters.

- T_{gap}: Constant time gap. In this study, values of 1.5 s, 2 s, 2.5 s, 3 s, 4 s, and 5 s are selected as test groups to evaluate the performance under different strategies.
- v_{ego}: Ego vehicle speed.
- G: Quadratic speed coefficient, accounting for increased safety margin at high speeds due to nonlinear risks (e.g., sudden deceleration of lead vehicle).

Through regression analysis, Fancher et al. further identified a negative correlation between T_{gap} and G [18]:

$$G = -0.0246 \cdot T_{gap} + 0.010819 \tag{3.12}$$

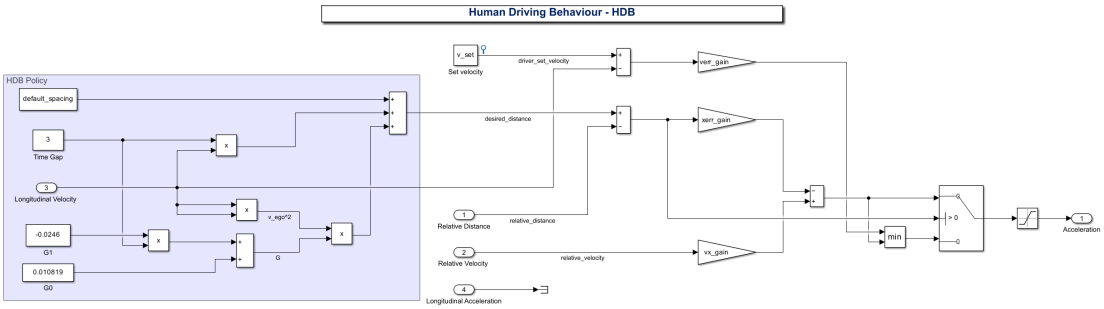

Figure 3.7: Modeling Structure of the Human Driving Behavior Policy

The HDB Policy captures nonlinear behavioral adjustments at various speeds and reflects comfort preferences and actual traffic flow behavior in mixed traffic. It is widely used in academic studies and advanced autonomous driving research to simulate human-like behaviors and evaluate ACC performance in hybrid human–machine environments.

3.3.4 Main Features of the Simulation Platform

The simulation platform developed in this study supports modular switching between different time gap policies, including CTG, CSF, and HDB. Users can conveniently select a desired Policy and adjust key parameters such as static distance and time gap values to match specific research objectives or driving scenarios.

The platform also enables fair and consistent performance comparisons. All policies operate under identical vehicle models, controller configurations, and scenario settings, ensuring that any observed differences in outcome can be attributed to the policies themselves. This design safeguards scientific rigor and comparability.

Furthermore, the platform accommodates a wide range of driving environments, including both urban and highway conditions, and provides multi-dimensional performance evaluation. Metrics span energy efficiency (e.g., energy consumption per 100 kilometers), comfort (e.g., RMS acceleration and jerk), and safety (e.g., minimum spacing and collision risk indicators). This comprehensive evaluation framework lays a robust foundation for policy selection and multi-objective optimization.

3.4 Chapter Summary

This chapter developed the key components of the Adaptive Cruise Control (ACC) system, including a high-fidelity longitudinal vehicle dynamics model, controller design, and modeling of three representative time-gap policies: Constant Time Gap (CTG), Constant Safety Factor (CSF), and Human Driving Behavior (HDB). By adopting a modular and hierarchical design framework, the ACC system was divided into an upper-layer policy module, a mid-layer controller, and a lower-layer dynamics response model. These layers function independently while maintaining tight integration, ensuring flexibility, scalability, and engineering feasibility of the overall system.

In terms of controller design, closed-loop PID-based logic was used. The controller receives error signals derived from the deviation between the desired and actual inter-vehicle distance, relative velocity, and set speed error, and outputs a target acceleration command, which is subsequently mapped into torque to drive vehicle response.

Regarding time gap policies, this study implemented a switchable modeling framework for three representative approaches. The CTG policy emphasizes a simple linear formulation; the CSF policy introduces braking constraints to enhance safety under extreme conditions; and the HDB policy is constructed using empirical driving data to replicate human-like behavior. All three policies were integrated into the simulation platform through standardized interfaces, ensuring fair comparison under identical control logic and driving conditions.

Additionally, this chapter established a policy selection and simulation scheduling mechanism, allowing users to flexibly switch between policies and parameter configurations. The platform supports various road scenarios, including urban and highway environments, and provides multi-dimensional performance metrics such as energy consumption, ride comfort, and safety. This facilitates comprehensive evaluation and informed decision-making regarding policy effectiveness.

In summary, Chapter 3 not only laid the technical foundation for ACC system modeling and policy implementation but also provided a unified and high-fidelity simulation framework to support the subsequent performance analysis. The next

chapter will leverage the models developed herein to conduct systematic comparisons of time gap policies under urban driving cycles.

Chapter 4

Performance Analysis of Time Gap Policies in Urban Driving Scenarios

4.1 Overview of Urban Driving Scenarios

Urban road traffic scenarios are characterized by high dynamism and uncertainty. Unlike highway scenarios where vehicles typically engage in stable cruising, urban traffic involves low-speed operation, frequent interference, and short-distance car-following. In actual operation, vehicle motion is often influenced by traffic lights, pedestrian crossings, and intersection congestion, resulting in significant speed fluctuations and frequent stop-and-go behavior. Moreover, urban driving is often subject to high traffic density and complex interactions, requiring Adaptive Cruise Control (ACC) systems to possess both real-time perception capabilities and highly responsive control performance.

In the performance evaluation of ACC systems, the use of representative driving cycles is an essential approach to assess the effectiveness of control policies. To accurately replicate the longitudinal dynamics typical of urban driving and conduct fair comparative tests across different time gap policies (CTG, CSF, HDB), this study adopts three internationally recognized urban driving cycles: the WLTP Class 3 Driving Cycle, the Artemis Urban Driving Cycle, and the China Light-Duty Vehicle Test Cycle for Passenger Car. These cycles represent various regional traffic patterns, urban densities, and driving behaviors, offering strong representativeness, wide applicability, and excellent generalization across testing conditions.

To ensure consistency and interoperability between different cycles on the simulation platform, a modular driving input framework was developed in Simulink.

The Driver Scenario Source module is used to load the reference speed profile of each cycle and transfer it to the Car-Following Scenario module, which in turn generates dynamic signals representing the behavior of the lead vehicle. All policy simulations are executed under a unified controller structure, identical vehicle dynamics model, and consistent sampling interval, thereby ensuring scientific validity and comparability of the performance results.

4.1.1 Description of the WLTP Class 3 Driving Cycle

The Worldwide Harmonized Light Vehicles Test Procedure (WLTP) [25], issued by the United Nations Economic Commission for Europe (UNECE), aims to enhance the consistency and representativeness of global vehicle energy consumption and emissions testing. Within the WLTP framework, the Class 3 Driving Cycle is designed to simulate medium-density urban traffic conditions and has been widely adopted in European and international standard evaluation procedures.

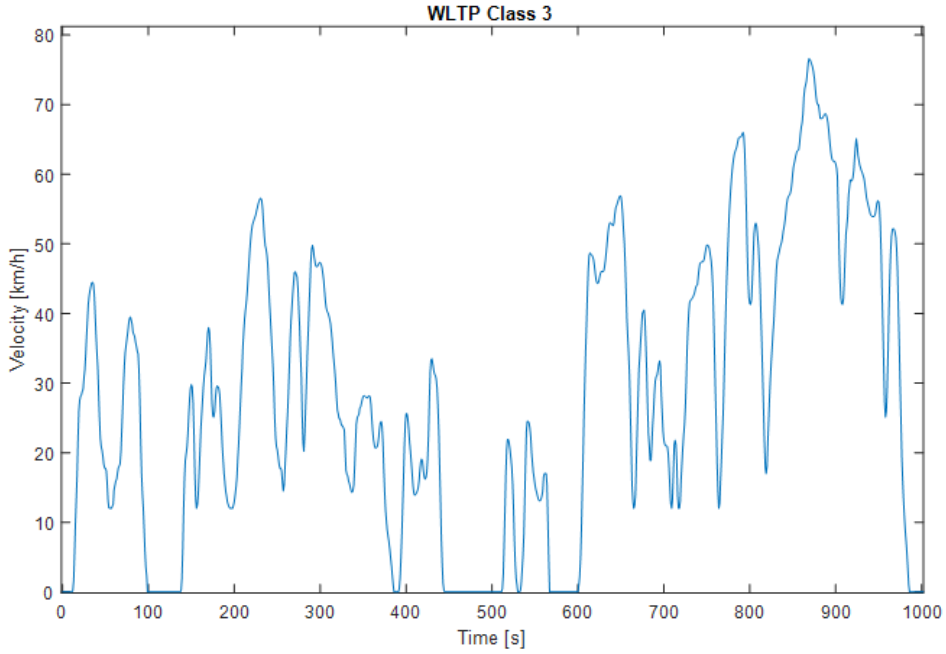

Figure 4.1: Speed–Time Curve of WLTP Class 3 Driving Cycle

As shown in the speed–time curve in Figure 4.1, the WLTP Class 3 Driving Cycle has a total duration of approximately 1000 seconds, with a peak speed close to 75 km/h and an average speed of around 34.2 km/h. The speed profile contains numerous acceleration and deceleration segments within the moderate speed range

of 20–50 km/h, interspersed with brief stopping and idling periods, effectively replicating typical traffic patterns on urban arterials or during off-peak hours.

The primary control challenges of this cycle are twofold. First, although the amplitude of speed fluctuations is moderate, the fluctuation duration is relatively long, requiring ACC policies to balance steady-state tracking with real-time adaptability. Second, the medium-frequency disturbances in the cycle place higher demands on the system's filtering capability and parameter tuning, necessitating a control policy that can achieve both fast responsiveness and smooth output to prevent oscillatory behavior or unnecessary energy loss.

4.1.2 Description of the Artemis Urban Driving Cycle

The Artemis Urban Driving Cycle was developed by the European ARTEMIS project team based on statistically derived real-world urban traffic data [26]. This cycle emphasizes alignment with actual driving behaviors and is considered more representative of real-world dynamics, particularly in terms of acceleration/deceleration patterns, traffic signal responses, and congestion characteristics.

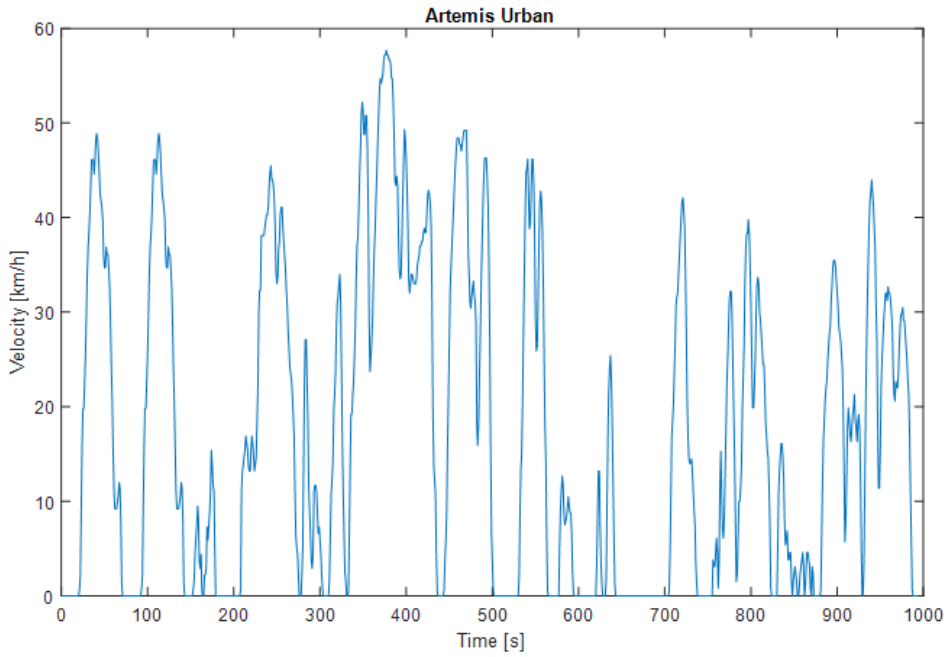

Figure 4.2: Speed–Time Curve of Artemis Urban Driving Cycle

As illustrated in the speed–time curve in Figure 4.2, the Artemis Urban Driving Cycle exhibits high-frequency fluctuation characteristics, with a peak speed of

approximately 58 km/h and frequent speed drops to 0 km/h. The average speed is only 18.9 km/h, making it a typical "stop-and-go–dominated" urban driving cycle. The profile clearly shows a segmented pattern, where every 100–200 seconds a full sequence of "start–accelerate–decelerate–stop" is repeated. This structure effectively simulates the driving rhythm in dense urban regions, such as city centers and commercial districts.

From a control perspective, the Artemis Urban Driving Cycle poses significant challenges to the dynamic responsiveness of ACC systems. The high-frequency disturbances require the controller to execute rapid acceleration adjustments while maintaining system stability and ride comfort. Overly aggressive responses may result in unnecessary acceleration and braking, leading to increased energy consumption and mechanical stress. Furthermore, due to the unpredictable behavior of the lead vehicle, improper configuration of time gap policies can result in deviations in the desired following distance, potentially causing delayed braking or unintended acceleration events.

4.1.3 Description of the China Light-Duty Vehicle Test Cycle for Passenger Car

The China Light-Duty Vehicle Test Cycle for Passenger Car was developed by the Ministry of Transport of China based on on-road measurements collected in key metropolitan areas such as Beijing, Shanghai, and Guangzhou. Designed to reflect the current realities of urban traffic in China, this cycle incorporates distinct localization characteristics and has been adopted in several national standards (e.g., GB 18352) as well as new energy vehicle assessment frameworks, making it highly representative and policy-relevant [27].

As shown in the speed–time profile in Figure 4.3, the total duration of the cycle is approximately 1250 seconds, with a peak speed of 63 km/h and an average speed of about 27.3 km/h. The trajectory exhibits a strongly nonlinear rhythm, alternating between intense acceleration phases and prolonged low-speed car-following segments. Notably, during the 400–800 second interval, the vehicle speed fluctuates sharply between 0 and 30 km/h, simulating typical traffic congestion conditions observed during morning and evening peak hours on Beijing's Second to Third Ring Roads.

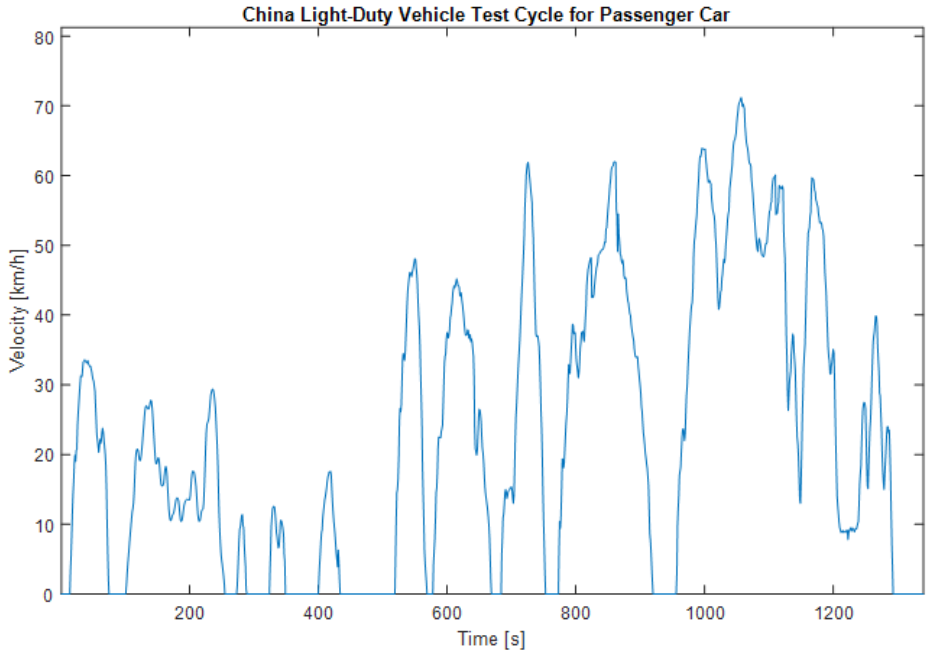

Figure 4.3: Speed–Time Curve of China Light-Duty Vehicle Test Cycle for Passenger Car

From a control standpoint, this cycle emphasizes the system's ability to maintain low-speed car-following stability and tolerate micro-level disturbances. Due to generally smaller inter-vehicle gaps in Chinese urban traffic, the behavior of the lead vehicle significantly affects the ego vehicle's control response. Time gap policies under this scenario must not only ensure safe spacing but also demonstrate robustness in handling complex and heterogeneous driving styles. In particular, adopting conservative policies (e.g., large time gaps) may lead to a decrease in traffic throughput on high-density roads, while overly aggressive policies, if not precisely controlled, may increase the risk of rear-end collisions.

4.2 Performance Comparison of Time Gap Policies under Different Urban Driving Cycles

To comprehensively evaluate the adaptability and performance of different time gap policies under representative urban traffic scenarios, this section conducts a systematic comparative analysis of the Constant Time Gap (CTG), Constant Safety Factor (CSF), and Human Driving Behavior (HDB) policies using the developed simulation platform. During testing, a baseline scenario—defined as the case without ACC control or time gap policy—is used as the reference condition. In this configuration,

the vehicle operates solely based on the prescribed driving cycle velocity profile, without any prediction of preceding vehicle behavior or adaptive buffer regulation. The resulting performance in terms of energy consumption, longitudinal dynamics, and jerk serves as a benchmark for evaluating the effectiveness of various policies. For each policy, multiple configurations of key control parameters are defined. The following metrics are recorded and compared across these configurations: target following distance, energy consumption level, longitudinal dynamic responsiveness (maximum and minimum acceleration), and ride comfort indicators (maximum and minimum jerk). All simulations are executed using a unified vehicle model and controller configuration, with the baseline scenario providing the reference for cross-policy comparison. This ensures consistency and scientific rigor in the evaluation process.

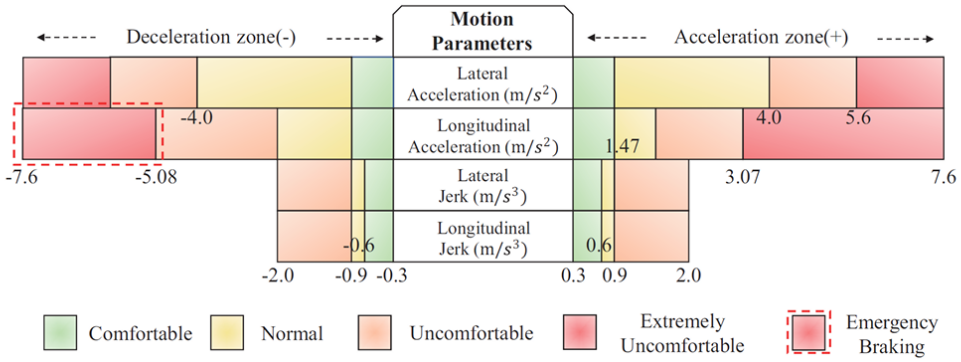

Figure 4.4: Typical comfort limits for longitudinal and lateral acceleration and jerk

To enhance the engineering relevance and comfort-oriented applicability of the conclusions, this study introduces a comfort evaluation threshold. As illustrated in Figure 4.4 [28], the physically acceptable range for longitudinal jerk is set at ± 2.0 m/s^3. Any parameter configurations exceeding this threshold, such as the jerk values observed under CTG and HDB policies when $T_{gap} = 1.5$ s, are considered either excessively aggressive or insufficiently stable. These behaviors may negatively affect the passenger experience. Therefore, such cases are excluded from the subsequent performance comparison to maintain the practical validity and scientific rigor of the analysis.

4.2.1 Performance of Time Gap Policies under the WLTP Class 3 Driving Cycle

Under the WLTP Level 3 driving cycle, a series of system simulations were performed based on the Simulink platform to evaluate the performance of each strategy under

different parameter settings. The simulation results are shown in Table 4.1, which provides the maximum target distance, maximum relative distance, battery energy consumption, extreme longitudinal acceleration (maximum and minimum values), and jerk value (maximum and minimum values) for the benchmark scenario and the constant time gap (CTG), human driving behavior (HDB), and constant safety factor (CSF) strategies. All performance indicators are evaluated based on the benchmark conditions to ensure consistency and fairness in horizontal comparisons.

Table 4.1: WLTP Class 3 Driving cycle

Baseline vehicle on WLTP Class 3			**0.648**	**1.643**	**-1.660**	**2.789**	**-2.808**
CTG $T_{\mathbf{gap}}$ [s]	$d_{\mathbf{des,max}}$ [m]	$d_{\mathbf{rel,max}}$ [m]	E [kWh]	$a_{\mathbf{max}}$ [m/s^2]	$a_{\mathbf{min}}$ [m/s^2]	$j_{\mathbf{max}}$ [m/s^3]	$j_{\mathbf{min}}$ [m/s^3]
1.5	34	34	0.634	2.094	-1.469	3.000	-2.053
2.0	44	44	0.617	1.342	-1.380	0.720	-0.602
2.5	55	54	0.605	1.263	-1.295	0.659	-0.563
3.0	65	65	0.594	1.193	-1.216	0.616	-0.528
4.0	86	85	0.576	1.073	-1.106	0.552	-0.487
5.0	107	104	0.561	1.006	-1.026	0.521	-0.456
HDB $T_{\mathbf{gap}}$ [s]	$d_{\mathbf{des,max}}$ [m]	$d_{\mathbf{rel,max}}$ [m]	E [kWh]	$a_{\mathbf{max}}$ [m/s^2]	$a_{\mathbf{min}}$ [m/s^2]	$j_{\mathbf{max}}$ [m/s^3]	$j_{\mathbf{min}}$ [m/s^3]
1.5	22	27	0.655	2.115	-1.834	2.994	-2.569
2.0	27	28	0.641	1.443	-1.458	0.807	-0.654
2.5	32	33	0.633	1.373	-1.401	0.763	-0.646
3.0	37	38	0.625	1.307	-1.351	0.723	-0.638
4.0	47	48	0.612	1.259	-1.268	0.666	-0.623
5.0	58	58	0.601	1.200	-1.217	0.622	-0.610
CSF $K_{\mathbf{safe}}$ [s]	$d_{\mathbf{des,max}}$ [m]	$d_{\mathbf{rel,max}}$ [m]	E [kWh]	$a_{\mathbf{max}}$ [m/s^2]	$a_{\mathbf{min}}$ [m/s^2]	$j_{\mathbf{max}}$ [m/s^3]	$j_{\mathbf{min}}$ [m/s^3]
1.25	102	95	0.569	1.161	-1.122	1.201	-0.537
1.50	116	106	0.561	1.125	-1.059	0.903	-0.520
1.75	130	117	0.554	1.092	-0.999	0.836	-0.509
2.00	144	127	0.547	1.061	-0.943	0.848	-0.498

This section will conduct a comprehensive analysis of the behavioral characteristics, energy-saving potential, and ride comfort of each strategy based on the numerical results shown in Table 4.1.

Baseline performance analysis

The simulation data shows that under the benchmark conditions, the total energy consumption reaches 0.648 kWh. The maximum acceleration is 1.643 m/s^2, and the minimum acceleration drops to -1.660 m/s^2. The maximum acceleration rate of change reached 2.789 m/s^3 and the minimum acceleration rate of change reached -2.808 m/s^3, both significantly exceeding the acceptable comfort threshold. These values indicate that the vehicle's longitudinal response has significant dynamic fluctuations. This pattern reflects that in the absence of a time gap management mechanism, the vehicle exhibits discontinuous acceleration and braking responses when subjected to external disturbances. This instability not only leads to reduced energy efficiency but also has a negative impact on ride comfort.

These findings highlight the importance of implementing a time gap strategy to improve control smoothness, reduce the acceleration rate of change, and improve

energy efficiency. They also provide a quantitative reference benchmark for evaluating the relative advantages and optimization potential of subsequent strategy configurations.

Performance of the CTG policy

The Constant Time Gap (CTG) policy computes the desired following distance using a linear function defined by a fixed time gap T_{gap} and a minimum static distance D_{min}. In this study, the time gap parameter was configured at 1.5 s, 2.0 s, 2.5 s, 3.0 s, 4.0 s, and 5.0 s.

In terms of energy consumption, simulation results indicate a clear optimization trend as the time gap increases. When $T_{\text{gap}} = 2.0$ s, the energy consumption is 0.617 kWh. At $T_{\text{gap}} = 5.0$ s, the consumption drops to 0.561 kWh, representing a reduction of approximately 13% compared to the baseline condition. This improvement is attributed to the larger buffer distance maintained during car-following, which reduces the frequency of aggressive acceleration and deceleration events and supports smoother and more stable power output.

Regarding acceleration and jerk performance, the CTG policy demonstrates relatively aggressive system responses at short time gaps (1.5 to 2.0 seconds). For example, when $T_{\text{gap}} = 1.5$ s, the maximum acceleration reaches 2.094 m/s^2, while the minimum acceleration drops to -1.469 m/s^2. This reflects the necessity for the system to execute rapid braking and acceleration to maintain the target distance under tight spacing, resulting in significant dynamic fluctuations. The corresponding jerk value reaches 3.000 m/s^3, which exceeds the acceptable comfort threshold of ± 2.0 m/s^3. Therefore, this configuration is excluded from the subsequent comparative analysis.

As the time gap increases beyond 3.0 s, the maximum jerk value decreases to 0.616 m/s^3. Compared to the baseline value of 2.789 m/s^3, this indicates a substantial improvement in ride comfort. Meanwhile, the extreme acceleration values converge toward ± 1.0 m/s^2, highlighting the balance between smooth vehicle dynamics and improved energy efficiency.

In terms of maximum relative distance, the CTG policy shows a proportional increase in both target and actual inter-vehicle distance with increasing T_{gap}. At $T_{\text{gap}} = 5.0$ s, the maximum actual relative distance reaches 104 m. This flexible and adjustable buffer is beneficial for accommodating variable traffic densities, though it may also lead to inefficient space utilization or delayed system responses in congested urban conditions.

In summary, the CTG policy demonstrates significant improvements in energy consumption and jerk performance relative to the baseline scenario. It is well-suited for low-complexity car-following applications in urban environments. However, its performance at short time gaps must be carefully managed by enforcing a lower

limit to ensure passenger comfort.

Performance of the HDB policy

The Human Driving Behavior (HDB) policy is based on behavior regression modeling using large-scale naturalistic driving datasets. It aims to capture the variation in the desired following distance as a function of vehicle speed. In this study, the time gap parameter T_{gap} is configured consistently with that of the CTG policy. The core objective of HDB is to replicate real-world following behavior by dynamically adjusting inter-vehicle spacing, thereby enhancing the coordination between ACC systems and human-driven vehicles.

In terms of energy performance, the HDB policy exhibits slightly higher energy consumption than CTG and CSF. At $T_{\text{gap}} = 5.0\,\text{s}$, the minimum energy consumption reaches 0.601 kWh, which is an improvement compared to the baseline (0.648 kWh) but remains higher than the values observed for CTG (0.561 kWh) and CSF (0.547 kWh). This is primarily attributed to the inclusion of a quadratic speed term in the regression model, which causes greater variation in the desired distance at medium to high speeds. Consequently, the system frequently adjusts acceleration commands, leading to increased energy fluctuation.

The analysis of acceleration and jerk indicates that HDB exhibits overly sensitive control responses at short time gaps. For instance, when $T_{\text{gap}} = 1.5\,\text{s}$, the maximum acceleration reaches $2.115\,\text{m/s}^2$, the maximum jerk peaks at $2.994\,\text{m/s}^3$, and the minimum jerk reaches $-2.569\,\text{m/s}^3$. All these values exceed the comfort threshold, indicating that while the controller closely mimics human-like responses, it compromises ride smoothness and system stability. Therefore, this configuration is excluded from further comparative analysis.

For configurations where $T_{\text{gap}} \geq 2.0\,\text{s}$, the jerk values decrease significantly, and control stability improves. The maximum jerk converges to the range of 0.6–$0.8\,\text{m/s}^3$, remaining within acceptable limits. The minimum acceleration gradually approaches $-1.2\,\text{m/s}^2$, reflecting a more tempered braking behavior.

Regarding maximum relative distance, HDB maintains values below 58 m, which is significantly shorter than those observed under CTG and CSF. This reflects the human tendency toward close following. While this behavior promotes lane capacity and road utilization, it may introduce elevated risks under high-frequency disturbances or in congested urban traffic scenarios.

Overall, compared to the baseline scenario, the HDB policy significantly reduces peak jerk and longitudinal acceleration, thereby improving ride comfort and energy efficiency. Additionally, its strength in behavioral realism and interactive consistency makes it particularly suitable for studies involving multi-vehicle coordination or mixed traffic control. However, its aggressive behavior under short time gap settings should be managed carefully to prevent degradation in passenger experience

or increases in energy consumption.

Performance of the CSF policy

The Constant Safety Factor (CSF) policy defines the desired inter-vehicle distance based on the vehicle's maximum braking capability and system reaction delay. The safety adjustment factor K is set to four values in this study: 1.25, 1.5, 1.75, and 2.0. Oriented toward active safety, this policy enhances the buffer margin during high-speed operations or abrupt traffic disturbances.

Energy performance is particularly outstanding. Simulation results show that the CSF policy achieves the lowest energy consumption among all tested policies. Specifically, at $K = 2.0$, energy consumption drops to 0.547 kWh, approximately 15% lower than the baseline value of 0.648 kWh. This highlights the CSF policy's potential for significant energy savings, making it well-suited for energy-efficient driving scenarios.

Acceleration and jerk remain consistently smooth. Across all configurations, the maximum acceleration remains within the range of 1.06 to 1.16 m/s^2, and the maximum jerk does not exceed 1.201 m/s^3. These results indicate excellent control of smoothness. The minimum acceleration is maintained around -1 m/s^2, ensuring moderate deceleration and minimizing passenger discomfort. Overall output fluctuations are minimal, and none of the CSF configurations exceed the safety threshold for jerk.

Maximum relative distance performance is also remarkable. When $K = 2.0$, the maximum relative distance reaches 127 m, indicating substantial safety redundancy. This characteristic is especially beneficial in multi-vehicle car-following or complex urban traffic scenarios where risk mitigation is critical.

In summary, the CSF policy outperforms the baseline and other tested policies across several key dimensions, including energy efficiency, control smoothness, and safety margins. It demonstrates the most balanced and optimal performance under the given test conditions.

4.2.2 Policy Performance under the Artemis Urban Driving Cycle

Under the Artemis Urban Driving Cycle, a systematic simulation analysis was conducted for each policy across different parameter configurations using the established simulation platform. The summarized results are presented as follows:

Table 4.2: Artemis Urban Driving cycle

Baseline vehicle on Artemis Urban			**0.438**	**3.279**	**-3.437**	**6.768**	**-6.210**
CTG $T_{\mathbf{gap}}$ [s]	$d_{\mathbf{des,max}}$ [m]	$d_{\mathbf{rel,max}}$ [m]	E [kWh]	$a_{\mathbf{max}}$ [m/s^2]	$a_{\mathbf{min}}$ [m/s^2]	$j_{\mathbf{max}}$ [m/s^3]	$j_{\mathbf{min}}$ [m/s^3]
1.5	26	30	0.395	2.093	-2.461	2.974	-1.960
2.0	34	34	0.376	1.688	-2.243	1.343	-1.291
2.5	42	41	0.363	1.522	-2.055	1.304	-1.242
3.0	50	49	0.352	1.432	-1.894	1.271	-1.199
4.0	66	64	0.333	1.304	-1.634	1.209	-1.124
5.0	82	78	0.318	1.194	-1.436	1.149	-1.056
HDB $T_{\mathbf{gap}}$ [s]	$d_{\mathbf{des,max}}$ [m]	$d_{\mathbf{rel,max}}$ [m]	E [kWh]	$a_{\mathbf{max}}$ [m/s^2]	$a_{\mathbf{min}}$ [m/s^2]	$j_{\mathbf{max}}$ [m/s^3]	$j_{\mathbf{min}}$ [m/s^3]
1.5	19	54	0.428	2.116	-3.042	2.966	-3.902
2.0	24	25	0.396	1.754	-2.443	1.346	-1.371
2.5	29	29	0.386	1.691	-2.302	1.305	-1.335
3.0	34	34	0.377	1.629	-2.177	1.272	-1.303
4.0	44	44	0.361	1.505	-1.964	1.210	-1.247
5.0	53	53	0.347	1.405	-1.790	1.150	-1.199
CSF $K_{\mathbf{safe}}$ [s]	$d_{\mathbf{des,max}}$ [m]	$d_{\mathbf{rel,max}}$ [m]	E [kWh]	$a_{\mathbf{max}}$ [m/s^2]	$a_{\mathbf{min}}$ [m/s^2]	$j_{\mathbf{max}}$ [m/s^3]	$j_{\mathbf{min}}$ [m/s^3]
1.25	66	60	0.337	1.585	-1.643	1.709	-1.153
1.50	74	67	0.330	1.523	-1.530	1.584	-1.152
1.75	82	73	0.324	1.459	-1.431	1.561	-1.149
2.00	90	78	0.319	1.395	-1.344	1.556	-1.146

Baseline performance analysis

In the baseline condition without ACC or time gap control, the battery energy consumption reached 0.438 kWh, the highest among all scenarios, indicating significant energy waste due to frequent braking and acceleration. The maximum longitudinal acceleration peaked at 3.279 m/s^2, and the minimum reached -3.437 m/s^2, suggesting a high occurrence of aggressive speed changes under urban traffic conditions. The peak jerk values were 6.768 m/s^3 and -6.210 m/s^3, both significantly exceeding the comfort threshold of ± 2.0 m/s^3. These results indicate that while the system responds rapidly without gap regulation, it leads to excessive dynamic shocks and inefficient energy use, severely compromising ride comfort.

Performance of the CTG policy

For the Artemis Urban cycle, the CTG policy was tested with time gap values of 2 s, 2.5 s, 3 s, 4 s, and 5 s (1.5 s was excluded due to jerk exceeding the ± 2.0 m/s^3 threshold). As T_{gap} increased, the maximum relative distance expanded from 34 m to 78 m.

In terms of energy efficiency, CTG demonstrated excellent performance. At $T_{\text{gap}} = 2$ s, energy consumption was 0.376 kWh, 14.2% lower than the baseline. When T_{gap} was extended to 5 s, consumption dropped to 0.318 kWh, representing a 27.4% improvement. This suggests that in the low-speed, high-frequency environment of the Artemis Urban cycle, increasing the time gap effectively reduces the burden caused by repeated braking and acceleration.

Regarding acceleration and jerk, comfort improved consistently. Maximum acceleration decreased from 1.688 m/s^2 to 1.194 m/s^2, and minimum acceleration

eased from $-2.243\,\mathrm{m/s^2}$ to $-1.436\,\mathrm{m/s^2}$. Jerk values remained within the comfort range, with maximum jerk ranging between 1.343 and $1.149\,\mathrm{m/s^3}$, and minimum jerk from -1.291 to $-1.056\,\mathrm{m/s^3}$. Overall, the CTG policy achieved a good balance between energy efficiency and comfort, making it suitable for urban environments with moderate traffic fluctuations.

Performance of the HDB policy

Under the Artemis Urban cycle, the HDB policy continued to exhibit close responsiveness to the lead vehicle, with maximum relative distance increasing from 25 m ($T_{\mathrm{gap}} = 2\,\mathrm{s}$) to 53 m ($T_{\mathrm{gap}} = 5\,\mathrm{s}$), generally lower than that of CTG for the same settings.

Energy-wise, HDB showed slightly higher values. At $T_{\mathrm{gap}} = 2\,\mathrm{s}$, energy consumption was 0.396 kWh, and it dropped to 0.347 kWh at $T_{\mathrm{gap}} = 5\,\mathrm{s}$, representing savings of 9.6% and 20.8% compared to the baseline, respectively. Though less efficient than CTG, the HDB policy still significantly outperformed the uncontrolled scenario.

For comfort, maximum acceleration reduced from $1.754\,\mathrm{m/s^2}$ to $1.405\,\mathrm{m/s^2}$, and minimum acceleration improved from $-2.443\,\mathrm{m/s^2}$ to $-1.790\,\mathrm{m/s^2}$. While substantially better than the baseline, these figures remained slightly higher than CTG's. The maximum jerk ranged from 1.346 to $1.150\,\mathrm{m/s^3}$, and the minimum from -1.371 to $-1.199\,\mathrm{m/s^3}$, with all values staying within acceptable thresholds.

Performance of the CSF policy

The CSF policy was tested with four safety adjustment factors: $K = 1.25$, 1.5, 1.75, and 2.0. In terms of distance metrics, the maximum relative distance increased from 60 m to 78 m, demonstrating strong buffer capacity.

Energy performance was particularly outstanding. Consumption dropped from 0.337 kWh ($K = 1.25$) to 0.319 kWh ($K = 2.0$), the lowest among all policies and 27.2% lower than the baseline. This confirms CSF's ability to reduce energy fluctuations by moderating brake response.

In terms of comfort, acceleration outputs remained stable. Maximum acceleration declined from $1.585\,\mathrm{m/s^2}$ to $1.395\,\mathrm{m/s^2}$, and minimum acceleration ranged from $-1.643\,\mathrm{m/s^2}$ to $-1.344\,\mathrm{m/s^2}$. Jerk values fluctuated minimally, with all maximum jerk values below $1.71\,\mathrm{m/s^3}$ and minimum jerk ranging from -1.153 to $-1.146\,\mathrm{m/s^3}$. The system responded smoothly, without harsh transitions, offering the best ride comfort among all policies.

Summary

The Artemis Urban Driving Cycle is characterized by frequent short-distance acceleration, deceleration, and idling phases, placing high demands on both responsiveness and smoothness of the control system. Under such conditions, the CSF policy delivered the greatest performance improvements across all indicators, demonstrating superior energy savings and minimal dynamic fluctuations. CTG followed closely with a simple structure and flexible gap configuration, performing consistently well under moderate-to-high time gaps. The HDB policy, while effective in replicating human-like behavior, requires further tuning to improve its energy efficiency and stability, particularly in high-frequency braking scenarios.

4.2.3 Policy Performance under the China Light-Duty Vehicle Test Cycle for Passenger Car

Under the China Light-Duty Vehicle Test Cycle for Passenger Car (referred to as the China City driving cycle), a series of simulations were conducted using the established platform to evaluate the performance of each time gap policy across multiple parameter settings. The summarized simulation results are presented as follows:

Table 4.3: China Light-Duty Vehicle Test Cycle for Passenger Car

	Baseline vehicle on CLTC		**0.615**	**2.091**	**-2.196**	**7.767**	**-6.450**
CTG $T_{\mathbf{gap}}$ [s]	$d_{\mathbf{des,max}}$ [m]	$d_{\mathbf{rel,max}}$ [m]	E [kWh]	$a_{\mathbf{max}}$ [m/s^2]	$a_{\mathbf{min}}$ [m/s^2]	$j_{\mathbf{max}}$ [m/s^3]	$j_{\mathbf{min}}$ [m/s^3]
1.5	32	32	0.588	1.791	-1.311	2.207	-0.965
2.0	42	41	0.579	1.022	-1.247	1.277	-0.946
2.5	52	51	0.571	0.962	-1.186	1.256	-0.926
3.0	62	60	0.565	0.926	-1.129	1.233	-0.906
4.0	82	79	0.553	0.856	-1.024	1.172	-0.865
5.0	102	98	0.542	0.790	-0.940	1.106	-0.824
HDB $T_{\mathbf{gap}}$ [s]	$d_{\mathbf{des,max}}$ [m]	$d_{\mathbf{rel,max}}$ [m]	E [kWh]	$a_{\mathbf{max}}$ [m/s^2]	$a_{\mathbf{min}}$ [m/s^2]	$j_{\mathbf{max}}$ [m/s^3]	$j_{\mathbf{min}}$ [m/s^3]
1.5	22	22	0.599	1.870	-1.383	2.383	-1.045
2.0	27	27	0.593	1.046	-1.341	1.423	-1.038
2.5	32	32	0.588	1.022	-1.302	1.408	-1.030
3.0	37	37	0.584	0.993	-1.267	1.393	-1.023
4.0	47	47	0.576	0.958	-1.203	1.362	-1.009
5.0	57	57	0.569	0.917	-1.147	1.339	-0.995
CSF $K_{\mathbf{safe}}$ [s]	$d_{\mathbf{des,max}}$ [m]	$d_{\mathbf{rel,max}}$ [m]	E [kWh]	$a_{\mathbf{max}}$ [m/s^2]	$a_{\mathbf{min}}$ [m/s^2]	$j_{\mathbf{max}}$ [m/s^3]	$j_{\mathbf{min}}$ [m/s^3]
1.25	95	86	0.548	1.496	-1.156	1.827	-0.853
1.50	107	96	0.543	1.423	-1.148	1.676	-0.833
1.75	120	105	0.538	1.350	-1.129	1.501	-0.795
2.00	132	115	0.533	1.298	-1.102	1.592	-0.759

Baseline performance analysis

In terms of energy consumption, the battery usage reached 0.615 kWh, significantly higher than any configuration with policy control. This indicates that the China City cycle, characterized by frequent acceleration and deceleration, imposes

intense power fluctuation on the electric drivetrain due to repeated start-stop actions, resulting in considerable energy loss.

Regarding comfort, the vehicle exhibited aggressive longitudinal dynamics. The maximum acceleration reached $2.091\,\mathrm{m/s^2}$, and the minimum dropped to $-2.196\,\mathrm{m/s^2}$. More critically, the jerk indicators showed extreme values, with the maximum jerk reaching $7.767\,\mathrm{m/s^3}$ and the minimum $-6.450\,\mathrm{m/s^3}$. These figures far exceed the $\pm 2.0\,\mathrm{m/s^3}$ comfort threshold, implying that passengers are likely to experience strong push-pull sensations and potential system oscillations. Such extreme dynamics not only compromise ride comfort but may also accelerate mechanical wear and thermal stress on components such as motors and braking systems.

Performance of the CTG policy

In this scenario, the CTG policy was tested with T_{gap} values of 2 s, 2.5 s, 3 s, 4 s, and 5 s (1.5 s was excluded due to excessive jerk). As the time gap increased, the maximum relative distance rose from 41 m to 98 m, showing a clear linear growth trend and effective distance control capability.

In terms of energy efficiency, the CTG policy demonstrated the typical characteristic of larger gaps leading to lower consumption. At $T_{\mathrm{gap}} = 2\,\mathrm{s}$, the energy consumption was 0.579 kWh, and it dropped to 0.542 kWh at $T_{\mathrm{gap}} = 5\,\mathrm{s}$—an 11.8% reduction compared to the baseline. This result validates that appropriate following buffers can effectively mitigate energy loss caused by abrupt vehicle dynamics.

As for comfort, acceleration outputs became progressively smoother. The maximum acceleration declined from $1.022\,\mathrm{m/s^2}$ to $0.790\,\mathrm{m/s^2}$, while the minimum reached $-0.940\,\mathrm{m/s^2}$. The jerk remained well-controlled, with values decreasing from 1.277 to $1.106\,\mathrm{m/s^3}$. All jerk measurements remained well below the $\pm 2.0\,\mathrm{m/s^3}$ comfort threshold. Compared to the baseline, longitudinal jolts were significantly reduced, improving passenger experience and confirming the CTG policy's effective modulation capability.

Performance of the HDB policy

Under the China City driving cycle, the HDB policy maintained similar behavioral characteristics as observed in the WLTP scenario. It exhibited a tendency toward closer vehicle following, with the maximum relative distance increasing from 27 m to 57 m, generally lower than the CTG results under the same time gap. This tighter following pattern may offer some advantages in terms of road space utilization, especially in low-speed, high-density urban traffic.

In terms of energy consumption, the HDB policy also showed a decreasing trend as T_{gap} increased: from 0.593 kWh ($T_{\mathrm{gap}} = 2\,\mathrm{s}$) to 0.569 kWh ($T_{\mathrm{gap}} = 5\,\mathrm{s}$).

Although these values outperform the baseline, they remain higher than those of CTG (0.542 kWh), indicating that the human-like responsiveness in HDB may cause additional energy usage under high-frequency acceleration-deceleration conditions.

In comfort analysis, the maximum acceleration ranged from $1.046\,\mathrm{m/s^2}$ to $0.917\,\mathrm{m/s^2}$, and jerk values remained within acceptable thresholds. The maximum jerk dropped from 1.423 to $1.339\,\mathrm{m/s^3}$, though still slightly higher than CTG, reflecting the more responsive yet slightly less stable behavior of the HDB policy in terms of passenger comfort.

Performance of the CSF policy

The CSF policy again demonstrated excellent performance under the China City driving cycle, with simulations conducted across four safety factors ($K = 1.25$ to 2.0). The maximum relative distance increased from 86 m to 115 m, highlighting the strategy's robust safety margin in complex urban environments.

From an energy standpoint, CSF continued to yield the lowest consumption across all policies. At $K = 1.25$, the consumption was 0.548 kWh, which further decreased to 0.533 kWh at $K = 2.0$—approximately 13.3% lower than the baseline. This validates CSF's advantage in dampening energy fluctuations through steady and controlled vehicle dynamics.

In terms of comfort, acceleration remained within a stable range of 1.496 to $1.298\,\mathrm{m/s^2}$. The maximum jerk ranged from 1.827 to $1.592\,\mathrm{m/s^3}$, and the minimum jerk stayed within -0.853 to $-0.759\,\mathrm{m/s^3}$. All values were well within the comfort threshold, and the minimal variability indicates a highly stable system. Such smooth dynamics enhance passenger comfort and contribute to reduced mechanical fatigue across vehicle subsystems.

Summary

The China City driving cycle represents the high-frequency, low-speed rhythm of typical Chinese urban traffic. Among the evaluated policies, CSF once again emerged as the best overall performer due to its superior energy-saving potential and high stability. The CTG policy also showed reliable and stable behavior when the time gap exceeded 3 s, making it suitable for low-speed urban commuting. The HDB policy demonstrated enhanced behavioral realism but revealed shortcomings in energy efficiency and output smoothness under intensive traffic conditions.

4.3 Energy Consumption Comparison Analysis

In the performance evaluation of Adaptive Cruise Control (ACC) systems, energy consumption serves as a key metric for assessing energy-saving potential and vehicle efficiency. To systematically analyze the energy performance differences of various time gap policies (CTG, HDB, CSF) across typical urban traffic environments, this study introduces the Energy Consumption Reduction Ratio (ECRR) as a unified evaluation indicator, defined as:

$$ECRR = \frac{E_{ref} - E_{ACC}}{E_{ref}} \times 100\% \tag{4.1}$$

where E_{ref} denotes the baseline energy consumption under the "no ACC, no time gap policy" condition, and E_{ACC} refers to the energy consumption when a specific time gap control policy is applied. A higher ECRR indicates greater energy-saving effectiveness; conversely, a negative ECRR implies that the policy results in additional energy losses.

4.3.1 ECRR Evaluation Results

To present the energy-saving capabilities of each policy under different traffic conditions, this study computes the ECRR values for each policy combination across the three representative driving cycles: WLTP Class 3 Driving Cycle, Artemis Urban Driving Cycle, and China Light-Duty Vehicle Test Cycle for Passenger Car. The energy-saving trends vary significantly across these driving cycles:

WLTP Class 3 Driving Cycle

Table 4.4: ECRR of WLTP Class 3 Driving cycle

Baseline vehicle on WLTP Class 3		**0.648**	
CTG $T_{\mathbf{gap}}$ [s]	$d_{\mathbf{rel,max}}$ [m]	E [kWh]	$E_{\mathbf{reduction}}$ [%]
2.0	44	0.617	4.8
2.5	54	0.605	6.6
3.0	65	0.594	8.2
4.0	85	0.576	11.0
5.0	104	0.561	13.3
HDB $T_{\mathbf{gap}}$ [s]	$d_{\mathbf{rel,max}}$ [m]	E [kWh]	$E_{\mathbf{reduction}}$ [%]
2.0	28	0.641	1.1
2.5	33	0.633	2.3
3.0	38	0.625	3.5
4.0	48	0.612	5.5
5.0	58	0.601	7.2
CSF $T_{\mathbf{gap}}$ [s]	$d_{\mathbf{rel,max}}$ [m]	E [kWh]	$E_{\mathbf{reduction}}$ [%]
1.25	95	0.569	12.1
1.50	106	0.561	13.4
1.75	117	0.554	14.5
2.00	127	0.547	15.5

The energy-saving potential is relatively limited. CTG achieves a maximum ECRR of 13.3%, while CSF slightly outperforms it with 15.5%. HDB performs weakly or even negatively, suggesting inefficiency in medium-to-high-speed scenarios.

Artemis Urban Driving Cycle

Table 4.5: ECRR of Artemis Urban Driving cycle

Baseline vehicle on Artemis Urban		**0.438**	
CTG $T_{\mathbf{gap}}$ [s]	$d_{\mathbf{rel,max}}$ [m]	E [kWh]	$E_{\mathbf{reduction}}$ [%]
2.0	34	0.376	14.2
2.5	41	0.363	17.2
3.0	49	0.352	19.8
4.0	64	0.333	24.0
5.0	78	0.318	27.4
HDB $T_{\mathbf{gap}}$ [s]	$d_{\mathbf{rel,max}}$ [m]	E [kWh]	$E_{\mathbf{reduction}}$ [%]
2.0	25	0.396	9.6
2.5	29	0.386	12.0
3.0	34	0.377	14.1
4.0	44	0.361	17.7
5.0	53	0.347	20.7
CSF $T_{\mathbf{gap}}$ [s]	$d_{\mathbf{rel,max}}$ [m]	E [kWh]	$E_{\mathbf{reduction}}$ [%]
1.25	60	0.337	23.1
1.50	67	0.330	24.7
1.75	73	0.324	26.0
2.00	78	0.319	27.3

All policies show significant improvement. CTG and CSF peak at 27.4% and 27.3% ECRR, respectively, with HDB achieving 20.7%. Frequent stop-and-go conditions enhance the benefits of smoother time gap strategies.

China Light-Duty Vehicle Test Cycle for Passenger Car

Table 4.6: ECRR of China Light-Duty Vehicle Test Cycle for Passenger Car

Baseline vehicle on CLTC		**0.615**	
CTG $T_{\mathbf{gap}}$ [s]	$d_{\mathbf{rel,max}}$ [m]	E [kWh]	$E_{\mathbf{reduction}}$ [%]
2.0	41	0.579	5.9
2.5	51	0.571	7.1
3.0	60	0.565	8.2
4.0	79	0.553	10.2
5.0	98	0.542	11.9
HDB $T_{\mathbf{gap}}$ [s]	$d_{\mathbf{rel,max}}$ [m]	E [kWh]	$E_{\mathbf{reduction}}$ [%]
2.0	27	0.593	3.6
2.5	32	0.588	4.3
3.0	37	0.584	5.0
4.0	47	0.576	6.3
5.0	57	0.569	7.5
CSF $T_{\mathbf{gap}}$ [s]	$d_{\mathbf{rel,max}}$ [m]	E [kWh]	$E_{\mathbf{reduction}}$ [%]
1.25	86	0.548	10.8
1.50	96	0.543	11.7
1.75	105	0.538	12.6
2.00	115	0.533	13.3

Though not as prominent as in Artemis, CSF maintains the lead with a 13.3% maximum ECRR. CTG performs moderately, while HDB consistently lags.

These ECRR values provide a quantitative reference for evaluating energy-saving effectiveness and support further strategy screening and optimization.

4.3.2 Joint Analysis of Energy Saving and Traffic Efficiency

Although certain time gap policies achieve notable energy savings as indicated by the Energy Consumption Reduction Ratio (ECRR), a practical trade-off often exists between energy efficiency and traffic throughput in real-world traffic operations. Specifically, increasing the time gap results in greater spacing between vehicles, which reduces lane capacity and negatively impacts the throughput of urban road networks. Therefore, using ECRR as the sole evaluation metric is insufficient for guiding real-world policy deployment.

To better account for the influence of time gap policies on urban traffic efficiency, this study introduces the maximum relative distance ($d_{\mathrm{rel,max}}$) as a proxy for spatial occupancy. The distribution of all tested policies is visualized in a two-dimensional space defined by 'maximum relative distance – ECRR'.As shown in the figure below:

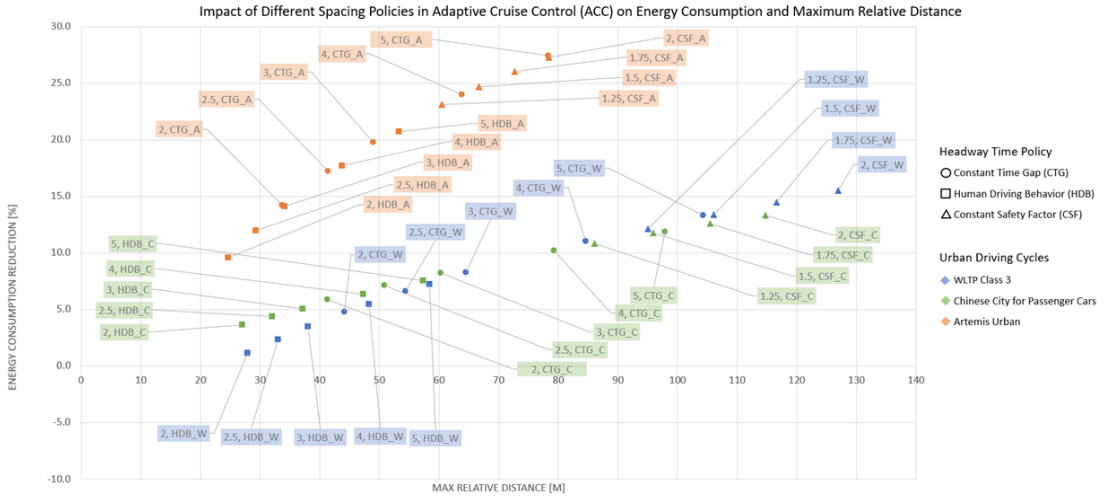

Figure 4.5: Energy Consumption and Maximum Relative Distance Across Time Gap Policies

According to engineering practice, car-following distances exceeding 70 meters significantly reduce road utilization efficiency. In contrast, minimal distances (e.g., below 40 meters) may trigger abrupt braking events, compromising both ride comfort and energy stability [4] [17]. Consequently, this study defines a desirable policy range in which the maximum relative distance falls between 40 and 70

meters. Policies within this range are considered to strike a balance between spatial efficiency and energy savings, supporting optimal traffic system performance.

Based on this evaluation framework, representative policy configurations that meet the dual criteria of high energy savings and acceptable spacing (40–70 meters) are identified. As shown in the figure below, these configurations fall within the red-bordered region, demonstrating notable energy advantages without sacrificing urban traffic throughput.

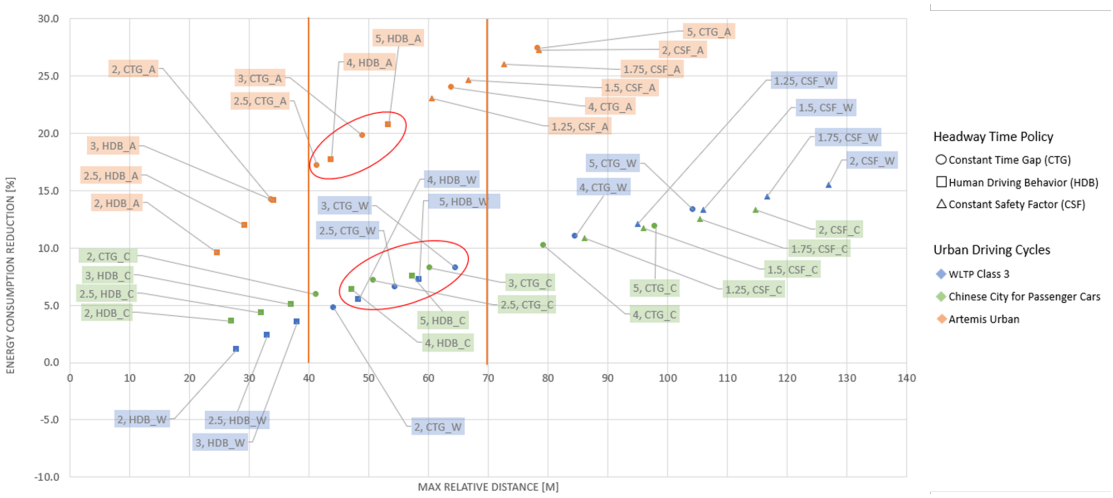

Figure 4.6: Energy Consumption and Maximum Relative Distance Across Time Gap Policies

- **CTG Policy**: $T_{\text{gap}} = 2.5$ s and 3.0 s
- **HDB Policy**: $T_{\text{gap}} = 4.0$ s and 5.0 s

These two groups of policy configurations not only demonstrate a consistent trend of energy savings across multiple driving scenarios (with ECRR values exceeding 8%), but also maintain maximum relative distances below the 70-meter threshold. This indicates that they offer substantial energy-saving potential without significantly compromising roadway capacity. Therefore, in the subsequent comfort evaluation—focused on maximum and minimum jerk metrics—these four configurations will be subjected to in-depth analysis. The goal is to identify optimal time gap policies that achieve a balanced trade-off among energy efficiency, ride comfort, and traffic throughput.

4.4 Comfort Evaluation

In the comprehensive assessment of time gap policy performance, ride comfort constitutes a critical evaluation metric. It is directly related to the smoothness

of longitudinal vehicle motion and the perceived comfort of passengers. This is particularly important in urban driving scenarios, where frequent acceleration and deceleration fluctuations can lead to passenger discomfort and fatigue.

To quantitatively evaluate the ability of different time gap policies to mitigate longitudinal acceleration disturbances, this study introduces the Acceleration Reduction Ratio (ARR) as the core evaluation index. It is defined as follows:

$$ARR = \frac{a_{\text{rms,ref}} - a_{\text{rms,ACC}}}{a_{\text{rms,ref}}} \times 100\% \tag{4.2}$$

where $a_{\text{rms,ref}}$ represents the root mean square (RMS) value of longitudinal acceleration under the baseline scenario without ACC control, and $a_{\text{rms,ACC}}$ corresponds to the RMS acceleration value under a given time gap policy. A higher ARR value indicates better performance in reducing acceleration fluctuations, which corresponds to improved ride comfort.

Building upon the previous energy consumption analysis, this section focuses on the four representative policy configurations previously identified as optimal: CTG with $T_{\text{gap}} = 2.5\,\text{s}$, CTG with $T_{\text{gap}} = 3.0\,\text{s}$, HDB with $T_{\text{gap}} = 4.0\,\text{s}$, and HDB with $T_{\text{gap}} = 5.0\,\text{s}$. The ARR metric is evaluated under three representative urban driving scenarios: WLTP Class 3, China City, and Artemis Urban. The comparative results are presented in Figure:

Table 4.7: Comfort Performance Comparison under Urban Driving Cycles

Driving Cycle	**WLTP**		**CLTC**		**Artemis urban**	
$a_{\text{rms,ref}}$ [m/s²]	**0.56**		**0.49**		**0.80**	
policy with T_{gap} [s]	a_{rms} [m/s²]	$a_{\text{rms,reduction}}$ [%]	a_{rms} [m/s²]	$a_{\text{rms,reduction}}$ [%]	a_{rms} [m/s²]	$a_{\text{rms,reduction}}$ [%]
CTG $T_{\text{gap}} = 2.5$	0.45	21.0	0.33	32.8	0.53	33.2
CTG $T_{\text{gap}} = 3$	0.42	25.4	0.31	35.5	0.50	37.5
HDB $T_{\text{gap}} = 4$	0.44	21.1	0.32	33.7	0.51	36.0
HDB $T_{\text{gap}} = 5$	0.42	25.9	24.0	0.31	36.6	41.0

To provide a more intuitive understanding of the comfort performance across different policies and urban driving scenarios, the Acceleration Reduction Ratio (ARR) results are further visualized in Figure 4.7:

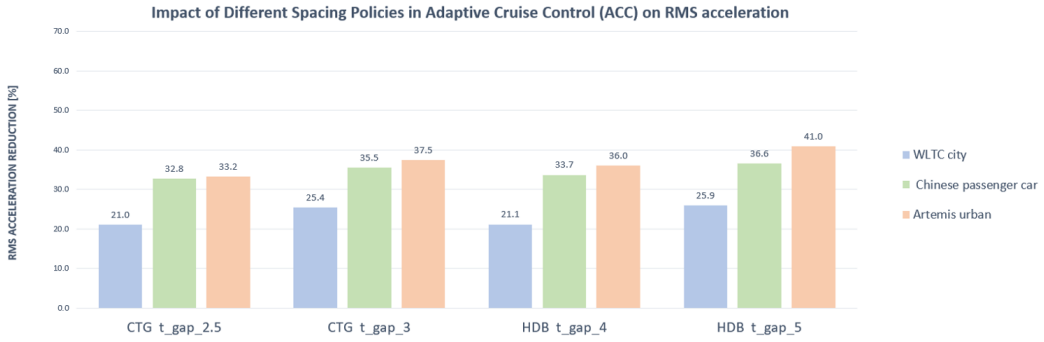

Figure 4.7: RMS Acceleration Reduction Comparison across Driving Cycles

This bar chart illustrates the comparative effectiveness of each policy in reducing RMS acceleration. The visualization highlights not only the overall superiority of the HDB(T_{gap}=5.0 s) configuration but also the consistent improvements observed with increasing time gaps. By translating numerical data into visual trends, this figure reinforces the insights derived from Table 4.7 and offers clearer support for cross-scenario evaluation.

4.4.1 Comparative Analysis of ARR across Policies

As illustrated in Figure 4.7, all four selected policies significantly reduce the fluctuation of longitudinal acceleration across the three representative urban driving cycles. Each achieves an Acceleration Reduction Ratio (ARR) exceeding 20%, demonstrating a positive contribution to ride comfort improvement. To further quantify the performance differences among these strategies, a comparative evaluation of ARR values under the three driving cycles is presented below.

Overall Performance

In terms of average ARR, the HDB(T_{gap}=5.0 s) policy exhibits the highest attenuation rate of acceleration fluctuations across all conditions, with ARR values of 25.9%, 36.6%, and 41.0%. The second-best performer is CTG(T_{gap}=3.0 s), with ARR values of 25.4%, 35.5%, and 37.5%, slightly lower than HDB(T_{gap}=5.0 s) but still indicating high levels of effectiveness.

By contrast, the CTG(T_{gap}=2.5 s) and HDB(T_{gap}=4.0 s) policies show moderate performance, with average ARR values fluctuating between 21.0% and 36.0%. These configurations provide a reasonable level of comfort but demonstrate slightly lower stability and therefore may have more limited applicability in scenarios requiring high comfort standards.

Cross-Cycle Consistency Analysis

To systematically evaluate the stability and adaptability of each time gap policy across different urban traffic environments, this section performs a cross-scenario consistency analysis of four candidate policies using the Acceleration Reduction Rate (ARR) metric under three representative urban driving cycles: WLTP Class 3, China City, and Artemis Urban.

Firstly, the CTG($T_{\text{gap}} = 3.0\,\text{s}$) policy achieved ARR values of 25.4%, 35.5%, and 37.5% across the three cycles respectively. These values are well-balanced, with a fluctuation range within 12.1% and consistently maintaining a medium-to-high level. This indicates that the CTG($T_{\text{gap}} = 3.0\,\text{s}$) policy provides stable control performance and good adaptability under varying urban traffic rhythms, demonstrating high consistency.

In contrast, although the HDB($T_{\text{gap}} = 5.0\,\text{s}$) policy achieved the highest ARR of 41.0% in the Artemis Urban cycle, it only reached 25.9% under the WLTP cycle, resulting in a maximum-minimum gap of 15.1%, slightly higher than that of the CTG($T_{\text{gap}} = 3.0\,\text{s}$) policy. This suggests that the HDB policy is more affected by scenario disturbances and therefore ranks second in stability.

On the other hand, the CTG($T_{\text{gap}} = 2.5\,\text{s}$) and HDB($T_{\text{gap}} = 4.0\,\text{s}$) policies showed ARR values of only 21.0% and 21.1% under the WLTP cycle, significantly lower than their performance in the other two cycles (both exceeding 25%). Although they performed well in intense car-following or low-speed fluctuating conditions (such as China City and Artemis Urban), their higher sensitivity to traffic rhythm variations limits their applicability across diverse scenarios.

In summary, from the ARR perspective, the CTG($T_{\text{gap}} = 3.0\,\text{s}$) policy stands out as the most consistent strategy across different driving cycles due to its low fluctuation and high absolute performance. The HDB($T_{\text{gap}} = 5.0\,\text{s}$) policy follows closely behind, offering exceptional comfort in some scenarios but with slightly reduced stability. The remaining two policies should be deployed cautiously, depending on specific scenario characteristics, to avoid potential degradation in control performance due to limited adaptability.

Summary

Based on the above comparative analysis, the following conclusions can be drawn:

- In terms of comfort, the HDB($T_{\text{gap}} = 5.0\,\text{s}$) policy performs best across all three cycles, showing high adaptability and reliability.
- The CTG($T_{\text{gap}} = 3.0\,\text{s}$) policy, though slightly less effective in comfort, remains a strong recommendation due to its simple model structure, stable control

logic, and balanced performance in both comfort and energy efficiency.

- The CTG($T_{\text{gap}} = 2.5\,\text{s}$) and HDB($T_{\text{gap}} = 4.0\,\text{s}$) policies demonstrate certain control capabilities but are highly influenced by traffic scenarios, and are therefore not recommended for independent deployment in complex urban environments.

4.5 Results Discussion

Building upon the quantitative analysis of energy efficiency (ECRR) and ride comfort (ARR) in previous sections, this chapter further explores the trade-offs and applicability of different time gap policies under typical urban driving conditions. The discussion not only guides the practical deployment of Adaptive Cruise Control (ACC) systems in urban environments but also offers a theoretical foundation for future multi-objective control design and model optimization across diverse driving contexts.

4.5.1 Multi-Objective Trade-off Analysis

Based on the simulation results, the three representative time gap policies—Constant Time Gap (CTG), Human Driving Behavior (HDB), and Constant Safety Factor (CSF)—demonstrated varying levels of performance in terms of energy consumption and longitudinal comfort across the WLTP Class 3 driving cycles, China Light-Duty Vehicle Test Cycle for Passenger Car, and Artemis Urban driving cycles:

- **Energy Efficiency Dimension:** The CSF policy consistently delivered the lowest energy consumption in all three driving cycles. Particularly under high K configurations, it achieved the highest Energy Consumption Reduction Ratio (ECRR), with average energy savings exceeding 15%. The CTG policy also showed favorable energy-saving potential at medium-to-large T_{gap} values. In contrast, the HDB policy, while behaviorally realistic, showed slightly inferior efficiency due to frequent dynamic responses.

- **Ride Comfort Dimension:** The HDB policy with $T_{\text{gap}} = 5.0\,\text{s}$ achieved the highest ARR values in all urban scenarios, indicating the strongest capability for suppressing longitudinal acceleration fluctuations. The CTG policy with $T_{\text{gap}} = 3.0\,\text{s}$ ranked second, also maintaining relatively low acceleration variability and stable performance.

- **Effectiveness under Traffic Efficiency Constraints:** When traffic efficiency is considered—specifically limiting the maximum relative distance to the 40–70 meter range—most CSF policy configurations are excluded due to their

extended spacing. As a result, only CTG policies with $T_{\text{gap}} = 2.5\,\text{s}$ and $3.0\,\text{s}$, and HDB policies with $T_{\text{gap}} = 4.0\,\text{s}$ and $5.0\,\text{s}$, remain within acceptable bounds. This highlights a key insight: although different policies have strengths in either comfort or efficiency, the ones suitable for real-world deployment must achieve balanced performance across spatial efficiency, energy saving, and dynamic control responsiveness.

Therefore, from the perspective of comprehensive performance, and based on a balanced evaluation of energy efficiency (ECRR) and ride comfort (ARR), the following conclusions can be drawn:

First, the CTG($T_{\text{gap}} = 3.0\,\text{s}$) policy demonstrates balanced performance across all three representative urban driving cycles. In terms of energy savings, this configuration achieves noticeable ECRR values in WLTP, China City, and Artemis Urban scenarios, consistently ranking in the upper-middle among all tested policies. Regarding comfort, the main advantages of this policy include its simple control logic, stable model structure, and high adaptability. It is also less sensitive to controller parameter tuning, making it particularly suitable for autonomous driving platforms operating under hardware constraints or variable urban conditions, with the potential for cross-scenario and cross-vehicle deployment.

Second, the HDB($T_{\text{gap}} = 5.0\,\text{s}$) policy is slightly less competitive in terms of ECRR (showing marginally higher energy consumption than CTG), but it remains highly valuable for comfort-dominant applications, such as high-end shared mobility services or urban autonomous taxis. The stability of its response, particularly at longer time gaps, further supports its suitability for deployment in low-speed urban environments where passenger comfort is prioritized.

Third, a clear "threshold effect" can be observed across multiple simulation results. Specifically, when the time gap exceeds 3.0 seconds for CTG and HDB policies, or when the safety factor $K \geq 1.75$ in CSF policies, performance metrics begin to converge and no longer exhibit significant improvements. This suggests that once certain control parameters surpass an effective threshold, further increases yield diminishing returns and may even lead to delayed responses or reduced traffic throughput. Therefore, control policy design should avoid overemphasizing large gaps or excessive safety margins and instead focus on identifying and fine-tuning optimal control intervals through systematic validation.

Finally, the simulation results reveal a general phenomenon: a policy that performs best in one dimension often fails to achieve optimal results in others. For example, although HDB($T_{\text{gap}} = 5.0\,\text{s}$) ranks highest in ARR, it lags behind CTG in energy efficiency. Similarly, while CSF excels in minimizing energy consumption, it is excluded from practical deployment due to exceeding the acceptable range for maximum relative distance. These findings underscore the importance of moving beyond single-metric optimization in ACC system design. A multi-objective

optimization framework that incorporates energy consumption, comfort, and traffic efficiency should be established. Advanced techniques such as weight balancing or reinforcement learning can be employed to achieve dynamic trade-offs. Only when a control policy satisfies all key performance constraints can it be considered viable for engineering implementation and real-world deployment.

4.5.2 Scenario-Based Analysis of Policy Applicability

Based on the performance evaluation of different time gap control policies under three representative urban driving cycles—WLTP Class 3 Driving Cycle, China Light-Duty Vehicle Test Cycle for Passenger Car, and Artemis Urban Driving Cycle—this section further explores the applicability and deployment suitability of each policy in real-world traffic scenarios.

WLTP Class 3 Driving Cycle: A Balanced Scenario with Medium Traffic Density

The WLTP Class 3 driving cycle is characterized by moderate speed ranges (average speed approximately 30-35 km/h) and regular acceleration/deceleration patterns. It represents typical conditions found on urban arterial roads and suburban commuting routes with medium traffic density. In such scenarios, vehicle operation is relatively stable, but still involves moderate braking responses and starting fluctuations, necessitating an ACC controller capable of responsive energy control and moderate dynamic damping.

Simulation results indicate that the CTG($T_{\text{gap}} = 3.0\,\text{s}$) policy demonstrates strong energy-saving performance in this scenario (ECRR $\approx 8.2\%$) while maintaining high comfort levels (ARR $\approx 37.5\%$). The relatively large time gap setting effectively prevents frequent braking-induced energy oscillations and provides sufficient buffer distance to mitigate longitudinal shocks. This makes it a highly balanced option suitable for routine deployment in most autonomous driving platforms.

Additionally, the HDB($T_{\text{gap}} = 5.0\,\text{s}$) policy achieves the highest ARR value (25.9%) in this driving cycle, offering superior ride comfort. This makes it particularly appropriate for vehicles equipped with advanced autonomous functions, ride-hailing platforms, or customized commuting services that prioritize comfort. In such use cases, it can serve as a "high-comfort mode" option, adding value across diverse deployment scenarios.

China Light-Duty Vehicle Test Cycle for Passenger Car: A Congested Urban Scenario with High Density and Frequent Stop-and-Go Behavior

The China Light-Duty Vehicle Test Cycle for Passenger Car reflects traffic conditions commonly observed in central areas of major metropolitan cities, characterized by high vehicle density, low speeds, and frequent braking. This scenario presents a typical pattern of frequent stop-and-go behavior, significant speed fluctuations, and dense traffic interference. Consequently, it imposes stringent requirements on the control policy in terms of smoothness, response delay, and system robustness.

Under this driving cycle, the HDB($T_{\text{gap}} = 5.0\,\text{s}$) policy demonstrates outstanding performance. Its human-like response pattern is more capable of handling complex urban stimuli such as sudden braking of the lead vehicle or intersection conflicts. In terms of acceleration and jerk regulation, this policy achieves a significantly higher ARR compared to other policies, effectively mitigating discomfort caused by urban congestion. Although its ECRR is slightly lower than that of CTG, the comfort priority generally outweighs energy efficiency in urban driving scenarios. Therefore, this policy is considered better aligned with actual commuting demands and is recommended for deployment in advanced cruise control systems operating in low-to-medium speed urban environments.

The CTG($T_{\text{gap}} = 3.0\,\text{s}$) policy also exhibits a certain degree of applicability. While maintaining basic energy-saving capabilities, it delivers comfort levels close to those of the HDB policy. This makes it suitable for vehicle platforms with limited computational or hardware resources, offering a more generalized solution for wide-scale deployment.

Artemis Urban Driving Cycle: A Compound Scenario with Varying Speeds and Frequent Idling

The Artemis Urban Driving Cycle captures the composite nature of typical European urban traffic environments. It comprises segments of abrupt acceleration, traffic light response zones, and extended periods of idling or low-speed cruising. This scenario imposes considerable challenges on Adaptive Cruise Control (ACC) policies in terms of responsiveness, predictive capability, and flexible regulation.

Simulation results indicate that both the CTG($T_{\text{gap}} = 3.0\,\text{s}$) and HDB($T_{\text{gap}} = 5.0\,\text{s}$) policies perform at a high level under this cycle. The CTG policy benefits from a moderate time gap that helps mitigate system load fluctuations. Meanwhile, the HDB policy demonstrates superior adaptability amid complex traffic rhythm variations, achieving the highest ARR value (41.0%), indicating stronger environmental adaptability.

In contrast, although the CSF policy continues to exhibit strength in energy consumption reduction (ECRR), it often results in a maximum relative distance that exceeds the defined upper limit for traffic efficiency (greater than 70 meters). This could lead to unnecessary spacing and reduced lane utilization in urban settings. Therefore, the CSF policy should be applied with caution in integrated

urban traffic control systems or be optimized through V2X-based coordination mechanisms.

Integrated Recommendation and Strategy Deployment Insights

The preceding analysis highlights the strong coupling between policy configurations and driving scenario characteristics. No single control scheme can be universally applied. Instead, strategy selection must be context-aware and scenario-specific:

- The CTG($T_{\text{gap}} = 3.0\,\text{s}$) policy is well-suited for most urban environments with moderate traffic density. It offers the lowest implementation cost and the highest adaptability, making it a reliable baseline configuration.
- The HDB($T_{\text{gap}} = 5.0\,\text{s}$) policy demonstrates significant advantages in comfort and is particularly suitable for service-oriented transportation systems or high-level autonomous driving scenarios.

Therefore, time gap configurations must be precisely adjusted according to specific driving conditions. A refined matching mechanism between T_{gap}, vehicle type, traffic density, and road classification should be established to achieve optimized energy efficiency management and enhanced ride comfort in urban autonomous driving systems.

Chapter 5

Performance Analysis of Time Gap Policies in Highway Driving Scenarios

5.1 Overview of Highway Driving Scenarios

Highway environments are characterized by medium to high average speeds, typically ranging from 60 km/h to 120 km/h. In contrast to urban roads, highways often exhibit more stable traffic flows, lower frequency of lane changes, and fewer disruptions from traffic signals or pedestrian interactions. These characteristics pose distinct operational demands on Adaptive Cruise Control (ACC) systems, particularly in terms of responsiveness, energy optimization, stability, and comfort at higher vehicle speeds.

First, the system must ensure smooth and predictive control behaviors to avoid unnecessary interventions that could disrupt the driving experience. Second, energy efficiency becomes more critical in highway conditions, where long segments of steady cruising and deceleration offer the potential for coasting and regenerative braking optimization. Third, maintaining stability and a safe margin becomes vital due to the increased kinetic energy at higher speeds, which amplifies the consequences of inadequate braking or insufficient headway. Lastly, driving comfort should be preserved even in the presence of high-speed acceleration, deceleration, or gradient changes, requiring effective control of longitudinal dynamics and acceleration rates.

Given these factors, highway scenarios offer a representative context for evaluating the performance of time gap policies under demanding yet structured conditions. To ensure that different traffic rhythms and control challenges are comprehensively addressed, this study adopts three internationally recognized driving

cycles: HWFET, US06, and Artemis Motorway. These test profiles collectively span a wide spectrum of average speeds, acceleration profiles, and energy-use behaviors, enabling a thorough assessment of the robustness and adaptability of each time gap policy.

5.1.1 Description of the HWFET Driving Cycle

The Highway Fuel Economy Test (HWFET) is a standardized high-speed driving cycle established by the U.S. Environmental Protection Agency (EPA), aimed at evaluating a vehicle's fuel or energy efficiency under mid- to high-speed steady-state highway conditions [29]. The cycle covers a distance of 16.5 km over a duration of 765 s, with an average velocity of approximately 77.7 km/h and a peak speed of 97.4 km/h. It primarily features extended segments of constant-speed cruising with minimal dynamic disturbance.

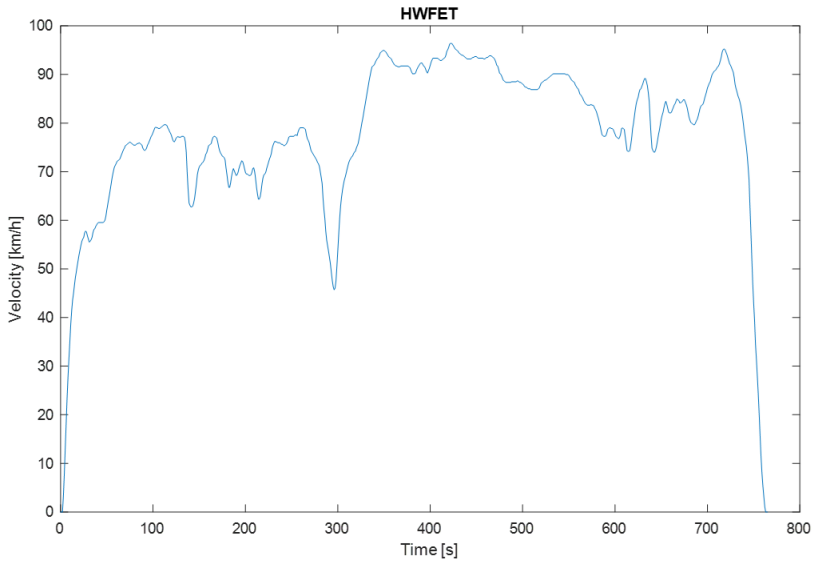

Figure 5.1: Speed–Time Curve of HWFET Driving Cycle

As illustrated in Figure 5.1, the HWFET velocity curve demonstrates an overall smooth profile, with several plateaus where the vehicle maintains speed near 90 km/h for prolonged periods. These flat segments represent ideal conditions for testing the energy-saving potential of ACC policies that emphasize coasting and regenerative braking. Minor fluctuations in the mid-phase (around 200–400 s) are present, but the overall acceleration remains moderate. A brief deceleration to under 50 km/h around 300 s introduces limited transient response requirements. Near the end of the cycle, a steep deceleration brings the vehicle speed to zero, simulating an off-ramp or highway exit scenario.

This relatively uniform structure allows for a clear assessment of how well time gap policies manage longitudinal control under stable highway cruising. In particular, it highlights the trade-off between energy consumption during light deceleration and maintaining headway consistency without unnecessary braking. As such, HWFET serves as a foundational benchmark for evaluating energy optimization strategies and basic control smoothness in highway scenarios.

5.1.2 Description of the US06 Driving Cycle

The US06 driving cycle is part of the U.S. FTP-75 framework and was developed to capture aggressive and non-ideal driving behaviors, including rapid accelerations, hard braking, and frequent transitions [30]. It covers 12.8 km over 596 s, with a maximum speed of 129.2 km/h and an average speed of 78.5 km/h. Unlike the smoother HWFET, US06 introduces intense transient events that challenge ACC system responsiveness and energy management.

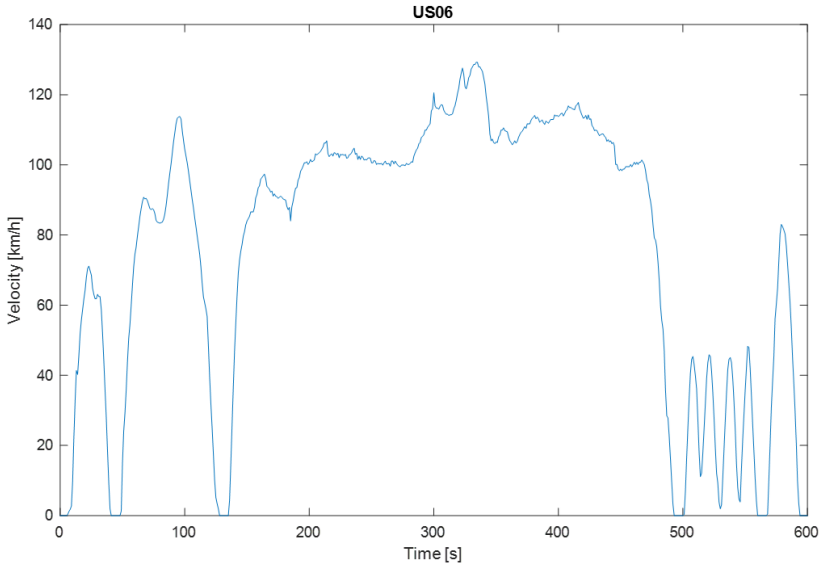

Figure 5.2: Speed–Time Curve of US06 Driving Cycle

As shown in Figure 5.2, the velocity profile of US06 is highly dynamic, marked by frequent and sharp velocity changes. In the initial 100 seconds, the vehicle undergoes several cycles of hard acceleration and complete stops, requiring the ACC controller to adapt to abrupt lead vehicle behavior. Between 200 and 400 seconds, a relatively stable cruising speed above 100 km/h is briefly maintained, though still punctuated by minor oscillations. Notably, the final 100 seconds of the cycle present a series of repeated accelerations and decelerations, resembling

real-world scenarios such as congestion waves or lane change-induced turbulence.

These features place demanding requirements on time gap policies. The ACC system must exhibit high-frequency adaptation to ensure collision avoidance without excessive braking, while also managing driver comfort during intense speed shifts. The cycle's inherently high energy usage also underscores the challenge of balancing safety with efficiency. Thus, the US06 cycle is essential for stress-testing the dynamic robustness and real-time adaptability of each time gap strategy.

5.1.3 Description of the Artemis Motorway Driving Cycle

The Artemis Motorway cycle originates from the EU-funded ARTEMIS project and is designed based on empirical high-speed driving data collected across various European motorway segments [26]. It spans 43.1 km over 1068 s, with an average speed of 94.0 km/h and a top speed of 130.0 km/h. Unlike purely synthetic cycles, Artemis includes a mix of real-world driving behaviors such as merging, lane changes, and varying speed limits, which create a semi-structured yet realistic profile.

Figure 5.3: Speed–Time Curve of Artemis Motorway Driving Cycle

Figure 5.3 depicts the Artemis Motorway velocity trajectory, which features several stages of linear acceleration reaching 120–130 km/h, followed by abrupt deceleration events, some of which reduce speed below 60 km/h in under 20 seconds. The distribution of speed changes is notably asymmetric: some phases reflect mild acceleration, while others simulate emergency-like braking. Around 600–800 seconds,

the velocity exhibits a wave-like pattern with moderate fluctuations, simulating terrain undulations or variable speed regulations. In the final segment of the cycle, a gradual speed reduction occurs, accompanied by irregular deceleration bursts, likely representing the exit from a highway or adaptation to traffic constraints.

Such complexity renders Artemis Motorway an ideal scenario to evaluate the holistic performance of ACC time gap policies. It tests the ability to handle prolonged high-speed cruising, sudden braking events, and transitional segments—all within a single cycle. Policies must balance comfort and safety while preserving energy efficiency across different sub-scenarios embedded in the cycle. Consequently, this cycle serves as a decisive test for validating both the control quality and adaptability of the proposed time gap control mechanisms.

5.2 Performance of Different Policies under Highway Driving Cycles

5.2.1 Performance under the HWFET Driving Cycle

This section presents a systematic evaluation of three representative time gap policies—Constant Time Gap (CTG), Human Driving Behavior (HDB), and Constant Safety Factor (CSF)—under the HWFET Driving Cycle across various parameter configurations. The assessment criteria include maximum target distance, maximum relative distance, battery energy consumption, longitudinal maximum and minimum acceleration, and jerk. The goal is to achieve a balanced trade-off between energy efficiency, control smoothness, and safety.

Table 5.1: HWFET Driving Cycle

	Baseline vehicle on HWFET		**1.707**	**1.454**	**-1.612**	**2.412**	**-1.937**
CTG $T_{\mathbf{gap}}$ [s]	$d_{\mathbf{des,max}}$ [m]	$d_{\mathbf{rel,max}}$ [m]	E [kWh]	$a_{\mathbf{max}}$ [m/s^2]	$a_{\mathbf{min}}$ [m/s^2]	$j_{\mathbf{max}}$ [m/s^3]	$j_{\mathbf{min}}$ [m/s^3]
1.5	43	42	1.702	1.374	-1.434	0.481	-0.473
2.0	56	55	1.699	1.272	-1.358	0.459	-0.448
2.5	70	69	1.697	1.185	-1.292	0.448	-0.428
3.0	83	82	1.696	1.118	-1.234	0.438	-0.412
4.0	110	108	1.692	1.007	-1.147	0.418	-0.390
5.0	137	134	1.689	0.915	-1.108	0.397	-0.370
HDB $T_{\mathbf{gap}}$ [s]	$d_{\mathbf{des,max}}$ [m]	$d_{\mathbf{rel,max}}$ [m]	E [kWh]	$a_{\mathbf{max}}$ [m/s^2]	$a_{\mathbf{min}}$ [m/s^2]	$j_{\mathbf{max}}$ [m/s^3]	$j_{\mathbf{min}}$ [m/s^3]
1.5	71	72	1.710	1.431	-1.538	0.483	-0.547
2.0	76	77	1.710	1.346	-1.496	0.459	-0.547
2.5	81	82	1.710	1.279	-1.458	0.457	-0.548
3.0	85	87	1.710	1.216	-1.424	0.469	-0.548
4.0	94	97	1.708	1.116	-1.363	0.494	-0.549
5.0	103	107	1.705	1.065	-1.311	0.519	-0.550
CSF $K_{\mathbf{safe}}$ [s]	$d_{\mathbf{des,max}}$ [m]	$d_{\mathbf{rel,max}}$ [m]	E [kWh]	$a_{\mathbf{max}}$ [m/s^2]	$a_{\mathbf{min}}$ [m/s^2]	$j_{\mathbf{max}}$ [m/s^3]	$j_{\mathbf{min}}$ [m/s^3]
1.25	156	150	1.678	1.128	-1.344	0.472	-0.313
1.5	179	171	1.674	1.093	-1.300	0.472	-0.294
1.75	202	192	1.671	1.062	-1.244	0.472	-0.292
2.0	225	213	1.670	1.035	-1.192	0.472	-0.289

The simulation results are summarized in Table 5.1, which details the performance metrics of the three policies under the HWFET cycle. To ensure fair horizontal comparisons, all indicators are collected based on unified initial speeds, simulation durations, and vehicle model parameters.

Baseline Scenario Analysis

According to the simulation results, the baseline energy consumption under the HWFET cycle is 1.707 kWh, representing the minimum energy required for a vehicle to complete the driving cycle through basic cruising and limited control intervention. In the absence of an ACC system for anticipatory deceleration or optimized coasting, this energy level remains relatively modest, although further improvements are possible, especially in terms of leveraging regenerative braking and minimizing dynamic interventions.

In terms of acceleration metrics, the maximum acceleration reaches 1.454 m/s^2, and the maximum deceleration is –1.612 m/s^2. This indicates that even within a relatively stable high-speed driving scenario, the vehicle still undergoes significant acceleration and deceleration events. These are often triggered by traffic flow variations, simulation-induced disturbances, or lead vehicle behaviors. Such dynamic responses tend to increase energy consumption and reduce ride comfort.

Additionally, the jerk values range from –1.937 m/s^3 to 2.412 m/s^3, suggesting clear discontinuities or shocks at the level of control signal derivatives. Without the involvement of advanced control strategies, these fluctuations may negatively impact passenger comfort and pose challenges to the stability of electric propulsion systems. Therefore, this baseline scenario not only serves as a reference lower bound for energy and stability assessments but also highlights the intensity of control efforts required in the absence of optimized policies, providing a clear direction for subsequent policy enhancements.

Performance Analysis of the CTG Policy

The Constant Time Gap (CTG) policy regulates the following distance between the ego vehicle and the preceding vehicle by setting a fixed time gap parameter T_{gap}. With a simple logic and stable performance, this policy has been widely applied in engineering practice. In this section, the CTG policy is tested under six configurations ranging from $T_{\text{gap}} = 1.5\,\text{s}$ to $5.0\,\text{s}$ to evaluate its impact on various performance metrics.

According to traffic safety research, maintaining a time headway of no less than 3 seconds is considered a fundamental safety threshold for highway scenarios. The relationship between time headway T_{gap} and relative distance d_{rel} satisfies:

$$d_{\text{rel}} = v_{\text{ego}} \cdot T_{\text{gap}}$$

where v_{ego} is the ego vehicle speed. Given the average speed of the HWFET cycle is approximately $v_{\text{avg}} = 77.7\,\text{km/h} = 21.6\,\text{m/s}$, the minimum safe distance under a 3-second headway is:

$$d_{\text{safe}} = 21.6\,\text{m/s} \times 3\,\text{s} = 64.8\,\text{m}$$

According to the tabulated data, the maximum relative distances for CTG($T_{\text{gap}} = 1.5\,\text{s}$) and CTG($T_{\text{gap}} = 2.0\,\text{s}$) are 42 m and 55 m, respectively, both significantly lower than the recommended 64.8 m. Due to this safety concern, these two configurations are excluded from the subsequent analysis.

Among the retained configurations ($T_{\text{gap}} = 2.5 \sim 5.0\,\text{s}$), increasing the time gap leads to a rise in maximum desired distance from 70 m to 137 m, all satisfying high-speed following safety requirements. Meanwhile, battery consumption decreases from 1.697 kWh to 1.689 kWh, indicating improved energy efficiency. The maximum acceleration drops from $1.185\,\text{m/s}^2$ to $0.915\,\text{m/s}^2$, and the maximum deceleration decreases from -1.292 m/s^2 to -1.108 m/s^2, showing smoother control intervention. Additionally, the maximum jerk value declines from $0.448\,\text{m/s}^3$ to $0.397\,\text{m/s}^3$, reflecting more gradual changes in control signals and improved comfort.

In summary, the CTG policy under the HWFET cycle exhibits a clear trend of "greater time gap leads to greater stability." Particularly when $T_{\text{gap}} \geq 3.0\,\text{s}$, the configuration outperforms the baseline in terms of energy efficiency, control smoothness, and safety redundancy, making it a promising and practical baseline control strategy for highway environments.

Performance Analysis of the HDB Policy

Under the HWFET driving cycle, which features high-speed steady-state conditions dominated by constant-speed cruising, the performance of the Human Driving Behavior (HDB) policy appears suboptimal. Simulation results indicate that for all tested time gap configurations ($T_{\text{gap}} = 1.5\,\text{s} \sim 5.0\,\text{s}$), the battery energy consumption consistently exceeds the baseline value (1.707 kWh). None of the configurations demonstrates an energy-saving advantage; the lowest energy consumption is 1.705 kWh, while the highest reaches 1.710 kWh. This indicates that the HDB policy fails to effectively utilize energy management mechanisms in this scenario, such as coasting control, anticipatory deceleration, and low-intervention car-following. Instead, the frequent adjustments in the following distance contribute to increased energy expenditure.

In terms of dynamic performance, although the acceleration magnitudes are generally comparable to those under the CTG policy, the jerk response exhibits

significant issues. Simulation data show that the maximum jerk value increases progressively from $0.483\,\mathrm{m/s^3}$ to $0.519\,\mathrm{m/s^3}$, while the minimum jerk decreases to $-0.550\,\mathrm{m/s^3}$. This reflects intensified responsiveness in acceleration and deceleration control. Similar to human drivers, the HDB policy tends to exhibit "micro-compensation behavior" even in speed-stable segments—frequent small throttle or brake inputs, which induce high-frequency control perturbations and lead to reduced ride comfort.

Additionally, with respect to maximum relative distance, the HDB policy fails to significantly improve safety margins even under $T_{\mathrm{gap}} \geq 3.0\,\mathrm{s}$. The maximum observed value is only 107 m, slightly below the performance of the CTG and CSF policies under comparable configurations. This suggests that the vehicle controlled by the HDB model does not adequately exploit the predictability of highway scenarios for proactive safety extension, further weakening its adaptability in this context.

In summary, although the HDB policy more closely reflects real human driving behavior in urban traffic or complex car-following scenarios, its "human-likeness" becomes a performance bottleneck in highly stable, high-speed, and predictable driving environments such as HWFET. Significant shortcomings are observed in terms of energy efficiency, comfort, and safety. Therefore, this study excludes the HDB policy entirely under this cycle, deeming it an unacceptable design option.

Performance Analysis of the CSF Policy

In the HWFET test scenario, the Constant Safety Factor (CSF) policy is evaluated under four configurations with safety factors $K = 1.25, 1.5, 1.75, 2.0$, corresponding to maximum desired distances of 156 m, 179 m, 202 m, and 225 m, respectively. Compared to the CTG policy, which yields a maximum desired distance of 137 m, the CSF policy provides a significantly larger following space. This enhances the system's buffering capacity in unexpected situations, thereby substantially improving safety redundancy.

In terms of energy efficiency, the CSF policy demonstrates outstanding performance. Battery energy consumption decreases from 1.678 kWh to 1.670 kWh, representing a reduction of approximately 2.2% relative to the baseline. Compared with the CTG policy (minimum energy consumption of 1.689 kWh), the CSF strategy proves more effective in energy-saving control. This advantage is attributed to its ability to maintain a low-intervention, coasting-dominated control mode during prolonged steady-speed segments. Especially in the low-acceleration HWFET scenario, this strategy can significantly reduce unnecessary activations of the powertrain.

Regarding comfort metrics, the CSF policy performs exceptionally well in terms of jerk. For all tested K values, the maximum jerk remains consistently below

0.472 m/s^3, and the jerk profile is relatively smooth with minimal fluctuation, as the minimum jerk remains above –0.313 m/s^3. This indicates that the control process is gentle and less abrupt, effectively mitigating discomfort during acceleration phases. Furthermore, the maximum acceleration is maintained below 1.128 m/s^2, which further confirms the moderate and uniform intervention of the powertrain system, contributing to a superior ride experience.

From the perspective of system stability, the CSF policy offers a structured approach to dynamic car-following, balancing safety margin maintenance with responsive adaptability, making it highly compatible with the characteristics of the HWFET cycle. Its linear proportional model provides predictable control logic and strong parameter tunability, facilitating real-world deployment. Compared to the HDB policy, the CSF approach features a simpler structure and does not rely on complex behavioral modeling, thereby offering greater control and explainability. Compared to the CTG policy, it further improves both energy efficiency and comfort, making it the most recommended solution in this study.

5.2.2 Policy Performance under the US06 Driving Cycle

Under the US06 Driving Cycle, a systematic simulation analysis was conducted for each policy across different parameter configurations using the established simulation platform. The summarized results are presented as follows:

Table 5.2: US06 Driving cycle

	Baseline vehicle on US06		**1.906**	**4.358**	**-3.367**	**9.016**	**-7.092**
CTG $T_{\mathbf{gap}}$ [s]	$d_{\mathbf{des,max}}$ [m]	$d_{\mathbf{rel,max}}$ [m]	E [kWh]	$a_{\mathbf{max}}$ [m/s^2]	$a_{\mathbf{min}}$ [m/s^2]	$j_{\mathbf{max}}$ [m/s^3]	$j_{\mathbf{min}}$ [m/s^3]
1.5	56	56	1.865	2.867	-2.679	2.688	-1.432
2.0	74	73	1.848	2.606	-2.573	1.859	-1.332
2.5	92	91	1.834	2.413	-2.458	1.822	-1.272
3.0	110	109	1.820	2.238	-2.340	1.782	-1.220
4.0	146	144	1.798	1.999	-2.109	1.699	-1.132
5.0	182	178	1.777	1.797	-1.895	1.613	-1.058
HDB $T_{\mathbf{gap}}$ [s]	$d_{\mathbf{des,max}}$ [m]	$d_{\mathbf{rel,max}}$ [m]	E [kWh]	$a_{\mathbf{max}}$ [m/s^2]	$a_{\mathbf{min}}$ [m/s^2]	$j_{\mathbf{max}}$ [m/s^3]	$j_{\mathbf{min}}$ [m/s^3]
1.5	70	76	1.908	3.323	-2.520	4.143	-1.601
2.0	72	81	1.910	2.895	-2.405	2.101	-1.493
2.5	74	86	1.921	2.773	-2.307	1.841	-1.400
3.0	76	91	1.932	2.677	-2.222	1.767	-1.361
4.0	80	180	2.423	3.892	-4.520	6.721	-5.450
5.0	85	233	2.542	3.980	-4.521	11.297	-8.331
CSF $K_{\mathbf{safe}}$ [s]	$d_{\mathbf{des,max}}$ [m]	$d_{\mathbf{rel,max}}$ [m]	E [kWh]	$a_{\mathbf{max}}$ [m/s^2]	$a_{\mathbf{min}}$ [m/s^2]	$j_{\mathbf{max}}$ [m/s^3]	$j_{\mathbf{min}}$ [m/s^3]
1.25	259	239	1.766	2.044	-1.904	1.976	-1.385
1.5	299	273	1.753	1.970	-1.773	1.970	-1.361
1.75	340	307	1.740	1.904	-1.662	1.950	-1.336
2.0	380	339	1.729	1.866	-1.553	1.918	-1.311

Baseline performance analysis

The simulation results show that the energy consumption reaches 1.906 kWh, significantly higher than the 1.707 kWh observed in the HWFET cycle. This

indicates that the frequent and abrupt speed adjustments in US06 lead to severe energy losses.

In terms of longitudinal dynamics, the system reaches a peak acceleration of $4.358\,\mathrm{m/s^2}$ and a peak deceleration of $-3.367\,\mathrm{m/s^2}$, both exceeding the commonly recommended comfort threshold of $\pm 2.5\,\mathrm{m/s^2}$. This suggests that the system, in the absence of active control, exhibits a pronounced tendency for high-rate, high-impact responses to disturbances.

Notably, the jerk (rate of change of acceleration) peaks at $9.016\,\mathrm{m/s^3}$, far beyond the typical comfort range of $\pm 2.0\,\mathrm{m/s^3}$. This indicates substantial discontinuities in the control output under frequent disturbances, which can cause not only discomfort for passengers but also lead to increased fatigue in mechanical systems and long-term reliability issues for vehicle components.

In conclusion, the baseline performance under the US06 cycle provides a critical reference benchmark for evaluating energy efficiency and ride comfort. It also highlights the pressing need for robust ACC control in high-speed urban traffic environments.

Performance Analysis of the CTG Policy

Under the US06 Driving Cycle, this study evaluates the adaptability of CTG to highly dynamic urban traffic conditions by testing six configurations ranging from 1.5 s to 5.0 s. However, in high-speed following scenarios, a 3-second headway is widely regarded as a minimum safety threshold. Considering that the average speed of the US06 cycle is 78.5 km/h (i.e., 21.8 m/s), the recommended safe distance is 65.4 m. According to the tabulated data, the maximum relative distances for CTG(T_{gap}=1.5 s) and CTG(T_{gap}=2.0 s) are only 39 m and 54 m, significantly below the safety requirement. These two configurations are thus excluded from subsequent analysis.

For the retained configurations ($T_{\mathrm{gap}} = 2.5 \sim 5.0\,\mathrm{s}$), the overall energy efficiency of the CTG policy improves progressively with increasing time gap. Battery energy consumption drops from 1.834 kWh to 1.777 kWh, suggesting reduced energy loss. Larger gaps allow earlier deceleration and longer coasting, enabling the system to respond more gently and reduce acceleration demand. In terms of dynamic performance, maximum acceleration decreases from $2.413\,\mathrm{m/s^2}$ to $1.797\,\mathrm{m/s^2}$, and maximum deceleration decreases from $-2.841\,\mathrm{m/s^2}$ to $-2.063\,\mathrm{m/s^2}$. Additionally, maximum jerk reduces from $1.822\,\mathrm{m/s^3}$ to $1.613\,\mathrm{m/s^3}$, which, although higher than that in HWFET, still outperforms the US06 baseline value of $9.016\,\mathrm{m/s^3}$.

These findings indicate that with appropriate gap configuration, the vehicle can better cooperate with the control system to reduce torque demand and smooth longitudinal dynamics. However, due to the limited adaptability of its fixed logic, the CTG policy may struggle to cope with intense dynamic phases in the US06

cycle (e.g., 0–100 km/h acceleration within 6 seconds). Hence, while CTG offers notable improvements in energy efficiency and comfort, it still falls short of the CSF policy in highly dynamic environments.

Performance Analysis of the HDB Policy

Simulation results show that under all tested time gaps $T_{\text{gap}} = 1.5 \sim 5.0\,\text{s}$, the HDB policy exhibits consistently high energy consumption. Notably, the most unfavorable configuration reaches 2.542 kWh, exceeding the baseline by more than 33%, indicating a complete failure in energy efficiency. The root cause lies in the HDB controller's inability to anticipate and smooth sudden changes in acceleration or braking, instead mimicking irregular and non-optimal human responses such as sudden braking followed by abrupt acceleration. This leads to increased control system load, frequent high-torque states, and excessive energy waste.

From a dynamic response perspective, the HDB policy demonstrates highly aggressive behavior. The maximum acceleration frequency reaches $3.9\,\text{m/s}^2$, and maximum deceleration hits $-4.521\,\text{m/s}^2$, both exceeding common tolerance thresholds. In terms of jerk, the peak value soars to $11.297\,\text{m/s}^3$ while the minimum falls to $-8.331\,\text{m/s}^3$, indicating intense fluctuations far beyond the baseline value of $9.016\,\text{m/s}^3$. These extremes reflect poor control and may result in discomfort due to excessive postural compensation and longitudinal oscillations for passengers.

From a control design perspective, the HDB policy proves structurally incompatible with the US06 driving environment, which is characterized by rapid acceleration-deceleration cycles. Although the policy emphasizes "human resemblance," its poor predictability and lack of control efficiency render it unsuitable for engineering applications. Therefore, this study regards the HDB policy as an "unacceptable" control configuration under the US06 cycle, and its deficiencies reflect the limitations of behavior-cloning-based policies in high-dynamic traffic conditions.

Performance Analysis of the CSF Policy

Under the US06 cycle, the CSF policy demonstrates remarkable energy-saving potential and control smoothness. As the safety factor K gradually increases from 1.25 to 2.0, the battery energy consumption decreases from 1.766 kWh to 1.729 kWh. This value is even lower than the minimum 1.777 kWh observed in the CTG group, indicating the CSF policy's structural efficiency in energy control. This advantage stems from its ability to extend throttle-off periods and delay power activation during speed reductions, enabling more efficient speed modulation and reduced energy waste.

From the perspective of longitudinal dynamic response, all CSF configurations maintain maximum acceleration below $2.044\,\text{m/s}^2$ and maximum deceleration within

$-1.904\,\mathrm{m/s^2}$, both more moderate than CTG and baseline results. Furthermore, the peak jerk value is consistently below $1.918\,\mathrm{m/s^3}$, and the entire jerk profile remains within the $\pm 2.0\,\mathrm{m/s^3}$ comfort threshold. This validates the CSF policy's superior smoothness and moderate responsiveness. Notably, CSF does not trade off comfort for excessive softness; instead, its control curve maintains proper curvature, enabling smooth dynamic adjustment even under rapid transitions typical of the US06 cycle.

In terms of distance control, the CSF policy outperforms CTG by actively adjusting the expected maximum relative distance. Especially under $K = 1.75 \sim 2.0$, the maximum relative distance reaches up to 142 m, ensuring sufficient headway buffer and enhancing safety redundancy. This "faster speed, greater distance" proportional control logic shows better adaptability in high-speed, complex driving conditions than the fixed-gap CTG policy.

Overall, the CSF policy not only performs reliably under steady-state conditions (e.g., HWFET), but also exhibits excellent energy control and adaptive safety across high-frequency, high-dynamic scenarios like US06. Its high interpretability and engineering feasibility enable efficient and smooth behavior under diverse traffic inputs, making it one of the most practical and adaptable time gap control policies in complex traffic environments.

5.2.3 Policy Performance under the Artemis Motorway Driving cycle

Under the Artemis Motorway Driving cycle, a series of simulations were conducted using the established platform to evaluate the performance of each time gap policy across multiple parameter settings. The summarized simulation results are presented as follows:

Table 5.3: Artemis Motorway Driving Cycle

Baseline vehicle on Artemis Motorway			**4.646**	**2.313**	**-3.440**	**6.273**	**-4.533**
CTG $T_{\mathbf{gap}}$ [s]	$d_{\mathbf{des,max}}$ [m]	$d_{\mathbf{rel,max}}$ [m]	E [kWh]	$a_{\mathbf{max}}$ [m/s^2]	$a_{\mathbf{min}}$ [m/s^2]	$j_{\mathbf{max}}$ [m/s^3]	$j_{\mathbf{min}}$ [m/s^3]
1.5	56	57	4.582	1.544	-2.450	1.563	-1.072
2.0	74	75	4.564	1.405	-2.277	1.294	-1.042
2.5	92	93	4.548	1.347	-2.129	1.234	-1.011
3.0	110	111	4.535	1.286	-2.001	1.179	-0.980
4.0	146	147	4.514	1.164	-1.791	1.081	-0.922
5.0	182	184	4.500	1.052	-1.625	1.001	-0.869
HDB $T_{\mathbf{gap}}$ [s]	$d_{\mathbf{des,max}}$ [m]	$d_{\mathbf{rel,max}}$ [m]	E [kWh]	$a_{\mathbf{max}}$ [m/s^2]	$a_{\mathbf{min}}$ [m/s^2]	$j_{\mathbf{max}}$ [m/s^3]	$j_{\mathbf{min}}$ [m/s^3]
1.5	70	74	4.656	1.800	-3.121	1.979	-1.198
2.0	72	79	4.667	1.553	-3.090	1.500	-1.212
2.5	74	84	4.687	1.522	-3.085	1.486	-1.232
3.0	76	89	4.735	1.479	-3.097	1.476	-1.315
4.0	80	261	6.677	3.846	-4.521	7.647	-5.775
5.0	85	299	6.818	3.914	-4.521	11.509	-4.292
CSF $K_{\mathbf{safe}}$ [s]	$d_{\mathbf{des,max}}$ [m]	$d_{\mathbf{rel,max}}$ [m]	E [kWh]	$a_{\mathbf{max}}$ [m/s^2]	$a_{\mathbf{min}}$ [m/s^2]	$j_{\mathbf{max}}$ [m/s^3]	$j_{\mathbf{min}}$ [m/s^3]
1.25	259	260	4.470	1.226	-1.342	1.103	-0.862
1.5	299	300	4.457	1.180	-1.267	1.042	-0.826
1.75	340	340	4.444	1.133	-1.222	0.983	-0.791
2.00	380	379	4.432	1.085	-1.174	0.926	-0.757

Baseline performance analysis

Simulation results show that the total battery energy consumption reaches 4.646 kWh, significantly higher than that in HWFET (1.707 kWh) and US06 (1.906 kWh), primarily due to the higher cruise speed, route length, and repeated acceleration-deceleration sequences. The maximum longitudinal acceleration is 2.313 m/s^2, and the maximum deceleration is –2.791 m/s^2. Moreover, jerk values fluctuate between -4.533 m/s^3 and 6.273 m/s^3, indicating substantial shock and discontinuity during dynamic transitions, particularly in deceleration phases.

Performance Analysis of the CTG Policy

The Constant Time Gap (CTG) policy was tested under the Artemis cycle using six time gap configurations ranging from 1.5 s to 5.0 s. As in previous scenarios, configurations with $T_{\text{gap}} = 1.5$ s and 2.0 s were excluded from detailed analysis due to insufficient relative distance that compromises safety, especially during high-speed braking or when merging from lower-speed segments.

Among the remaining configurations, the CTG policy shows a gradual improvement in energy efficiency and dynamic performance as the time gap increases. Battery energy consumption decreased from 4.548 kWh at $T_{\text{gap}} = 2.5$ s to 4.500 kWh at $T_{\text{gap}} = 5.0$ s, indicating a mild energy-saving trend. Maximum acceleration reduced from 2.002 m/s^2 to 1.598 m/s^2, and jerk decreased from 1.204 m/s^3 to 1.001 m/s^3. Although the energy-saving gains were less pronounced than those observed in HWFET and US06, the reduction in jerk signifies improved ride comfort in this scenario.

Notably, the CTG policy showed limitations in handling the hybrid speed

transitions inherent in Artemis. While the policy performed reasonably well in high-speed sections, it exhibited delayed responses during transitions from low to high speeds, particularly in segments between 400-600 seconds. This structural rigidity prevented the full exploitation of regenerative braking or coasting opportunities. Consequently, although the CTG strategy under Artemis maintained acceptable performance in terms of stability and smoothness, its lack of adaptability limits its potential in complex real-world scenarios.

Performance Analysis of the HDB Policy

The Human Driving Behavior (HDB) policy continued to exhibit structural disadvantages under the Artemis Motorway conditions. Designed to simulate real human driving behavior, the HDB policy adjusts following distances dynamically based on perceived traffic density and driving aggressiveness. However, in complex environments with frequent speed transitions, this behavioral mimicry does not yield better comfort or safety. Instead, it introduces significant instability and excessive energy demand.

Simulation results revealed that for all tested configurations ($T_{\text{gap}} = 1.5\,\text{s} \sim 5.0\,\text{s}$), battery consumption was consistently above the baseline. The highest recorded value reached 6.818 kWh, and the lowest remained at 4.656 kWh, entirely failing the energy efficiency objective of ACC systems. Moreover, the HDB policy triggered frequent oscillatory responses during periods of speed fluctuation, causing unnecessary activation of the propulsion and braking systems.

The jerk indicators confirmed poor performance in terms of ride comfort. In the $T_{\text{gap}} = 4.0\,\text{s}$ and $5.0\,\text{s}$ configurations, jerk peaked at $7.647\,\text{m/s}^3$ and $11.509\,\text{m/s}^3$, respectively, significantly exceeding safety and comfort thresholds. Such values not only impair ride quality but also reflect control logic incapable of managing moderate-speed transitions effectively. Peak acceleration remained above $2.9\,\text{m/s}^2$ and deceleration approached -$3.0\,\text{m/s}^2$, indicating a lack of proper damping and smoothing capacity.

Therefore, the HDB policy was excluded entirely from the Artemis-based analysis due to its structural incompatibility with complex motorway dynamics. Its behavior-mimicking control structure lacked both the flexibility and predictive capability required to handle hybrid transitions smoothly, rendering it unsuitable for energy-efficient or comfortable ACC deployment in realistic highway conditions.

Performance Analysis of the CSF Policy

The Constant Safety Factor (CSF) policy once again demonstrated strong adaptability and stability under the Artemis Motorway driving cycle. By applying different safety coefficients $K = 1.25 \sim 2.0$, the vehicle dynamically adjusted its

desired following distance according to its current speed, enabling smooth transitions between high-speed cruising and low-speed phases. This ensured that both energy efficiency and longitudinal comfort were effectively maintained throughout the cycle.

Simulation results showed that the CSF strategy consistently limited the maximum longitudinal acceleration to below $1.226\,\mathrm{m/s^2}$ and the maximum deceleration to -1.823 $\mathrm{m/s^2}$, demonstrating improved control smoothness compared to both the baseline and other policies. The jerk value remained well-controlled, with the maximum not exceeding $1.103\,\mathrm{m/s^3}$, indicating excellent ride comfort. In particular, the CSF strategy performed well during the middle segments of the cycle (e.g., 600–800 seconds), where alternating coasting and acceleration phases occurred. Despite the presence of complex velocity transitions, the controller managed to suppress sudden acceleration surges or harsh braking, highlighting its robustness in variable-speed scenarios.

In terms of energy consumption, the CSF strategy outperformed both CTG and HDB policies. The battery energy usage decreased from 4.470 kWh at $K = 1.25$ to 4.432 kWh at $K = 2.0$, showing a steady improvement. This reduction is attributed to the policy's proactive approach in maximizing coasting opportunities and reducing unnecessary propulsion torque in long, gentle deceleration phases. Moreover, its velocity-proportional spacing logic inherently accommodates the high-speed nature of the Artemis cycle, extending inter-vehicle distances appropriately to minimize control oscillations without sacrificing responsiveness.

Overall, the CSF policy under the Artemis Motorway cycle proves to be a robust and efficient time gap control solution. Its smooth torque modulation, adaptive distance regulation, and energy-saving benefits make it highly suitable for real-world deployment in mixed-speed highway environments. With both structural simplicity and operational versatility, it is the most capable policy across all tested configurations.

5.3 Energy Consumption Comparison Analysis

To identify control strategies that balance energy efficiency and general applicability across various driving cycles, this study evaluates simulation results using the Energy Consumption Reduction Rate (ECRR) as a key performance metric. ECRR is defined as the percentage reduction in battery energy consumption compared to the corresponding baseline scenario, reflecting the strategy's potential to improve energy efficiency. Tables 5.4, 5.5, and 5.6 present the simulation results under HWFET, US06, and Artemis Motorway cycles, respectively. For each strategy configuration, they report the maximum relative distance ($d_{\mathrm{rel,max}}$), battery energy consumption (E_{battery}), and its reduction rate ($E_{\mathrm{battery,\ reduction}}$) relative to the baseline.

Table 5.4: ECRR of HWFET Driving cycle

Baseline vehicle on HWFET		**1.707**	
CTG $T_{\mathbf{gap}}$ [s]	$d_{\mathbf{rel,max}}$ [m]	E [kWh]	$E_{\mathbf{reduction}}$ [%]
2.5	69	1.697	0.6
3.0	82	1.696	0.6
4.0	108	1.692	0.9
5.0	134	1.689	1.1
CSF $T_{\mathbf{gap}}$ [s]	$d_{\mathbf{rel,max}}$ [m]	E [kWh]	$E_{\mathbf{reduction}}$ [%]
1.25	150	1.678	1.7
1.50	171	1.674	2.0
1.75	192	1.671	2.1
2.00	213	1.670	2.2

Table 5.5: ECRR of US06 Driving cycle

Baseline vehicle on US06		**1.906**	
CTG $T_{\mathbf{gap}}$ [s]	$d_{\mathbf{rel,max}}$ [m]	E [kWh]	$E_{\mathbf{reduction}}$ [%]
2.5	91	1.834	3.8
3.0	109	1.820	4.5
4.0	144	1.798	5.7
5.0	178	1.777	6.7
CSF $T_{\mathbf{gap}}$ [s]	$d_{\mathbf{rel,max}}$ [m]	E [kWh]	$E_{\mathbf{reduction}}$ [%]
1.25	239	1.766	7.3
1.50	273	1.753	8.0
1.75	307	1.740	8.7
2.00	339	1.729	9.3

Table 5.6: ECRR of Artemis Motorway Driving cycle

Baseline vehicle on Artemis Motorway		**4.646**	
CTG $T_{\mathbf{gap}}$ [s]	$d_{\mathbf{rel,max}}$ [m]	E [kWh]	$E_{\mathbf{reduction}}$ [%]
2.5	93	4.548	2.1
3.0	111	4.535	2.4
4.0	147	4.514	2.8
5.0	184	4.500	3.1
CSF $T_{\mathbf{gap}}$ [s]	$d_{\mathbf{rel,max}}$ [m]	E [kWh]	$E_{\mathbf{reduction}}$ [%]
1.25	260	4.470	3.8
1.50	300	4.457	4.1
1.75	340	4.444	4.3
2.00	379	4.432	4.6

From the tabulated data, the CSF strategy demonstrates superior energy-saving capabilities across all three driving scenarios. For example, in the US06 cycle, as the safety factor K increases, the maximum relative distance expands up to 339 m, with battery consumption decreasing from 1.766 kWh to 1.729 kWh, corresponding to an ECRR improvement from 7.3% to 9.3%. The CTG strategy, although effective, exhibits slightly lower ECRR values, with a maximum of 6.7% under the same cycle.

Figure 5.4 further illustrates these trends by plotting each strategy's $d_{\mathrm{rel,max}}$ against its ECRR value.

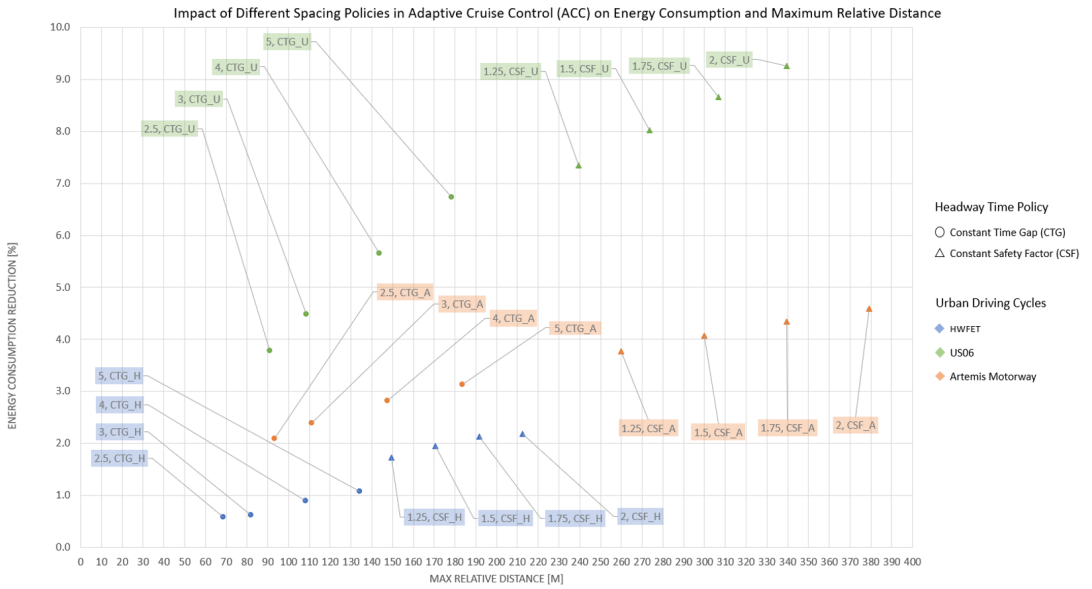

Figure 5.4: Energy Consumption and Maximum Relative Distance Across Time Gap Policies

A layered pattern is evident: while ECRR generally increases with following distance, the trend is weaker in the HWFET scenario. Notably, about the CTG strategy in HWFET, despite a large time gap setting ($T_{\text{gap}} = 5.0\,\text{s}$) yielding $d_{\text{rel,max}} = 134\,\text{m}$, achieves only a 1.1% ECRR, indicating that energy gains from enlarged spacing are marginal in steady-state cruise conditions.

In contrast, CSF strategies exhibit both higher $d_{\text{rel,max}}$ and superior energy reduction across dynamic cycles such as US06 and Artemis. For example, in US06, CSF_U ($K = 1.5$) attains an ECRR of 8.0% at a spacing of 273 m, whereas CTG_U ($T_{\text{gap}} = 5.0\,\text{s}$) at a similar range yields only 6.7%. This highlights CSF's stronger adaptive capacity under high variability traffic conditions.

Based on these findings, strategy selection should not focus solely on the optimal ECRR within a single driving cycle but should consider consistency and engineering feasibility across multiple conditions. Following the comprehensive discussion and simulation validation, four candidate strategies were selected for further multi-objective evaluation:

- $\text{CTG}(T_{\text{gap}} = 2.5\,\text{s})$
- $\text{CTG}(T_{\text{gap}} = 5.0\,\text{s})$
- $\text{CSF}(K = 1.25)$
- $\text{CSF}(K = 1.75)$

These configurations share several desirable characteristics:

- No configuration violates safety thresholds or leads to excessive energy consumption, ensuring baseline feasibility.

- All present stable downward trends in energy use compared to baseline, with ECRR values ranging from 0.6% to 9.3%.

- Maximum relative distances are contained within a practical range of 70 m to 300 m, avoiding excessive traffic space occupancy.

In summary, the four selected strategies demonstrate consistent energy-saving performance and inter-scenario adaptability, laying the foundation for further evaluation in comfort, dynamics, and normalized multi-index comparisons.

5.4 Comfort Evaluation

In the comprehensive evaluation of time gap policies, ride comfort plays a critical role alongside energy efficiency. To quantitatively evaluate the longitudinal comfort performance of each policy configuration, this study introduces the Acceleration Reduction Ratio (ARR) as the core metric, which has been defined earlier. ARR reflects the extent to which a given strategy suppresses longitudinal acceleration disturbances, where higher ARR values indicate better suppression effects and enhanced comfort.

Based on previous selections of representative policies, four configurations were chosen for cross-scenario comfort evaluation: CTG with $T_{\text{gap}} = 2.5\,\text{s}$, CTG with $T_{\text{gap}} = 5.0\,\text{s}$, CSF with $K = 1.25$, and CSF with $K = 1.75$. The comparative results under three driving cycles—HWFET, US06, and Artemis Motorway—are shown in Table 5.7 and visualized in Figure 5.5.

Table 5.7: Comfort Performance Comparison under Highway Driving Cycles

Driving Cycle	**HWFET**		**US06**		**Artemis Motorway**	
$a_{\text{rms,ref}}$ [m/s²]	**0.30**		**1.00**		**0.56**	
policy with T_{gap} [s]	a_{rms} [m/s²]	$a_{\text{rms,reduction}}$ [%]	a_{rms} [m/s²]	$a_{\text{rms,reduction}}$ [%]	a_{rms} [m/s²]	$a_{\text{rms,reduction}}$ [%]
CTG $T_{\text{gap}} = 2.5$	0.263	12.4	0.775	22.2	0.406	27.2
CTG $T_{\text{gap}} = 5$	0.230	23.3	0.615	38.2	0.320	42.7
CSF $K = 1.25$	0.233	22.2	0.661	33.6	0.295	47.1
CSF $K = 1.75$	0.218	27.4	0.596	40.1	0.263	52.9

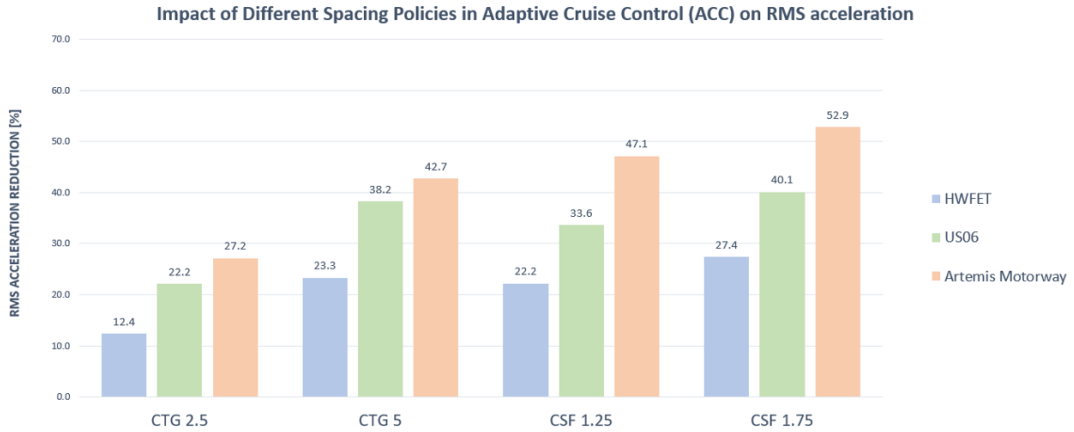

Figure 5.5: RMS Acceleration Reduction Comparison across Driving Cycles

The results reveal that all four selected time gap configurations significantly reduce RMS acceleration, indicating a notable improvement in ride comfort. Among them, the CSF strategy with $K = 1.75$ demonstrates the highest ARR values across all scenarios, peaking at 52.9% under the Artemis Motorway cycle. This suggests that increasing the safety factor K in CSF can more effectively suppress acceleration fluctuations, especially in high-speed or aggressive deceleration environments.

On the other hand, the CTG with $T_{\text{gap}} = 5.0\,\text{s}$ also shows a considerable improvement in comfort, achieving more than 40% ARR under the US06 and Artemis cycles. This reflects the advantages of longer headway in mitigating impact and improving comfort. However, under HWFET with a more stable speed profile, the performance advantage of a larger T_{gap} is less obvious than that of CSF.

Furthermore, while CTG with $T_{\text{gap}} = 2.5\,\text{s}$ yields acceptable comfort benefits under Artemis (27.2%) and US06 (22.2%), its effectiveness under HWFET drops to just 12.4%. This highlights a key limitation: shorter headways may not consistently perform well across all traffic dynamics.

In terms of cross-cycle stability, both CSF policies maintain high and stable ARR values, with CSF ($K = 1.75$) delivering the highest uniformity and improvement. In summary, comfort evaluation based on ARR values confirms the superiority of CSF strategies—particularly with larger safety factors—in improving ride quality. CTG policies with large headways also exhibit strong comfort potential, though with slightly lower consistency.

5.5 Results Discussion

5.5.1 Multi-Objective Trade-off Analysis

To conduct a balanced evaluation of different time gap policies, this study adopts a two-dimensional analysis framework integrating energy efficiency and ride comfort. The Energy Consumption Reduction Ratio (ECRR) and Acceleration Reduction Ratio (ARR) are selected as core evaluation metrics, which respectively reflect the energy-saving capability and the effectiveness in mitigating longitudinal disturbances. A higher ECRR indicates better battery energy savings, while a higher ARR corresponds to improved driving smoothness and ride quality.

The results show that, in terms of energy savings, the CSF policy with $K = 2.0$ achieves the highest ECRR across multiple driving cycles, reaching up to 9.3% in the US06 cycle. It is followed by CTG with $T_{\text{gap}} = 5.0\,\text{s}$ and CSF with $K = 1.75$, which also perform well. CTG with $T_{\text{gap}} = 2.5\,\text{s}$ performs relatively poorly, especially under low-speed scenarios such as HWFET, where the energy-saving effect is only 0.6%.

In terms of ARR, which evaluates driving smoothness and passenger comfort, CSF policies again show a clear advantage. In particular, CSF($K = 1.75$) achieves ARR values exceeding 40% across all three driving cycles, indicating superior jerk suppression capabilities. CTG with $T_{\text{gap}} = 5.0\,\text{s}$ also performs relatively well, while CTG with $T_{\text{gap}} = 2.5\,\text{s}$ shows poor jerk control due to its short headway and rigid response.

Overall, from the cross-cycle perspective, CSF($K = 1.75$) demonstrates optimal performance across both metrics. Although CSF($K = 2.0$) achieves the best ECRR, it imposes excessive following distances, resulting in poor spatial efficiency and limited comfort benefits. CTG with $T_{\text{gap}} = 5.0\,\text{s}$ shows acceptable comfort improvements and moderate energy savings, making it suitable as an alternative when stability and simplicity are preferred.

5.5.2 Scenario-Based Analysis of Policy Applicability

Following the comprehensive metric evaluation, it is essential to analyze the real-world applicability of each time gap policy under different driving scenarios. As different traffic conditions vary significantly in speed profiles, acceleration patterns, and dynamic fluctuations, practical deployment decisions should be based not only on numerical superiority but also on contextual adaptability.

In highway cruising scenarios such as HWFET, vehicles typically operate at high speeds with low acceleration variance, and system performance relies heavily on maintaining longitudinal stability. In such cases, CTG policies with large time gaps (e.g., $T_{\text{gap}} = 5.0\,\text{s}$) perform effectively, providing noticeable energy savings

(up to 1.1%) and maintaining relative distances within acceptable limits (134 m). Therefore, CTG is applicable in steady cruising with low traffic density.

In contrast, highly dynamic cycles like US06 and Artemis Motorway demand rapid responses and disturbance tolerance. CSF policies, with their adaptive structure, show distinct advantages. For instance, CSF($K = 1.75$) achieves ECRR values of 9.3%, and ARR values exceeding 40% under both cycles, demonstrating stable comfort and energy-saving capabilities. HDB policies, although inspired by human behavior, suffer from overreaction patterns, resulting in excessive jerk and poor energy performance. These characteristics render them unsuitable for high-speed, dynamic environments.

In summary, CSF policies offer the best adaptability across various scenarios due to their flexible structure and balanced performance. CTG policies are suitable in simple and stable environments, while HDB policies are not recommended due to poor control stability. Policy selection should be aligned with traffic characteristics and sensor accuracy to ensure optimal integration of ACC systems into real-world operations.

Chapter 6

Conclusion and Future Work

6.1 Conclusions

This thesis centers on the impact of time gap policies in Adaptive Cruise Control (ACC) systems, focusing on three representative approaches—Constant Time Gap (CTG), Constant Safety Factor (CSF), and Human Driving Behavior (HDB)—and conducts comprehensive modeling, parameterization, and multi-dimensional performance evaluation within a high-fidelity Simulink simulation environment under typical urban and highway driving conditions. The research considers the diversity of traffic scenarios and engineering application needs, constructing an evaluation index system that integrates energy consumption, comfort, and safety, and introduces a baseline without ACC or time gap policy to ensure the scientific validity and consistency of cross-policy comparisons.

In urban driving scenarios, through systematic simulation of WLTP Class 3, Artemis Urban, and the China city driving cycles, it is demonstrated that all time gap policies significantly improve energy efficiency and ride comfort, effectively suppressing frequent stop-and-go and acceleration events. The CSF policy consistently achieves the lowest energy consumption, minimum acceleration, and jerk values in all groups, thus theoretically offering dual advantages in fuel economy and ride quality. However, due to its considerable maximum inter-vehicular distance—often exceeding 70 meters—CSF greatly reduces space utilization and thus lacks engineering feasibility for urban deployment. To balance spatial efficiency and energy saving, this thesis proposes a selection mechanism with a maximum inter-vehicular distance constraint of 40–70 meters, identifying CTG ($T_{\text{gap}} = 2.5\,\text{s}$, $3.0\,\text{s}$) and HDB ($T_{\text{gap}} = 4.0\,\text{s}$, $5.0\,\text{s}$) as the optimal candidates that meet requirements for energy, comfort, and road capacity. Further comfort evaluation reveals that HDB ($T_{\text{gap}} = 5.0\,\text{s}$) consistently achieves the highest acceleration root mean square reduction rate (ARR), providing the best ride experience in all urban cycles. CTG

($T_{\text{gap}} = 3.0\,\text{s}$), with its simplicity and strong cross-cycle consistency, is recommended as the most universal strategy for urban conditions. In summary, CTG ($T_{\text{gap}} = 3.0\,\text{s}$) should be prioritized as the standard configuration for city driving, while HDB ($T_{\text{gap}} = 5.0\,\text{s}$) suits high-end comfort-oriented scenarios.

In highway scenarios, the thesis evaluates HWFET, US06, and Artemis Motorway cycles through systematic simulation. Policies not meeting the minimum safety headway of 3 seconds are excluded. Results indicate that the CSF policy, with its dynamic safety factor, maintains the greatest improvement in energy consumption and optimal comfort across all high-speed conditions, particularly excelling in highly dynamic scenarios (US06, Artemis Motorway) with strong disturbance suppression. The CTG policy, in high-speed, low-disturbance scenarios such as HWFET, is advantageous for its stable structure and ease of parameter tuning, making it suitable as a conservative engineering baseline. HDB, due to frequent responses and "human-like" micro-adjustments, suffers from increased energy use and excessive jerk in dynamic highway environments, limiting its engineering applicability.

Further multi-objective analysis shows that CSF ($K = 1.75$) delivers the optimal balance of energy consumption and comfort in highway conditions; however, its maximum following distance far exceeds that of CTG ($T_{\text{gap}} = 5.0\,\text{s}$), resulting in lower space utilization. Therefore, while CSF is highly recommended for scenarios with stringent energy and comfort requirements but relaxed road capacity constraints, it is not suitable where space efficiency is critical. In comparison, CTG ($T_{\text{gap}} = 5.0\,\text{s}$) achieves nearly equivalent comfort and energy savings with a more reasonable maximum gap, thus slightly superior in spatial efficiency. Nevertheless, both large-gap strategies can significantly limit road throughput, which must be considered for high-volume highways.

Overall, this research establishes a generalizable and reusable modeling and evaluation framework for ACC time gap policies, systematically clarifies their performance boundaries and application domains under various scenarios, and provides robust theoretical and engineering references for adaptive, multi-objective, and intelligent ACC policy design in future applications.

6.2 Summary of Limitations and Prospects

This thesis presents a systematic exploration of time gap policies for Adaptive Cruise Control, aiming to offer both a clear comparison and practical insights for real-world applications. By designing a unified simulation platform and evaluating multiple policies under representative urban and highway driving cycles, the study highlights how energy consumption, comfort, and safety can be balanced through appropriate policy selection. The work also demonstrates the importance of carefully setting evaluation metrics and using a consistent baseline, so that results are meaningful

for both theory and practice.

At the same time, it should be acknowledged that this research has certain limitations. The scenarios are based on standard driving cycles and idealized simulation conditions, which, while useful for controlled comparison, cannot capture all the variability and unexpected events of real-world traffic. The policies discussed are static and do not adapt to changing traffic, driver intentions, or sudden hazards. Likewise, some factors—such as extreme emergencies, real-world actuator constraints, and the behavior of advanced electrified powertrains—were beyond the scope of this work.

Looking ahead, several directions could be taken to build on these results. Future studies may explore adaptive policies that respond dynamically to traffic and environment, perhaps with support from V2X or infrastructure data. Extending the approach to include lane changing, merging, or collaborative platooning could offer new insights for more advanced automated driving systems. Finally, validating the findings in hardware-in-the-loop setups or real vehicle tests, and considering more complex or unexpected traffic scenarios, will help bridge the gap between simulation and deployment, making ACC systems safer and more robust in everyday use.

List of Tables

List of Figures

Bibliography

[1] On-Road Automated Driving (ORAD) Committee. *Taxonomy and Definitions for Terms Related to Driving Automation Systems for On-Road Motor Vehicles*. Apr. 2021. DOI: https://doi.org/10.4271/J3016_202104. URL: https://doi.org/10.4271/J3016_202104 (cit. on pp. 1, 24).

[2] *Taxonomy and Definitions for Terms Related to Driving Automation Systems for On-Road Motor Vehicles*. URL: https://www.sae.org/standards/content/j3016_202104/. (accessed: 30.04.2021) (cit. on p. 2).

[3] Rajesh Rajamani. *Vehicle Dynamics and Control*. 2nd. New York: Springer, 2012. URL: https://link.springer.com/book/10.1007/978-1-4614-1433-9 (cit. on pp. 4, 26).

[4] Martin Treiber and Arne Kesting. *Traffic Flow Dynamics: Data, Models and Simulation*. Springer, 2013. URL: https://link.springer.com/book/10.1007/978-3-642-32460-4 (cit. on pp. 4, 60).

[5] Ardalan Vahidi and Antonio Sciarretta. «Energy saving potentials of connected and automated vehicles». In: *Transportation Research Part C: Emerging Technologies* 95 (2018), pp. 822–843. DOI: 10.1016/j.trc.2018.08.004 (cit. on p. 5).

[6] MathWorks. *Adaptive Cruise Control with Sensor Fusion*. Online; accessed 2025-05-13. 2025. URL: https://www.mathworks.com/help/driving/ug/adaptive-cruise-control-with-sensor-fusion.html (cit. on p. 9).

[7] A. AL-Ali, S. Al-Sharaeh, and S. Mohammed. «Modeling and Simulation of Adaptive Cruise Control System». In: *ResearchGate* (2020). Online. URL: https://www.researchgate.net/publication/340519532_Modeling_and_Simulation_of_Adaptive_Cruise_Control_System (cit. on pp. 9, 10).

[8] SAE International. *Evaluating the Impact of Sensor Accuracy on Adaptive Cruise Control Systems*. Tech. rep. Online. SAE International, 2025. URL: https://www.sae.org/publications/technical-papers/content/2025-01-5011/ (cit. on p. 10).

[9] Shaimaa K. El-Baklish, Anastasios Kouvelas, and Michail A. Makridis. «Driving towards stability and efficiency: A variable time gap strategy for Adaptive Cruise Control». In: *Transportation Research Part C: Emerging Technologies* 174 (2025), p. 105074. DOI: 10.1016/j.trc.2025.105074. URL: https://www.sciencedirect.com/science/article/pii/S0968090X25000786 (cit. on p. 10).

[10] Haohua Zhang. «Enhancing vehicle safety-the role of PID control in adaptive cruise control systems». In: *AIP Conference Proceedings, 2024 2nd International Conference on Computer Science and Mechatronics (ICCSM 2024)*. Vol. 3194. 1. 2024, p. 050023. DOI: 10.1063/5.0222898. URL: https://pubs.aip.org/aip/acp/article-abstract/3194/1/050023/3325254/Enhancing-vehicle-safety-the-role-of-PID-control (cit. on p. 13).

[11] MathWorks. *Adaptive Cruise Control System Using Model Predictive Control*. Online; accessed 2025-07-10. 2025. URL: https://ww2.mathworks.cn/help/mpc/ug/adaptive-cruise-control-using-model-predictive-controller.html (cit. on p. 14).

[12] Y. Lin, J. McPhee, and N. L. Azad. «Adaptive Cruise Control Based on Safe Deep Reinforcement Learning». In: *Sensors* 24.8 (2024), p. 2657. DOI: 10.3390/s24082657. URL: https://www.mdpi.com/1424-8220/24/8/2657 (cit. on p. 14).

[13] Buğra Kabasakal and Murat Üçüncü. «The Design and Simulation of Adaptive Cruise Control System». In: *International Journal of Automotive Science and Technology* 6.3 (2022), pp. 242–256. DOI: 10.30939/ijastech..1038371. URL: https://dergipark.org.tr/en/pub/ijastech/article/1038371 (cit. on p. 14).

[14] Clement Uchechukwu Mba and Carlo Novara. «Evaluation and Optimization of Adaptive Cruise Control Policies Via Numerical Simulations». In: *International Conference on Vehicle Technology and Intelligent Transport Systems (VEHITS)*. 2016, pp. 13–19. DOI: 10.5220/0005621100130019. URL: https://www.researchgate.net/publication/302973842_Evaluation_and_Optimization_of_Adaptive_Cruise_Control_Policies_Via_Numerical_Simulations (cit. on p. 17).

[15] Junmin Wang and Rajesh Rajamani. «Should adaptive cruise-control systems be designed to maintain a constant time gap between vehicles?» In: *IEEE Transactions on Vehicular Technology* 53.5 (2004), pp. 1480–1490. DOI: 10.1109/TVT.2004.832386. URL: https://ieeexplore.ieee.org/document/1337326 (cit. on p. 18).

[16] T. Yu, Y. Tang, R. Chen, and S. Zhao. «Optimization of Adaptive Cruise Control Strategies Based on the Responsibility-Sensitive Safety Model». In: *Vehicles* 7.2 (2025), p. 28. DOI: 10.3390/vehicles7020028. URL: https://www.mdpi.com/2624-8921/7/2/28 (cit. on p. 20).

[17] Michail Makridis, Konstantinos Mattas, and Biagio Ciuffo. «Response Time and Time Headway of an Adaptive Cruise Control. An Empirical Characterization and Potential Impacts on Road Capacity». In: *IEEE Transactions on Intelligent Transportation Systems* 21.4 (2020), pp. 1677–1686. DOI: 10.1109/TITS.2019.2948646. URL: https://ieeexplore.ieee.org/document/8884686 (cit. on pp. 21, 60).

[18] Cunxue Wu, Zhongming Xu, Yang Liu, Chun Yun Fu, Kuining Li, and Minghui Hu. «Spacing Policies for Adaptive Cruise Control: A Survey». In: *IEEE Access* 8 (2020), pp. 50149–50162. DOI: 10.1109/ACCESS.2020.2978244. URL: https://ieeexplore.ieee.org/document/9026788 (cit. on pp. 22, 40).

[19] International Organization for Standardization. *ISO 26262: Road vehicles—Functional safety*. Standard. 2018 (cit. on p. 23).

[20] Julia Nilsson, Mattias Brännström, Jonas Fredriksson, and Erik Coelingh. «Longitudinal and Lateral Control for Automated Yielding Maneuvers». In: *IEEE Transactions on Intelligent Transportation Systems* 17.5 (2016), pp. 1404–1414. DOI: 10.1109/TITS.2015.2504718. URL: https://ieeexplore.ieee.org/document/7378957 (cit. on p. 26).

[21] SHRP 2. *Naturalistic Driving Study: Dataset and Documentation*. https://insight.shrp2nds.us/. 2015 (cit. on p. 26).

[22] Clara Marina Martinez, Mira Heucke, Fei-Yue Wang, Bo Gao, and Dongpu Cao. «Driving Style Recognition for Intelligent Vehicle Control and Advanced Driver Assistance: A Survey». In: *IEEE Transactions on Intelligent Transportation Systems* 19.3 (2018), pp. 666–676. DOI: 10.1109/TITS.2017.2706978. URL: https://ieeexplore.ieee.org/document/8002632 (cit. on p. 26).

[23] Hans B. Pacejka. *Tire and Vehicle Dynamics*. 3rd. Oxford: Butterworth-Heinemann, 2012. ISBN: 978-0-08-097016-5 (cit. on p. 32).

[24] MathWorks. *Tire (Magic Formula)*. Online; accessed 2025-07-14. 2025. URL: https://it.mathworks.com/help/sdl/ref/tiremagicformula.html (cit. on p. 32).

[25] United Nations Economic Commission for Europe. *UN Regulation No. 154 – Worldwide harmonized Light vehicles Test Procedure (WLTP)*. Standard. 2021. URL: https://unece.org/transport/documents/2021/02/standards/un-regulation-no-154-worldwide-harmonized-light-vehicles-test (cit. on p. 44).

[26] Michel André. «The ARTEMIS European driving cycles for measuring car pollutant emissions». In: *Science of The Total Environment* 334–335 (2004), pp. 73–84. DOI: 10.1016/j.scitotenv.2004.04.070. URL: https://www.sciencedirect.com/science/article/pii/S0048969704003584 (cit. on pp. 45, 73).

[27] DieselNet. *China Light-Duty Vehicle Test Cycle (CLTC)*. Online; accessed 2025-07-14. 2023. URL: https://www.dieselnet.com/standards/cycles/cltc.php (cit. on p. 46).

[28] Jeroen van Hegelsom. «Real-Time MPC Strategy for Predictive Adaptive Cruise Control». Master Thesis, CST2023.048. MA thesis. Eindhoven University of Technology, 2023. URL: https://research.tue.nl/en/studentTheses/real-time-mpc-strategy-for-predictive-adaptive-cruise-control (cit. on p. 48).

[29] U.S. Environmental Protection Agency. *Highway Fuel Economy Test (HWFET) Cycle*. Online, accessed 2024-07-10. 2021. URL: https://www.epa.gov/vehicle-and-fuel-emissions-testing/dynamometer-drive-schedules (cit. on p. 71).

[30] U.S. Environmental Protection Agency. *Supplemental Federal Test Procedure (SFTP) US06*. Online, accessed 2024-07-10. 2021. URL: https://www.epa.gov/vehicle-and-fuel-emissions-testing/dynamometer-drive-schedules (cit. on p. 72).